بسم الله الرحمن الرحيم

Sudan University of Science and Technology

College of Graduate Studies

Optical Characterization of Thick Films for Some Oxides Fabricated by Pulsed Laser Deposition

التوصيف البصري للاغشية السميكة لبعض الاوكسيدات المصنعة بواسطة الترسيب بالليزر النبضئ

A thesis submitted in fulfillment of the requirements for the degree of doctor of philosophy in laser application in physics

By:

Omar Ahmed Mohammed Elnour

Supervised:

Prof. Dr. Nafie A. Almuslet

November 2016

الآيـة

قَالَ تَعَالَىٰ: أَعُوذُ بِٱللَّهِ مِنَ ٱلشَّيْطَٰنِ ٱلرَّجِيمِ ﴿ ۞ ٱللَّهُ نُورُ ٱلسَّمَٰوَٰتِ وَٱلْأَرْضِ ۚ مَثَلُ نُورِهِۦ كَمِشْكَوٰةٍ فِيهَا مِصْبَاحٌ ۖ ٱلْمِصْبَاحُ فِى زُجَاجَةٍ ۖ ٱلزُّجَاجَةُ كَأَنَّهَا كَوْكَبٌ دُرِّىٌّ يُوقَدُ مِن شَجَرَةٍ مُّبَٰرَكَةٍ زَيْتُونَةٍ لَّا شَرْقِيَّةٍ وَلَا غَرْبِيَّةٍ يَكَادُ زَيْتُهَا يُضِىٓءُ وَلَوْ لَمْ تَمْسَسْهُ نَارٌ ۚ نُّورٌ عَلَىٰ نُورٍ ۗ يَهْدِى ٱللَّهُ لِنُورِهِۦ مَن يَشَآءُ ۚ وَيَضْرِبُ ٱللَّهُ ٱلْأَمْثَٰلَ لِلنَّاسِ ۗ وَٱللَّهُ بِكُلِّ شَىْءٍ عَلِيمٌ ﴿٣٥﴾ فِى بُيُوتٍ أَذِنَ ٱللَّهُ أَن تُرْفَعَ وَيُذْكَرَ فِيهَا ٱسْمُهُۥ يُسَبِّحُ لَهُۥ فِيهَا بِٱلْغُدُوِّ وَٱلْءَاصَالِ ﴿٣٦﴾ رِجَالٌ لَّا تُلْهِيهِمْ تِجَٰرَةٌ وَلَا بَيْعٌ عَن ذِكْرِ ٱللَّهِ وَإِقَامِ ٱلصَّلَوٰةِ وَإِيتَآءِ ٱلزَّكَوٰةِ ۙ يَخَافُونَ يَوْمًا تَتَقَلَّبُ فِيهِ ٱلْقُلُوبُ وَٱلْأَبْصَٰرُ ﴿٣٧﴾ ﴾ النور: ٣٥ - ٣٧

Dedication

To……

Soul of my mother

My father

My family

Omar

Acknowledgement

The investigations in this work have been carried out under the supervision of **Prof. Dr. Nafie Abd Alatif Almuslet**. I express my deep sense of gratitude for his excellent guidance, competent advice, keen observations and persistent encouragement as well as personal attention given to me during the entire course of work, without which the successful completion of this work would not have been possible. I am deeply indebted to him for his kindness, constant encouragement and support.

With a sense of gratitude, I am thankful to all the office and library staff of the institute of laser –Sudan University of Science and Technology and the technical staff for all the help and cooperation.

Abstract

The main aim of this study was to deposit thick films of Titanium dioxide, Zinc oxide and Aluminum oxide, all deposited individually on a glass substrate by pulsed laser technique . In this technique a Q-Switch Nd:YAG laser with wavelength 1064 nm, pulse energy 500, 600, and 700 mJ, respectively, was used. The repetition rate was 20, 30 and 40Hz. In the beginning of the process, disks of these oxides were fabricated via mixing with Potassium Bromide of equal weight ratios: 50% - 50% for all oxides. In order to make these disks, the materials were compressed via a compressor of high pressure.

Laser beam of pulse energy 500mJ and10ns pulse duration with frequency of20Hz,was focused on Titanium dioxide disk and plasma was obtained from each disk and deposited on the glass substrate.

The former procedure was repeated with increasing repetition rate to (30) Hz then (40) Hz. Afterward, the same above procedure was repeated by increasing the laser pulse energy to (600 mJ), then to (700 mJ).

All above mentioned steps were repeated with ZnO and Al_2O_3 disks.

The thickness of each film was measured by the scanning electron microscope, and the relation between the film thickness and the repletion rate for each energy of the pulsed laser was plotted.

The measurements of the transmitted intensity for some lasers were carried out from which the refractive indices, absorption coefficients were calculated, the transmission percentage for each film was measured too,

Consequently, the relations between the refractive indices and absorption coefficients with wavelength were plotted.

Same steps were repeated for all films. A comparison was done between the optical properties (transmission spectrum, refractive indices and absorption) of the films, where it was noticed that these optical properties depend on the thickness of the thick film.

Results revealed that it is possible to use these films of filters at at certain wavelengths, or reflectors for other wavelengths. Finally future work were recommended.

المستخلص

إن الهدف الرئيس لهذه الدراسة هو ترسيب اغشية سميكة من اكسيد التيتانيوم واكسيد الزنك واكسيد الألمونيوم كل علي انفراد على سطح شريحة زجاجية وذلك بواسطة تقانة الترسيب بالليزر النبضي حيث استخدم ليزر نيوديوم – ياق ذي التشغيل المفتاحي و ذي الطول الموجي 1064 نانومتر بطاقة نبضة 500 و 600 و 700 ملي جول على التوالي وعند معدل تكرار 20و30و 40هيرتز. في البداية تم تصنيع اقراص من كل من هذه الاكسيدات بخلطها مع بروميد البوتاسيوم بنسب وزنية ثابتة متساوية 50%−50% للكل حيث تم كبسها بواسطة مكبس ذي ضغط عالي لتكوين الاقراص.

تم تركيز الليزر بطاقة نبضة (500) ملي جول وزمن نبضه (10) نانو ثانية وبتكرارية (20) هيرتز علي اقراص TiO_2 وتم ترسيب البلازما الناتجة من كل قرص علي الشريحة الزجاجية . ثم اعيدت نفس الخطوة بزيادة معدل التكرارية (30) هيرتز ثم (40) هيرتز. وبعدها اعيدت نفس الخطوات أعلاه بزيادة طاقة النبضة الئ (600) ملي جول وبعدها (700) ملي جول.

كل الخطوات اعلاه تمت اعادتها لأقراص من ZnO و Al_2O_3 وبذلك اصبحت هنالك 3 مجموعات من الاغشية السميكه. ولقياس سمك كل غشاء استخدم المجهر الالكتروني الماسح ثم رسمت العلاقة بين سمك الغشاء ومعدل التكرارية لكل طاقة من طاقات الليزر المستخدمة.

ومن ثم اجريت قياسات للشدة النافذة من هذه الليزرات ومنها تم حساب معاملات الانكسار والامتصاص وقيست النفاذية لكل غشاء باعتبار ان المادة لا تمتص الشدة. ومن ثم تم رسم العلاقاتبين: النفاذية (كنسبة مئوية) و معاملات الانكسار والامتصاص مع الاطوال الموجية.

اجريت نفس الخطوات لكل الاغشية وتمت مقارنة الخصائص البصرية (طيف النفاذ ومعاملات الانكسار والامتصاص) لكل الاغشية حيث لوحظ اعتماد هذه الخصائص علئ سمك الغشاء.

اظهرت النتائج المتحصل عليها امكانية استخدام الاغشية من اكاسيد التيتانيوم والزنك و الالمونيم علي سطح الزجاج كمرشح عند بعض الاطوال الموجية . او عاكس لبعض الاطوال الموجية الأخرى. كما تم وضع بعض التوصيات لأعمال مستقبلية.

TABLE OF CONTENTS

الآية	i
Dedication	ii
Acknowledgement	iii
Abstract	vi
المستخلص	iv
Table of contents	vi
List of Figures	x
List of Tables	xiii
Chapter One **Thick Films, Basic Concepts**	
1.1 Introduction	1
1.2 Aims of the work	2
1.3 Outline of thesis	2
1.4 Optical coatings	2
1.4.1 Deposition process	3
1.4.2 Deposition parameters	3
1.4.3 Types of thick films	4
1.4.4 Thick film Preparation Techniques	4
1. 5 Physical Vapour Processes (PVD)	4
1.5.1 Thermal evaporation by resistive heating	6
1.5.2 Electron beam evaporation	7
1.5.3 Ion plating	8
1.5.4 Molecular Beam Epitaxy	9
1.5.5 Glow-Discharge Technologies	10
1.5.6 Electrodeposited coatings	10
1.5.7 Sputtering	12
1.6 Chemical Vapor Deposition	12
1.6.1 Photochemical deposition	14
1.6.2. Electrochemical deposition	15
1.6.3. Spray pyrolysis deposition	17

1.6.4 Chemical bath deposition	18
1.6.5 Spin Coating	19
1.7 The major advantages of the CVD	21
Chapter Two Pulsed laser deposition, Basic concept	
2-1 Introduction	23
2.2 Laser – target interaction	24
2.2.1 The ablation process	25
2.2.2 Practical considerations	27
2.3 Plume expansion	28
2.3.1 In vacuum	29
2.3.2 In a background atmosphere	31
2.4 Film deposition	32
2.4.1 Typical growth modes	32
2.4.2 Characteristics of PLD growth	34
2.4.3 Structure development	36
2.4.4 Particulate formation	37
2-4-5 Advantages and disadvantages of PLD	37
2.5 The Optical Properties	38
2.6 Literature Review	42
Chapter Three The Experimental Part	
3.1 Introduction	48
3.2 Deposition Equipments	48
3.2.1 Nd: YAG Laser	48
3.2.2 Target holder	49
3.2.3 Substrate holder	49
3.3 Target materials	49
3.3.1 Titanium Dioxide (TiO_2)	50
3.3.2 Sapphire (Al_2O_3)	51
3.3.3 Zinc oxide (ZnO)	52
3.3.4 Potassium Bromide (KBr)	54
3.4 The Pressing Machine and its Parts	55
3.5 Procedure of the PLD	56
3.6 Fabrication of the thick films by (PLD)	57
3.7 Scanning electronic microscope	57
3.8 Characterization of thick films	59
3.8.1 The Lasers Sources	59
3.8.1.1 Diode Laser (532nm)	60
3.8.1.2 Monochromatic LED (660 nm)	60
3.8.1.3 He-Ne Laser (632.8nm)	60

3.8.1.4 Diode laser (675 nm)	60
3.8.1.5 Diode Laser (820 nm)	61
3.8.1.6 Diode laser 915nm	61
3.9 Determination of the films optical properties	61
Chapter Four Results and discussion	
4.1 Introduction	64
4.2Thickness measurement	64
4.3 The optical properties of (TiO_2) thick films	69
4.4 The optical properties of Al_2O_3 thick films	75
4.5 The optical properties of (ZnO) thick films	75
4.6 Conclusions	83
4.7 Future work	84
References	85
Appendix	94

LIST OF FIGURES

Figure	Page
Figure.1.1: (a) Resistance–heated vacuum evaporation, (b) a selection of vacuum evaporation (Courtesy Leybold – Heraeus)	6
Fig.1.2:Electron beam heated vacuum evaporation (270°deflection)	7
Fig.1.3: Resistance heated ion plating	8
Figure.1.4: plating bath	11
Figure.1.5:Sequence of gas transport and reaction processes contributing to CVD film growth	13
Figure.1.6: Schematic diagram of the PCD method	14
Figure.1.7: Schematic diagram of the 3-electrodes electrochemical cell Apparatus.	16
Figure.1.8: Schematic diagram of spray pyrolysis apparatus.	17
Figure.1.9: Schematic diagram of the CBD method	18
Figure.1.10: stages of spin –coating process	20
Figure.2.1: Schematic presentation of the pulsed laser deposition process.	24
Figure.2.2: Schematic presentation of the laser target interactions during a high-power laser pulse.	26
Figure.2.3: Frank - van der Merwe nucleation and growth	34
Figure.2.4: The optical spectrum of solar radiation	40
Figure 2.5: The solar reflectance spectrum	41
Figure 3.1 ZnO disk after being ablated by the laser	50
Figure 3.2: Crystal structure of TiO_2. Red and grey spheres are oxygen and titanium atoms, respectively.	51
Figure (3.4). Tablets of the three groups of materials obtained by the compression method**.**	56
Figure (3.5) : schematic diagram of PLD technique setup	56
Figure 3.6. Schematic representation of a scanning electron microscope	57
Figure 3.7 a photograph of the PLD setup.	62
Figure (4. 1): SEM image of the TiO_2 thick films sample A1.	65
Figure (4. 2: SEM image of the TiO_2 thick films sample A2.	65
Figure (4. 3): SEM image of the TiO_2 thick films sample A3.	65
Figure (4. 4): SEM image of the TiO_2 thick films sample A6.	66
Figure (4. 5): SEM image of the TiO_2 thick films sample A7.	66
Figure (4. 6): SEM image of the TiO_2 thick films sample A8.	66
Figure (4. 7): SEM image of the TiO_2 thick films sample A9.	67
Figure (4. 8): SEM image of the TiO_2 thick films sample A1.	67
Figure (4.9) SEM image of the Al_2O_3 thick films sample B1.	67
Figure (4.10) SEM image of the Al_2O_3 thick films sample B2.	68

Figure (4.11) SEM image of the Al_2O_3 thick films sample B3.	68
Figure (4.12) SEM image of the Al_2O_3 thick films sample B4.	68
Figure (4.13) : The thickness of thin films in the Repetition Rate (20,30 and 40Hz) at pulse energy (500mJ)	69
Figure (4.14) : The thickness of thin films in the Repetition Rate (20,30 and 40Hz) at pulse energy (500mJ)	69
Figure (4-15): Transmission spectra of samples (A_1, A_2, A3) versus wavelengths at 500 mJ and, 20, 30, 40Hz RR.	70
Figure (4-16): Transmission spectra of samples (A_4, A_5, A6) versus wavelengths at 500 mJ and 20, 30, 40Hz RR.	71
Figure (4-17): Transmission spectra of samples (A_7, A_8, A9) versus wavelengths at 600 mJ and 20, 30, 40Hz RR.	71
Figure (4.19): The absorption coefficient of samples (A_1,A_2,A_3) versus wavelengths at 500 mJ and 20,30,40 Hz RR	72
Figure (4.20): The absorption coefficient of samples (A_5,A_6,A_7) versus wavelengths at 600 mJ and 20,30,40 Hz RR	72
Figure (4.21): The absorption coefficient of samples (A_7,A_8,A_9) versus wavelengths at 700 mJ and 20,30,40 Hz RR	73
Figure (4.22): The refractive indices of samples (A_1, A2, A3) versus wavelengths at 500 mJ and 20, 30, 40 Hz RR.	73
Figure (4.23): The refractive indices of samples (A_4, A5, A6) versus wavelengths at 600 mJ and 20, 30, 40 Hz RR.	75
Figure (4.24): The refractive indices of samples (A_7, A8, A9) versus wavelengths at 700 mJ and 20, 30, 40 Hz RR.	76
Figure (4.25): Transmission spectra of samples (B_1, B2) versus wavelengths at 500 mJ and 20, 30, 40 Hz RR.	76
Figure (4.26): Transmission spectra of samples (B_4, B5, B6) versus wavelengths at 600 mJ and 20, 30, 40 Hz RR.	77
Figure (4.27): Transmission spectra of samples (B_7, B8, B9) versus wavelengths at 700 mJ and 20, 30, 40 Hz RR.	77
Figure (4.28): The absorption coefficient of samples (B_1, B2, B3) versus wavelengths at 500 mJ and 20, 30, 40 Hz RR.	79
Figure (4.29): The absorption coefficient of samples (B_4, B5, B6) versus wavelengths at 500 mJ and 20, 30, 40 Hz RR.	79
Figure (4.30): The absorption coefficient of samples (B_7, B8, B9) versus wavelengths at 500 mJ and 20, 30, 40 Hz RR.	79
Fig (4.31): The refractive indices of samples (B_1, B2, B3) versus wavelengths at 500 mJ and 20, 30, 40 Hz RR.	80
Figure (4.32): The refractive indices of samples (B_4, B5, B6) versus wavelengths at 600 mJ and 20, 30, 40 Hz RR.	80
Figure (4.33): The refractive indices of samples (B_7, B8, B9) versus wavelengths at 700 mJ and 20, 30, 40 Hz RR.	80
Fig (4.34): Transmission spectra of samples (C_1, C2, C_3) versus wavelengths at 500 mJ and 20, 30, 40 Hz RR.	80
Fig (4.35): Transmission spectra of samples (C_4, C5, C_6) versus	82

wavelengths at 700 mJ and 20, 30, 40 Hz RR.	
Fig (4.36): Transmission spectra of of samples (C_7, C8, C9) versus wavelengths at 500 mJ and 20, 30, 40 Hz RR.	82
Fig (4.37): The absorption coefficient of samples (C_1,$C_2$$C_3$) Versus wavelengths at500 mJ and 20, 30, 40 Hz RR.	82
Fig (4.38): The absorption coefficient of samples (C_4,C_5,C_6) Versus wavelengths at 600 mJ and 20, 30, 40 Hz RR.	83
Fig (4. 39): The absorption coefficient of samples (C_7,C_8,C_9) Versus wavelengths at 700 mJ and 20, 30, 40 Hz RR.	83
Fig (4.40): The refractive indices of samples (C_1,C_2,C_3) versus wavelengths at 500 mJ and 20,30,40 Hz RR	83

LIST OF TABLES

Tables	Page
Table 1.1: methods for deposition of thick films	5
Table 2-1: Typical PLD parameters.	28
Table 3-1: The specifications of Nd: YAG Laser	51
Table 3.2: Potassium Bromide properties	55
Table 3.3: Sapphire, Al_2O_3 Properties	56
Table 3.4:Physical properties of ZnO wurtzite structure	58
Table 3.5: Specification of diode Laser (532nm)	60
Table 3.6: Specification of HeNe Laser (632.8nm)	60
Table 3.7: Specification of diode Laser omega XP.	61
Table (4.1) : samples that were prepared by Nd:YAG (1064 nm) laser	67
Table (4-2):The thicknesses of the thick film	67

Chapter One

Thick Films, Basic Concepts

1-1 Introduction:

The field of material science and engineering community's ability to conceive the novel materials with extraordinary combination of chemical, physical and mechanical properties has changed the modern society. There is an increasing technological progress. Modern technology requires thin and thick films for different applications (West, 2003).

Thick film technology is the basic of development in solid state electronics. The usefulness of the optical properties of metal films, and scientific about the behavior of two-dimensional solids has been responsible for the immense interest in the science and technology of the thick films. Thick film studies have directly or indirectly advanced many new areas of research in solid state physics and chemistry which are based on phenomena uniquely characteristic of the thickness, geometry, and structure of the film (West, 2003).

When we consider a very low thick film of some substance, we have a situation in which the two surfaces are so close to each other that they can have a decisive influence on the internal physical properties and processes of the substance, which differ, therefore, in a profound way from those of a bulk material. The decrease in distance between the surfaces and their mutual interaction can result in the rise of completely new phenomena. Here the one dimension of the material is reduced to an order of several atomic layers which creates an intermediate system between macro systems and molecular systems, thus it provides us a method of investigation of the microphysical nature of various processes. However the physical properties of the films like electrical resistivity do not substantially differ from the properties of the bulk material .For a thin film the limit of thickness is considered between tenths of nanometer and several micrometers. Thin and thick film materials are the key elements of continued technological advances made in the fields of

optoelectronic, photonic, and magnetic devices. The processing of materials into films allows easy integration into various types of devices. The properties of material significantly differ when analyzed in the form of thick and thin films. Most of the functional materials are rather applied in thick film form due to their specific electrical, magnetic, optical properties or wear resistance. Thick film technologies make use of the fact that the properties can particularly be controlled by the thickness parameter. Thick films are formed mostly by deposition, either physical or chemical deposition methods.

1.2Aims of the work:

The aims of this study are:

- The fabrication of thick films of TiO_2, Al_2O_3, and ZnO on glass substrate by pulsed laser deposition method.
-The determination of the optical properties of these films in range of wavelengths between (532-915) nm.

1-3 Outlines of the thesis:

This thesis is divided into four chapters, each covering a specific subject. Chapter one is concerned in thick film and different methods for fabricating films. Chapter two introduces the pulsed laser deposition techniques and the literature review. Chapter three presents the materials and the experimental part designed for this work. In chapter four the results are presented and discussed, followed by the conclusions and recommendations

1-4 Optical coatings:

An important aspect of modern films design work is the use of computers to match the multilayer parameters to a set of optical specifications such as a desired reflectance curve.

There are several basic approaches to the design of films multilayer coatings. This includes graphical, analytical and digital design methods. Antireflection (AR) coatings: There are primary reasons for using (AR) coating:

1-Transmission decreases due to reflections between the surfaces.

2- The multiple reflections between the surfaces of the elements cause unwanted light to fall onto the image plane, reducing the contrast and definition of image.

For light normally incident on an air/glass interface with the glass having a refractive index of (1.5), the intensity of the reflected light will be 4% of the incident light. For an optical system containing ten such surfaces, the transmitted beam will lose $1/3$ of its intensity from reflection losses alone.

Surface reflection losses on an optical element can be reduced significantly by adding an antireflection (AR) coating.

1.4.1 Deposition process:

Methods of deposition processes proceed along the following sequence of steps:

1- Transition of condensed phase, which may be solid or liquid, into the gaseous state. 2- Vapor traversing the space between the evaporation source and substrate at reduced gas pressure. 3- Condensation of vapor upon arrival at the substrates.

1.4.2 Deposition parameters:

Some parameters effects on the deposition processes:

1- Nature and condition of the substrate.

2- Cleanliness of the substrate.

3- Substrate temperature.

4- Evaporation rate.

5- Effects of post annealing of film.

1.4.3 Types of films:

There are many types of films divided according to their kind or sort:

Metallic films: This is a kind of metallic films (-e.g.) Al thick film, Ag and Gold thick films.

Dielectric films like: Antireflection (AR) coatings, Broadband (AR) coating and High reflection coating.

1.4.4 Thick film Preparation Techniques:-

Generally, any film deposition follows the sequential steps: a source material is converted into the vapor form (atomic/molecular/ionic species)from the condensed phase (solid or liquid), which is transported to the substrate and then it is allowed to condense on the substrate surface to form the solid film (Kaydanov *et al*, 2000) Depending on how the atoms/molecules/ions/clusters of species are created for the condensation process, the deposition techniques are broadly classified into two categories, physical methods and chemical methods.Chemical deposition, chemical vapour deposition, and spray pyrolysis are examples of chemical method of thick film deposition. Thermal evaporation, ebeam evaporation, rf and dc sputtering and pulsed laser deposition (PLD) are examples of physical methods of thin film preparation.

The methods summarized in table (1.1) are often capable of producing films defined as films, i.e. 1μm or less and films defined as thick films, i.e. 1μm or more. However, there are certain techniques which are only capable of producing thick films and these include screen printing, glazing, electro phoretic deposition, flame spraying and painting.

1.5 Physical Vapour Processes (PVD):

PVD processes proceed along the following sequence of steps:

a) The solid material to be deposited is physically converted to vapour phase.

b) The vapour phase is transported across a region of reduced pressure from the source to the substrate.

c) The vapour condenses on the substrate to form the thick film.

The conversion from solid to vapour phase is done through physical dislodgement of surface atoms by addition of heat in evaporation deposition or by momentum transfer in sputter deposition. The category of PVD technique is the group of so called augmented energy techniques including ion, plasma or laser assisted depositions.

Table (1.1) methods for deposition of thick and thin films:

EVAPORATIVE METHODS	
Vacuum Evaporation	
Conventional vacuum evaporation	Molecular-beam epitaxy (MBE)
Electron-beam evaporation	Reactive evaporation
GLOW-DISCHARGE PROCESSES	
Sputtering	Plasma Processes
Diode sputtering	Plasma-enhanced CVD
Reactive sputtering	Plasma oxidation
Bias sputtering (ion plating)	Plasma anodization
Magnetron sputtering	Plasma polymerization
Ion beam deposition	Plasma nitridation
Ion beam sputter deposition	Plasma reduction
Reactive ion plating	Microwave ECR plasma CVD
Cluster beam deposition (CBD)	Cathodic arc deposition
GAS-PHASE CHEMICAL PROCESSES	
Chemical Vapor Deposition (CVD)	Thermal Forming Processes
CVD epitaxy	Thermal oxidation
Atmospheric-pressure CVD (APCVD)	Thermal nitridation
Low-pressure CVD (LPCVD)	Thermal polymerization
Metalorgainc CVD (MOCVD)	Ion implantation
Photo-enhanced CVD (PHCVD)	
Laser-induced CVD (PCVD)	
Electron-enhanced CVD	
LIQUID-PHASE CHEMICAL TECHNIQUES	
Electro Processes	Mechanical Techniques
Electroplating	Spary pyrolysis
Electroless plating	Spray-on techniques
Electrolytic anodization	Spin-on techniques
Chemical reduction plating	Liquid phase epitaxy
Electrophoretic deposition	
Chemical displacement plating	

1.5.1 Thermal evaporation by resistive heating:

Thermal evaporation is the most widely used technique for the preparation of thick films of metals, alloys, and also many compounds, as it is very simple and convenient. Here the only requirement is to have a vacuum environment in which sufficient amount of heat is given to the evaporants to attain the

vapour pressure necessary for the evaporation. The evaporated material is allowed to condense on a substrate kept at suitable temperature.When evaporation is made in vacuum, the evaporation temperature will be considerably lowered and the formation of the oxides and incorporation of impurities in the growing layer will be reduced. Evaporation is normally done at a pressure of 10^{-5} Torr. At this pressure a straight line path for most of the emitted vapour atoms is ensured for a substrate to source distance of nearly 10 to 50cm (look *et al*, 2002). The characteristics and quality of the deposited film will depend on the substrate temperature, rate of deposition, ambient pressure, etc. and the uniformity of the film depends on the geometry of the evaporation source and its distance from the source fig (1.1). The deposition by thermal evaporation is simple, convenient and is widely used. Excellent and detailed reviews on the know-how of the thermal evaporation have been discussed by Holland (Joseph *et al*, 2001).

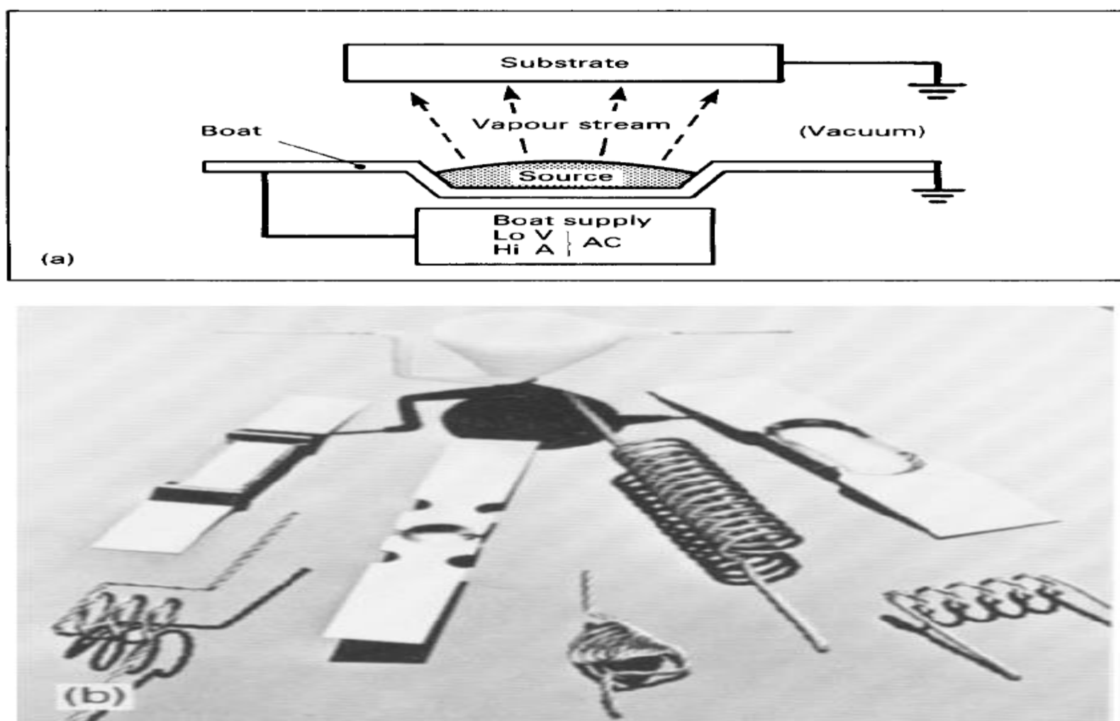

Fig (1.1) (a) Resistance –heated vacuum evaporation, (b) a selection of vacuum evaporation (Courtesy Leybold – Heraeus)

1.5.2 Electron beam evaporation:

In electron beam evaporation (EBE) a stream of electrons is accelerated through fields of typically 5–10kV and focused onto the surface of the material for evaporation. The electrons lose their energy very rapidly upon striking the surface and the material melts at the surface and evaporates. That is, the surface is directly heated by impinging electrons, in contrast to conventional heating modes. Direct heating allows the evaporation of materials from water-cooled crucibles fig (1.2). Such water-cooled crucibles are necessary for evaporating reactive and in particular reactive refractory materials to avoid almost completely the reactions with crucible walls. This allows the preparation of high purity films because crucible materials or their reaction products are practically excluded from evaporation (Anisimov*et al*, 1993).Electron beam guns can be classified into thermionic and plasma electron categories. In the former type the electrons are generated thermionically from heated refractory metal filaments, rods or disks. In the latter type, the electron beams are extracted from plasma confined in a small space.The copper electrodes for the electrical characterisation of the ZnO:Al thick films were evaporated using a 3kW electron beam source and a six-inch diameter diffusion pump backed by a rotary pump.

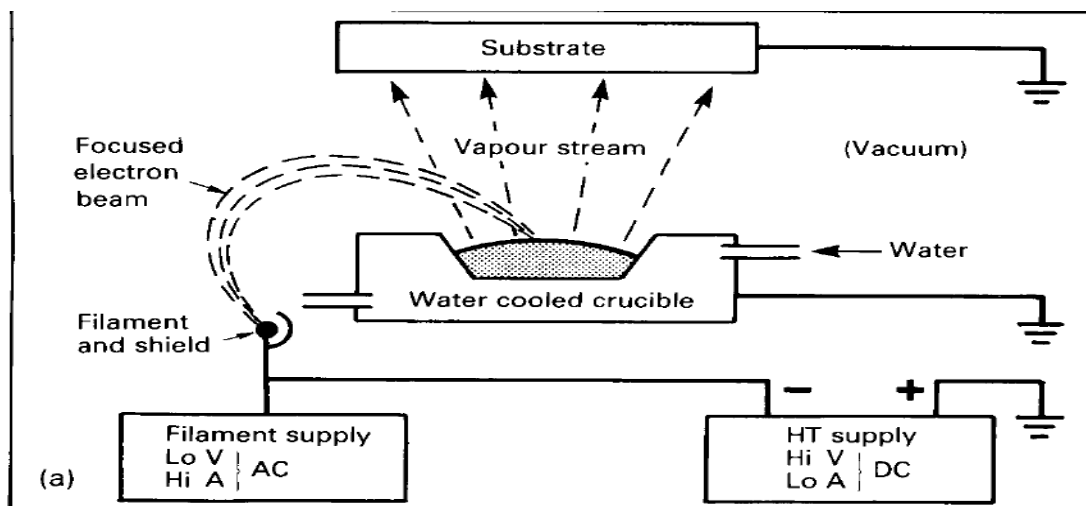

Fig (1.2) Electron beam heated vacuum evaporation (270°deflection)

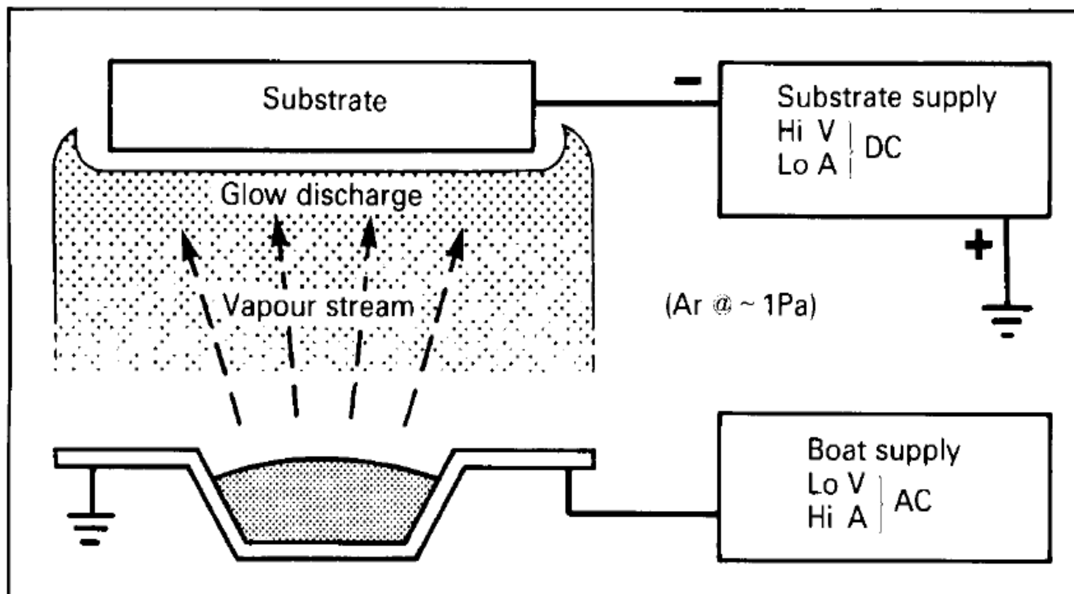

Fig (1.3) Resistance heated ion plating

1.5.3 Ion plating

A dynamic pressure of some 1Pa of a gas such as argon is maintained by a continuous gas bleed and throttled pumping (a dynamic pressure is preferred to prevent the build-up of out gassed impurities in the chamber), and the substrate is negatively biased at 1-2 kV with respect to the grounded evaporation source .

Evaporant atoms gain energy by collision with the ionised argon but contrary to the earlier belief, from which the name ion plating originated, the degree of ionisation of the vapour stream is probably no more than 0.1%; the term ion plating is therefore largely a misnomer, but is widely used. The combination of high energy (approximately 10 eV) evaporant atoms plus continuing substrate bombardment by gas ions results in excellent film adhesion and, by correct choice of deposition parameters, in a dense coating. At the same time the presence of the gas ensures a good throwing power (Fig. 1.3).The evaporant charge is melted as in vacuum evaporation and gas ionisation may be advantageously increased by a device such as a heated filament electron emitter. There are several variants of the technique and all claim high film adhesion and density but all require the substrate to be held at a high DC potential or to be connected to an RF (radiofrequency) supply.

1.5.4 Molecular Beam Epitaxy (MBE):

MBE (Gossard, 1988) is a sophisticated, finely controlled method for growing single-crystal epitaxial films in a high vacuum (10^{-11} torr). The films are formed on single-crystal substrates by slowly evaporating the elemental or molecular constituents of the film from separate Knudsen effusion source cells (deep crucibles in furnaces with cooled shrouds) onto substrates held at a temperature appropriate for chemical reaction, epitaxy, and re-evaporation of excess reactants. The furnaces produce atomic or molecular beams of relatively small diameter, which are directed at the heated substrate, usually silicon or gallium arsenide. Fast shutters are interposed between the sources and the substrates.

By controlling these shutters, one can grow superlattices with precisely controlled uniformity, lattice match, composition, dopant concentrations, thicknesses, and interfaces down to the level of atomic layers.

The most widely studied (Narayana and Gibson, 2002) materials are epitaxial layers of III-V semiconductor compounds, but silicon, metals, silicides, and insulators can also be deposited as single-crystal films by this versatile and uniquely precise method. Complex layer structures and superlattices for fabricating gallium arsenide heterojunction solid-state lasers, discrete microwave devices, optoelectronic devices, waveguides, monolithic integrated optic circuits, and totally new devices, have been created. An additional important advantage of MBE is the low temperature requirement for epitaxy, which for silicon is in the range of 400°C to 800°C, (Knodle et al, 1986) and for gallium arsenide, 500°C to 600°C. Several production systems with associated analytic equipment are now available. (Narayana and Gibson, 2002). The extremely limited product throughput, the complex operation, and the expensive equipment are, at present, the major limitations of this promising deposition technology for production applications.

1.5.5 Glow-Discharge Technologies

The electrode and gas-phase phenomena in various kinds of glow discharges (especially rf discharges) represent a rich source of processes used to deposit and etch films. Creative exploitation of these phenomena has resulted in the development of many useful processes for film deposition (as well as etching), as listed in Table (1.1)

1.5.6 Electrodeposited coatings:

Electrodeposition is a well-established process for applying metallic coatings to improve surface properties of materials used in engineering practice.

Although the principles are similar to those involved in the application of relatively thick coatings for decorative and corrosion protection purposes, engineering electrodeposition differs in several important respects and constitutes a specialised process in its own right, for the sake of completeness. Basic principles electrodeposition or electroplating involves making the component to be coated the negative electrode or cathode in a cell containing a liquid or electrolyte which must allow the passage of electric current (Fig. 1.4).

This electrolyte is usually a solution in water of a salt of the metal to be deposited, and is maintained at a controlled temperature which can be up to about 60 "C. The electrical circuit is completed by a positive electrode or anode which is generally made out of the metal to be deposited and is located a short distance away from the cathode. Under the action of a direct current applied at a low voltage, positively charged metal ions in the electrolyte move towards the cathode, where they undergo conversion to metal atoms and deposit on the cathode, i.e. the component surface.

Electrodeposition is used extensively not only to apply coatings to new components to confer the required surface properties, but also to restore the dimensions of parts that have either worn excessively in service or been so over-machined as to be outside required tolerances. Another application is production of free-standing bodies by deposition on to shaped mandrels

which are capable of subsequent removal. This process, known as electroforming, enables the shape and surface finish of the mandrel to be faithfully reproduced and in this way constitutes a simple method of fabricating parts of intricate shape in a single operation.Two techniques are available for electrodeposition of coatings for engineering purposes, following the principles outlined earlier: vat and selective plating.

The characteristics of both processes and the complementary processes of electroless or autocatalytic deposition and hard anodizing (Grainger, 1998).

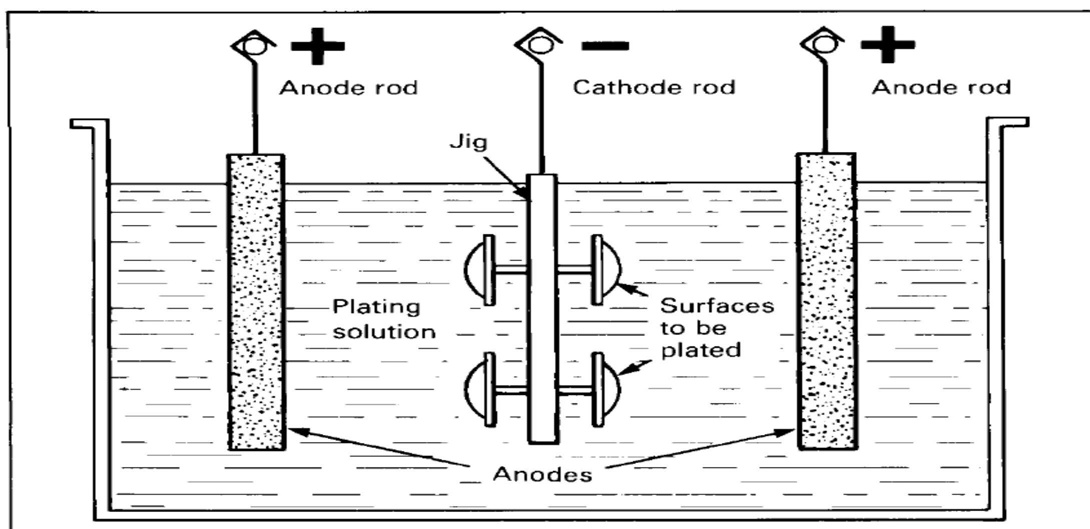

Figure (1.4) plating bath

1.5.7 Sputtering:

If a surface is bombarded with energetic particle, it is possible to cause ejection of the surface atoms, a process known as sputtering. These ejected atoms can be condensed on to a substrate to form a thick film. Such a process can be realised by forming positive ions of a heavy neutral gas such as Argon and bombarding the surface of the target material by making the surface the cathode in an electrical circuit. Such a method of obtaining a film has various advantages over normal evaporation techniques, in as much as no container contamination will be obtained. It is possible to deposit alloys without worrying about any fractionation of the materials. High melting point materials can be used as easily as low melting point ones and finally, using an R.F. technique, both metals and insulators can be deposited.

1.6 Chemical Vapor Deposition:

Chemical vapor deposition (CVD) is the process of chemically reacting a volatile compound of a material to be deposited, with other gases, to produce a nonvolatile solid that deposits atomistically on a suitably placed substrate. It differs from physical vapor deposition (PVD), which relies on material transfer from condensed-phase evaporant or sputter target sources. Because CVD processes do not require vacuum or unusual levels of electric power, they were practiced commercially prior to PVD. A century ago CVD methods were used to deposit a protective tungsten coating on carbon filaments in an attempt to extend the life of incandescent lamps. Today, high-temperature CVD processes for producing thick films and coatings have found increasing applications in such diverse technologies as the fabrication of solid-state electronic devices, the manufacture of ball bearings and cutting tools, and the production of rocket engine and nuclear reactor components. In particular, the need for high-quality epitaxial (single crystal) films in both silicon and compound-semiconductor technology, coupled with the necessity to deposit associated insulating and passivating films, has served as a powerful driver spurring the development of CVD processing methods. A schematic view of the silicon MOS transistor structure in Fig. 1.9 indicates the extent to which CVD materials monopolize the films deposited above the original wafer. With the exception of the gate oxide and metals Al-Cu, Ti/TiN, and $TiSi_2$, all films are deposited by some variant of CVD processing. They include the (epitaxial) Si substrate, polysilicon, various SiO2 films, low-temperature oxide (LTO), borophosphosilicate glass (BPSG), and W plugs. Silicon nitride is another CVD material commonly used in these devices. Among the reasons for the growing adoption of CVD methods is the ability to produce a large variety of films and coatings of metals, semiconductors, and inorganic as well as organic compounds in either a crystalline or vitreous form, possessing desirable properties. Furthermore, the ability to controllably create films of widely varying stoichiometry makes CVD unique among deposition

techniques. Other advantages include the affordable cost of the equipment and operating expenses, the suitability for both batch and semicontinuous operation, and the compatibility with other processing steps. Because of this, many variants of CVD processing have been researched and developed, including atmospheric pressure (APCVD), low-pressure (LPCVD), plasma-enhanced (PECVD), and laser-enhanced (LECVD) chemical vapor deposition. Hybrid processes combining features of both physical and chemical vapor deposition have also emerged. The fundamental sequential steps that occur in every CVD process are sketched in Fig. (1.5) and include:

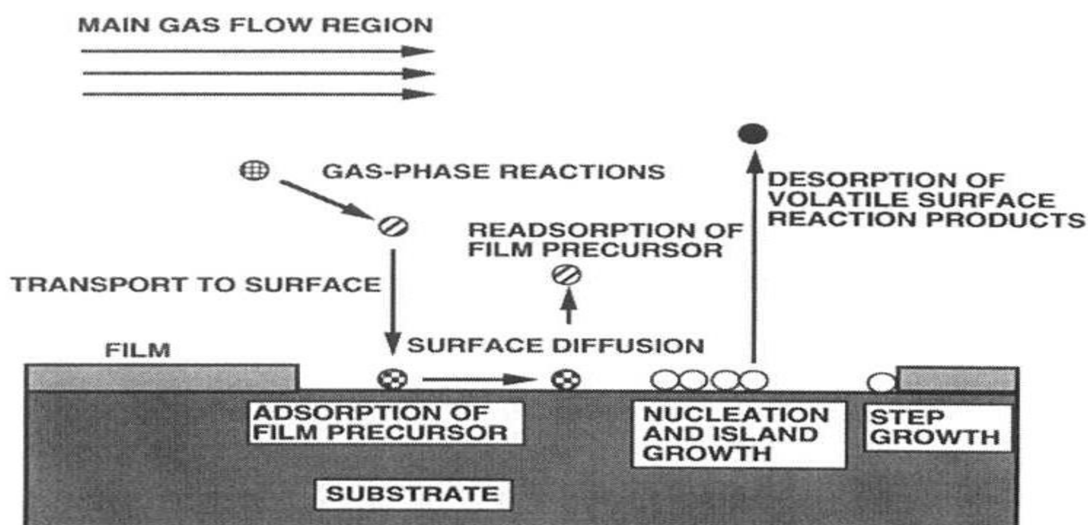

Figure (1.5) Sequence of gas transport and reaction processes contributing to CVD film growth.

1. Convective and diffusive transport of reactants from the gas inlets to the reaction zone.

2. Chemical reactions in the gas phase to produce new reactive species and by-products.

3. Transport of the initial reactants and their products to the substrate surface.

4. Adsorption (chemical and physical) and diffusion of these species on the substrate surface.

5. Heterogeneous reactions catalyzed by the surface leading to film formation.

6. Desorption of the volatile by-products of surface reactions.

7. Convective and diffusive transport of the reaction by-products away from the reaction zone.

1.6.1 Photochemical deposition:

Photochemical deposition (PCD) method involves direct irradiation of precursor bath with ultraviolet light. In PCD, the energy is absorbed by the precursor species. The absorbed photon may promote electrons to excited states (Fig. 1.6). If UV or visible radiation is used, the ground state energy is increased by single-or multi-photon absorption process at longer wavelengths. The simplicity of the method allows the deposition of thick films depending on the reaction conditions and the substrates, which are not affected by the UV light. For this reason, photochemical deposition gains attention in the field of thick film technology. The PCD technique is simple, cheap, better controllability and is capable for large area deposition (Chowdhuryand Ichimura, 2010). PCD offers several advantages, which includes low-temperature selected area deposition, freedom of substrate selection (Hugonnot, 2007), and reaction controlled by optical modulation. Problems that arise includes: low deposition rate (Podder*et al*, 2005) and it was observed that the substrate position affects the deposited film thickness and it is difficult to control this position precisely (Chowdhuryand Ichimura, 2010).

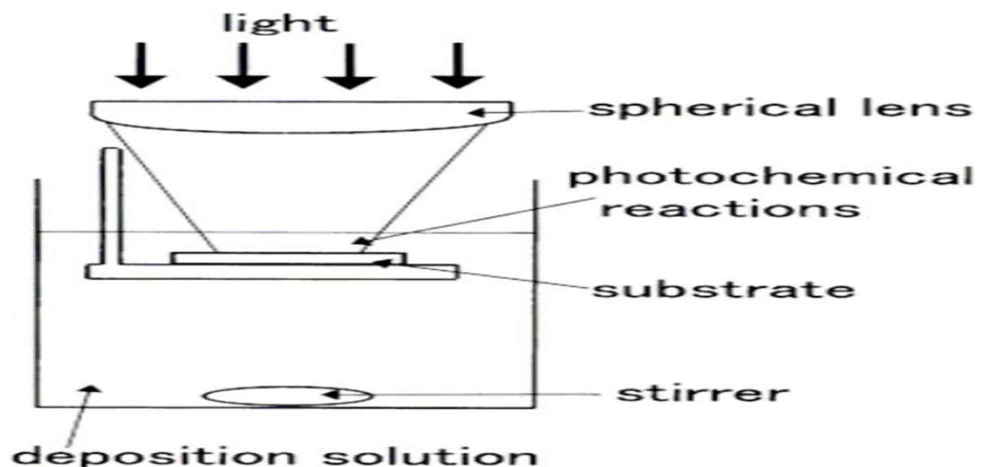

Fig1.6: Schematic diagram of the PCD method.

1.6.2. Electrochemical deposition

(a) Anodic oxidation:

A large number of metals (called valve metals) tend to form a protective oxide film of limited thickness. The anodization process involves the migration of ions of oxygen, metal, or both depending on the material, through the existing oxide film. The details of the ion transport process, however, are still a subject of some debates. Growth rate of an anodic film depends on the current density and the temperature of the electrolyte. Anodic oxidation has been extensively utilized in producing ultra-thin and thick oxide films for tunnel devices, capacitors, protective layers, etc. A serious disadvantage of anodization in aqueous solution is that, in some cases, it results in the incorporation of water and OH ions into the films producing deleterious effects on their dielectric behavior.

(b) Electrolytic deposition

Electrochemical (Electrolytic) deposition (ECD) is a technique in which a film of solid metal is deposited from a solution of ions onto an electrically conducting surface. Based on applied electric field across the electrolysis cell, ECD techniques can be classified in three different deposition categories figure (1.7): (i) at a constant potential (potentiostatic) (ii) at a constant current densities (galvanostatic) and iii) using periodic pulsed potential (two or three step voltage bias). In the case of pulsed deposition, the potential values and duration of time of each voltage step play significant role to control the properties of the deposited films.

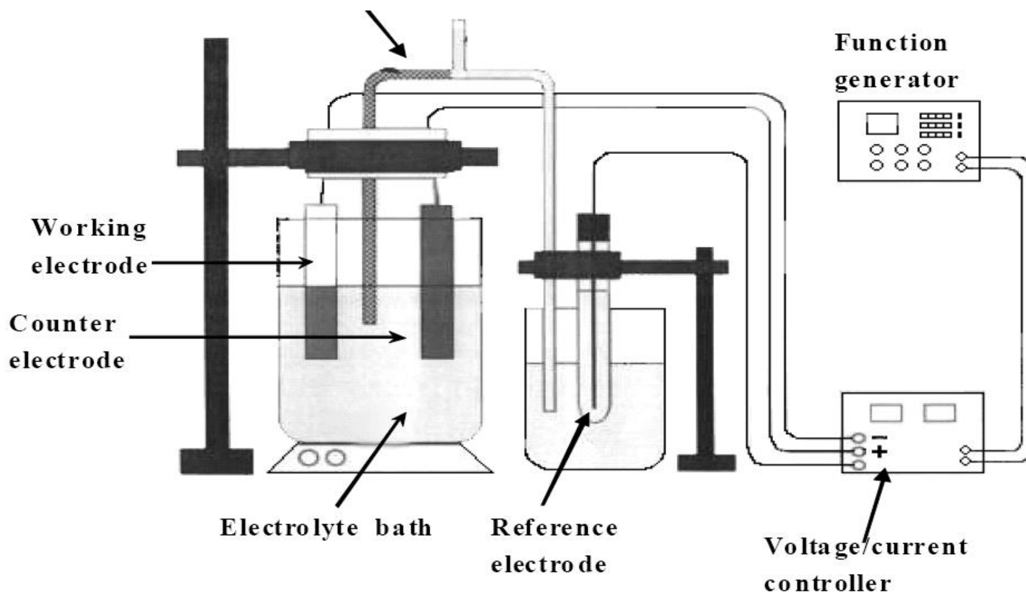

Fig. 1.7: Schematic diagram of the 3-electrodes electrochemical cell Apparatus.

1.6.3. Spray pyrolysis deposition (SPD):

The thermal decomposition of a compound to yield a deposit of the stable reside is called pyrolysis. Schematic diagram of spray pyrolysis technique is shown in figure 1.8.

Spray pyrolysis, which is the main concern of this work, involves spraying of solution usually aqueous, contained soluble salts of the constituent atoms of the desired compounds on the heated substrates.

It is already known that the process of spray deposition is one of the simplest and least expensive one of all the film deposition methods available to date. Because of this extreme simplicity one has to face a number of difficulties in controlling the process variables.

Moreover the qualities of the deposited films are relatively inferior to those films obtained in other complex methods. It is needed to improve the process of deposition and to reduce the cost of production, since for solar cell and other device technology the low cost production of semiconducting films has become a necessary precondition.

Chemical pyrolysis method can be defined as a material synthesis, in which the constituents of the vapor phase react to form a solid film at some surface

thus; the occurrence of the chemical reaction is an essential characteristic of the pyrolysis method. This method has some similarity to the chemical bath deposition method.

To understand the process, one must know which chemical reactions occur in the reactor and to what extent. Furthermore, the effects of process variables such as temperature, pressure, input concentrations and flow rates on these reactions must be understood. The nature and extent of chemical reactions can be deduced, if one knows the composition of solid and vapor phases in the pyrolysis system. The composition of the solid product can be analyzed after the deposition but that of the vapor phase must be determined in situ at the particular reaction condition, otherwise high temperature species may disappear or change on cooling to room temperature.

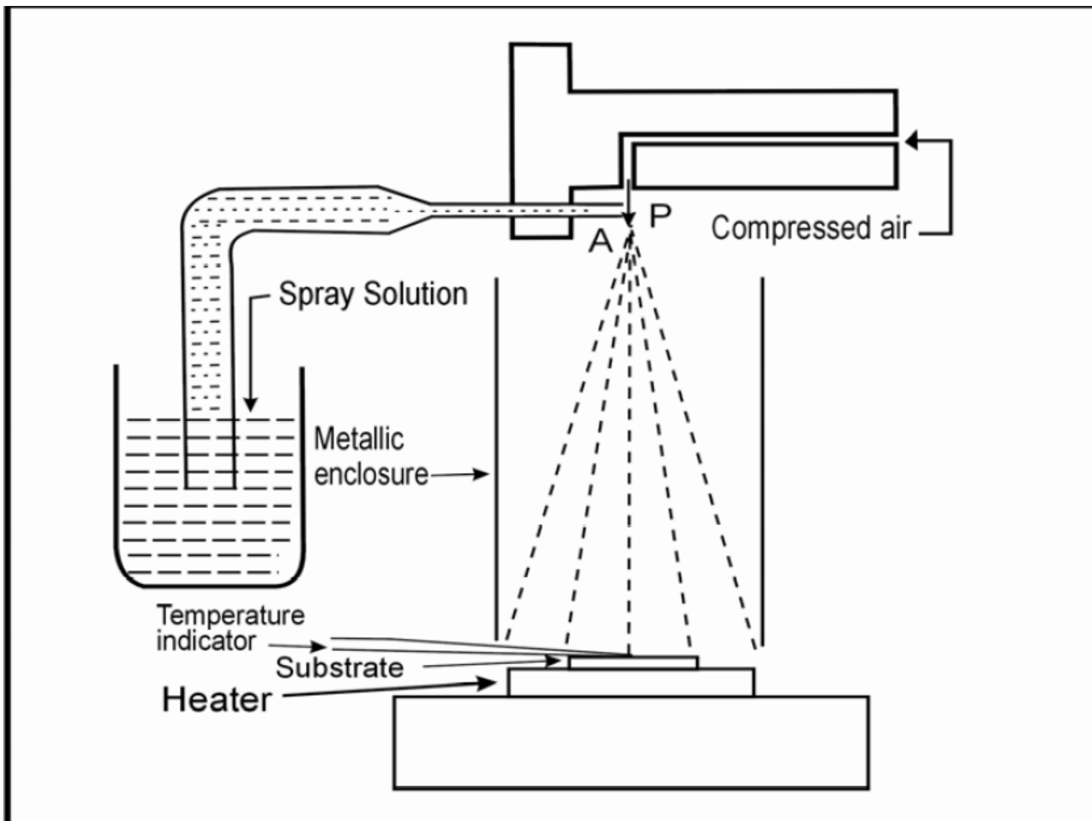

Fig.1.8: Schematic diagram of spray pyrolysis apparatus.

1.6.4 Chemical bath deposition (CBD)

CBD is an aqueous analogue of CVD. The technology is based on slow controlled precipitation of the desired compound from its ions in a reaction bath solution. A ligand or complexing agent acting as a catalyst is usually employed in a bath to control the reaction in a suitable medium as indicated by the pH of deposition solution to obtain crystal growth. Otherwise, spontaneous reaction and sedimentation of materials will be obtained. The condition for compound to be deposited from a solution bearing its ions is that its ionic product (I.P) should be greater than the solubility product (Ksp). The complexing agent of a metal in solution forms a fairly stable complex ions of the metal and provides a controlled release of free ions according to an equilibrium reaction of the form: $M(A)^{2+} = M^{2+} + A$, where M^{2+} is the metal ions and A is the complexing agent. The concentration of an ion at any temperature is given by $[M^{2+}]\ [A]\ /M\ (A)\ ^{2+} = Kd$, where Kd is the dissociation or instability constant of the complex ion. The negative ions required for the precipitation of the compound are also generated slowly by suitable complex compounds. The deposition compounds are also generated slowly by suitable complex compounds. The deposition technique can be improved by controlling the addition of another complexing agent with pH opposed to that of bath constituents. This could vary the deposition conditions at different suitable pH values. A schematic diagram of CBD technique is shown in Fig. 1.9

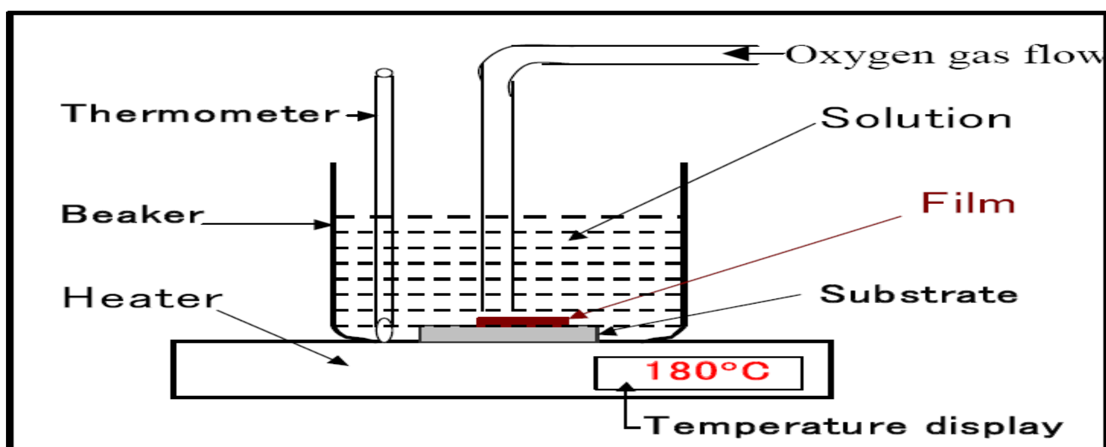

Figure (1.9): Schematic diagram of the CBD method.

The advantages of CBD technique are low cost, large area deposition and relatively low deposition temperature (usually less than $80C^{O}$). Additionally, chemical bath deposition is becoming an alternative deposition technique for thick films of compound materials like chalcogenides, oxides and halides. A major success can be found in the recent period with the deposition of semiconducting cadmium sulfide or zinc sulfide buffer or window layers in efficient copper indium diselenide or cadmium telluride film solar cells.

However, CBD has some drawbacks: (1) in the classical beaker configuration, the material yield during film formation is very low, about a few percent, leading to an unnecessary waste production and increased treatment costs. The reason is that the volume to surface ratio is very high and that only a small part of the solution is contributing to the film formation, the remaining one leading to the formation of colloids in the bulk of the solutions. (2) The formation of particles leads not only to the generation of significant amount of waste but also to the creation of defects in the deposited film.

1.6.5 Spin Coating:

The spin coating method proceeded to overcome some limitations in the size of substrates. Nowadays it is even possible to deposit high-quality; antireflective and conductive thick films on the top of screens. By this development spin coating is again a method with a high potential in industrial fabrication processes. From a phenomenological point of view, Bomside et al. divided spin coating into four steps: deposition, spin-up, spin-off and evaporation, even evaporation will occur at all steps (Burnside et al, 1989). This is visualized in Figure (1.11)

There are two forces balancing the quality of the resulting coating: the centrifugal force, which drives the viscous sol radially outwards, and the viscous force (friction), which acts radially inwards (Higgins, 1986). During spin-up, centrifugal forces overwhelm the force of gravity, and the rapid thinning squelches all inertial forces other than centrifugal force. The

thickness of an initially uniform film can be calculated by the empirical equation.

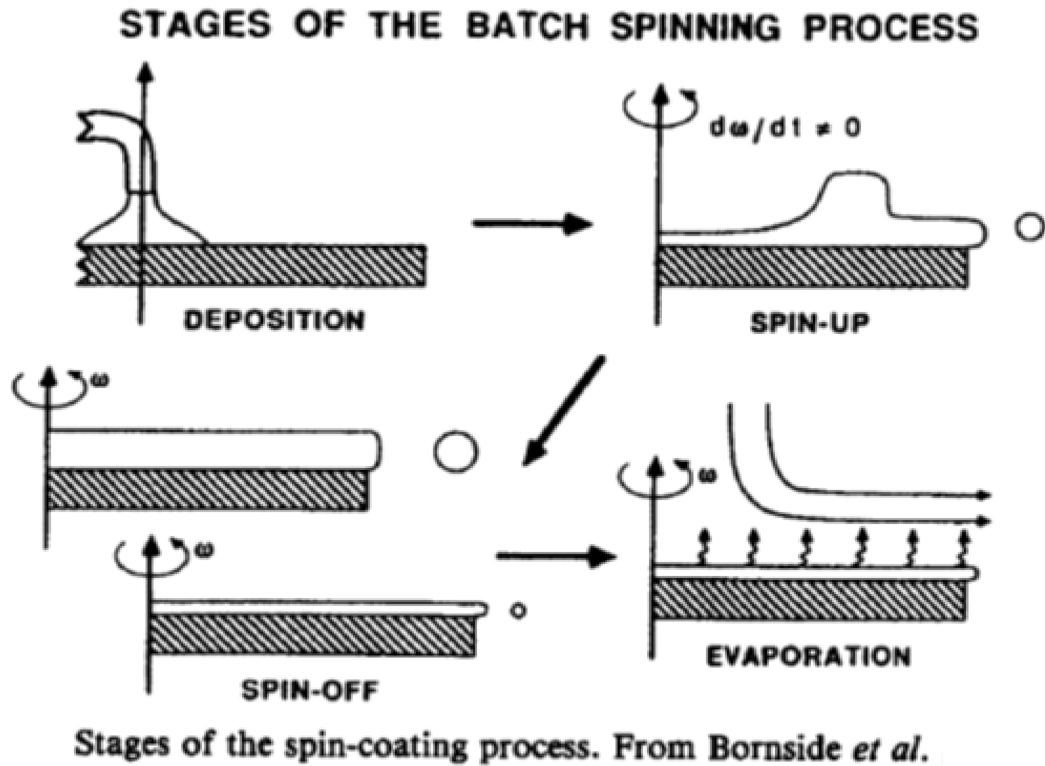

Stages of the spin-coating process. From Bornside *et al.*

Figure 1.10 stages of spin –coating process

$$h\ (t) = h_0 / (1 + 4\ \rho\omega^2\ h_0^2 / 3\ \eta)^{1/2}\ h_0$$

Where$h_0$the initial thickness, t is time andω is the angular velocity, $\rho$and η assumed constant. It is evident that evaporation takes place during the three staring stages. Therefore, Meyerhofer developed a model which separates spin-off from evaporation stages .The final thickness and the total elapsed time to achieve this thickness are:

$$h_{final} = (1 - \rho_{\mathring{A}} / \rho_A)\ (3\ \eta\ m / 2\ \rho_{\mathring{A}}\ \omega^2)^{1/3}$$

Where PA is the mass of volatile solvent per unit volume, PA is its initial value and e is the evaporation rate that depends on the mass transfer

coefficient. The equations are based on the assumption that all liquids used behave in a Newtonian way.

Therefore, in reality, it is often observed that the film inside is thicker than on the outside of the substrate. This problem could be technically solved by a spinning coating apparatus with employed dispensing systems that provide the liquid with a radially moving arm.

The major advantages of the CVD techniques are as follows:

(1) In general, low-vacuum facilities are required and, thus, a relatively simples etup and fast recycling are possible; (2) high (-1 ~m/min) deposition rates are possible; (3) it is possible to deposit compounds with easily controlled stoichiometry; (4) it is relatively easy to dope the deposits with controlled amounts of impurities; (5) it is possible to deposit multicomponent alloys; (6) refractory materials can be deposited at relatively lower temperatures as compared to vacuum evaporation; (7) epitaxial layers of high perfection and low impurity content can be easily grown; (8) objects of complex shapes and geometries can be coated; and (9) *in situ* chemical vapor etching of the substrates prior to deposition is possible. However, the technique also has some drawbacks: (1) The generally complex thermodynamics and reaction kinetics are poorly understood; (2) higher substrate temperatures are required than those in the corresponding PVD techniques; (3) the reactive gases used for deposition and the volatile reaction products formed are, in most cases, highly toxic, explosive, or corrosive; (4) the corrosive vapors may attack the substrate, the deposited film, and the materials of the deposition setup; (5) the volatile products generated during the deposition process may lead to incorporation of impurities in the film; (6) the high substrate temperatures may lead to diffusion, alloying, or chemical reaction on the substrate surface, thus restricting the choice of the substrate; (7) high substrate temperatures may also give rise to segregation effects

when metastable multi component materials are being deposited; (8) it is difficult to control the uniformity of the deposit; and (9) masking of the substrate is generally difficult.

Chapter Two

Pulsed laser deposition, Basic concepts

2-1 Introduction:

Already in the 1960s, just a few years after the first commercial Ruby laser became available, the first laser deposition experiments were performed (Vilanova, 2006). However, it was not until almost 20 years later that scientists really became interested in pulsed laser deposition (PLD). In the late 1980s, reliable short pulsed ultraviolet (UV) lasers became commercially available and PLD proved to be efficient in growing high-quality high-temperature superconductor (HTS) films (Dijkkamp *et al*, 1987). Since then, the PLD technique has experienced explosive growth and researchers have studied the deposition of HTS films and other multicomponent oxide films.

The advantages of PLD are the simplicity and versatility of the experiment. With the use of a high-power pulsed UV-laser and a vacuum chamber, a variety of stoichiometric oxide films can be grown in a reactive oxygen background gas without the need for further processing.

Compared with other vacuum deposition techniques such as, e.g., sputtering and chemical vapour deposition, the PLD technique is operationally simpler, faster and more versatile. Some disadvantages of the PLD technique are that problems with particulates can occur, that large area covering is difficult and that the upper deposition rate limit is unknown.

The PLD process, shown schematically in Figure 2-1, can be divided into (at least) three steps:

1. Laser - target interaction
2. Plume expansion
3. Film deposition

Here "plume" means the ensemble of particles ejected from the target following a laser pulse.

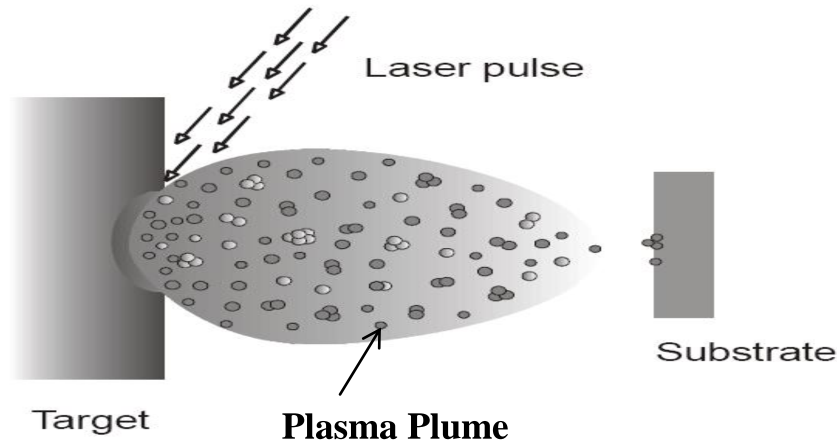

Figure 2-1 Schematic presentation of the pulsed laser deposition process.

Table 2-1 Typical PLD parameters.

Parameter	Typical values
Materials examples	Tio_2 ,AL_2O_3, ZnO
Laser wavelength	1064 nm
Laser pulse width	6 – 50 ns
Laser repetition rate	20,30,40 Hz
Laser fluence	500-700mJ
Substrate examples	glass

The time scales involved in the three process steps are very different. Typically, the laser-target interactions occur within nanoseconds, whereas the plume expansion in a background gas takes place within microseconds. Depending on the experimental conditions, the film growth process following a laser pulse can in principle continue to develop until the next laser pulse occurs milliseconds later.

In the following sections each process step will be described separately.

2.2 Laser – target interaction

When a pulsed high-power laser interacts with a target material, the process is often referred to as “laser ablation”. Here ”ablation” covers a variety of processes that occur during the interaction such as absorption, surface melting and vaporisation, ejection of particles, and plasma formation and expansion. If the laser power density is high enough ($\sim 10^9$W/cm^2), this interaction may resemble an explosion (Ferrante1 *et al*, 2001).

2.2.1 The ablation process

The ablation process is complex and very material dependent as well as highly dependent on laser parameters such as wavelength, pulse length and power density.

A general description is complex and it is more convenient to describe a typical ablation scenario as a function of laser pulse time. A schematic presentation of the ablation process for a 30 ns long high-power laser pulse is shown in figure (2-2).

The laser - target interaction can be divided into several stages.

1- As the laser pulse hits the target, photons are immediately absorbed in a surface layer by electronic processes. The absorption depth depends on the optical penetration depth of the material, which can be in the order of a few nanometers at the vaporisation temperature (Kaczmarek, 1997). The absorbed energy is transported into the material either by electrons (in metals) or by phonons (in non-metals). The energy relaxation time in metals is very fast, $\sim 10^{-14}$ s, whereas it is much slower, $\geq 10^{-12}$ s, in non-metals (Mohammed, 2015). However, compared with the laser pulse duration, the absorbed energy is rapidly converted into heat.

2- Thereby the surface is heated beyond the melting temperature of the target material (which is, e.g., $\sim 1400 C^{\circ}$for YBCO (Tonooka*et al*, 2009) and the surface melts.

3- The melted surface starts to vaporise. The high temperatures generated at the target surface (up to several thousand degrees celcius) cause emission of many species from the target – ions, electrons, neutral atoms and molecules (Sharma AK, 2001). Further irradiation by the laser light ionises the evaporated material by single-photon and nonresonant multiphoton processes and an expanding plasma (i.e. an electrified gas of electrons, ions and neutrals that maintains quasi charge neutrality) is formed above the target surface.

4- Once formed, the plasma absorbs the laser radiation by inelastic free electron scattering also called inverse-Bremsstrahlung, which results in

further heating of the plasma. The absorption of the radiation by the plasma is a function of the plasma density, the plasma temperature and the laser

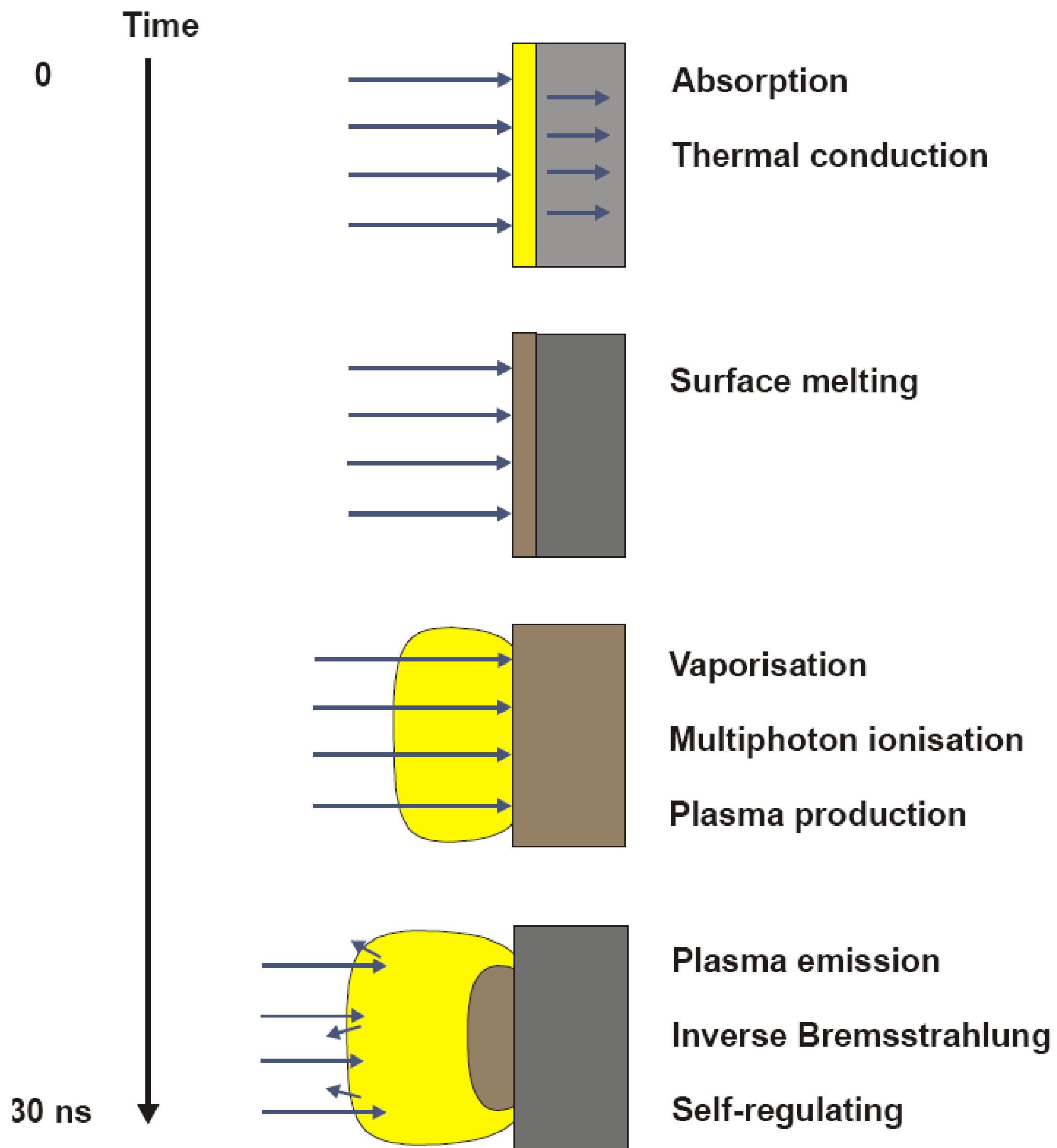

Figure 2-2 Schematic presentation of the laser target interactions during a high-power laser pulse.

Frequency (Cheung and Horwitz, 2013). For sufficiently long laser pulses (and/or high laser power densities), the electron density above the target surface can become so dense that the plasma becomes opaque and no laser-target interaction is possible.

However, as the plasma expands, it becomes less dense and the laser may again interact with the target surface and in this way a self-regulating process

is established. The hot plasma also emits light, partly by Bremsstrahlung at the early stage of plume expansion, but also by emission from atoms, ions and molecules, which is seen as a luminous region just above the target surface.

As indicated above, a variety of different interactions are involved in a laser ablation process. Not only the interaction between the laser and the target has to be considered, but also laser-vapour, vapour-target, laser-plasma and plasma target interactions play a role. Several theoretical models and model calculations that try to describe this ablation process exist – see, e.g., Phipps and Dreyfus (Coutal *et al,* 1996). However, the existing models usually deal with parts of the interaction only and/or with specific materials.

2.2.2 Practical considerations

2.2.2.1 Laser power density

A characteristic feature of laser ablation is the existence of a laser ablation threshold, i.e. for all materials there exists a threshold laser power density below which ablation, i.e. measurable material removal, is not possible. This threshold power density may be lower for non-metals than for metals, which is due to the poor energy transport in non-metals giving rise to higher surface temperatures during the ablation process. Typical threshold laser power densities are in the order of $10^7 - 10^8$ W/cm^2. Above the ablation threshold, the ablation rate increases nonlinearly with increasing laser power density.

For optimum laser deposition, the laser power density should neither be too low nor too high. If the power density is too close to the ablation threshold, the material removal is low and non-stoichiometric transfer of target material is possible for multicomponent targets (Smith, 1995). If the power density is too high, however, a large amount of the laser energy is ”wasted” in plume heating and ionization instead of being used for heating the target surface. See the final ablation stage above.

2.2.2.2 Laser wavelength

The laser wavelengths used for laser deposition are typically between 200 and 400nm. This is mainly because most materials used for deposition exhibit strong absorption in this spectral region. Absorption coefficients tend to increase with decreasing wavelength in this region and the optical penetration depths of the target materials are correspondingly reduced.

Wavelengths in the visible or infrared part of the photonic spectrum are problematic as they greatly enhance the inverse-Bremsstrahlung. Below 200 nm, strong absorption of molecular oxygen can make the beam control setting in this spectral region difficult if film deposition is performed in an oxygen background gas. Furthermore, the optics is more difficult at shorter UV-wavelengths as special and expensive components are needed at these wavelengths (Hansen, 1997).

2.2.2.3 Target surface modifications

The laser ablation process alters the target surface topology and can change the chemical composition of the target surface as well. After several laser pulses, an initially flat target surface will typically convert to a rough surface morphology exhibiting small structures like cones, ripples or ridges. In order to obtain steady state laser ablation, preconditioning (preablation) of the target is necessary.

In a laser deposition experiment, the laser light is usually incident at 30°-$45^{\circ}$to the target surface. Thereby, the laser-plasma interaction is reduced and any laser-substrate interaction avoided. A drawback of this geometry is that the laser-may etch a trench into the target so that the plume tilts back towards the laser-beam (Greer *et al*, 1997).

2.3 Plume expansion:

Provided that the laser power density on the target is above the threshold for plasma creation, expanding plasma is formed above the target surface during ablation. This plasma formation threshold is typically higher than the power density threshold for laser ablation.

In PLD the plasma plume typically expands in a background atmosphere. However, in order to describe plume expansion in an atmosphere, some knowledge of plume expansion in vacuum is necessary.

2.3.1 In vacuum

During irradiation of a target, in vacuum, with a high-power laser pulse of around 30ns duration, a bubble of hot plasma is formed ≤ approximately 50μm from the target surface. As soon as the plasma is created, the plasma particles-interact and tend to “lose memory” of the primary ablation mechanisms. Thus, the plasma expansion can be described by certain characteristics, i.e. secondary ablation mechanisms (Lowndes *et al*, 1998) which to some extent are independent of the primary mechanisms. The expansion characteristics are described-below.

Knudsen layer formation

Initially, the density of ablated particles may be high, i.e. in the range of 10^{18} $–10^{20}cm^2$ and, in addition, the ablated particles close to the target surface have an anisotropic velocity distribution (all velocity vectors point away from the target surface). However, this anisotropic velocity distribution is transformed into an isotropic one by collisions among the ablated particles. This happens within a few mean-free paths from the surface, a region known as the Knudsen layer (Allmen, and Blatter, 1998). It is mainly within this Knudsen layer that laser energy is absorbed in the plasma (Lowndes *et al*, 1998).

High temperatures

Estimated initial plasma temperatures for PLD materials are in the range from 5000 K to 15000 K.

Forward-directed plume

After the laser pulse has terminated, inter-particle collisions can lead to a highly anisotropic expansion of the plasma plume, which will typically be peaked in the forward direction, i.e. normal to the target surface. In a model by Singh and Narayan (see, e.g., (Singh and Narayan, 1998), where they

model the plasma as a fluid - using the equations of gas dynamics followed by an adiabatic expansion - they show that the acceleration of the plasma varies inversely with its dimensions. Consequently, the highest velocities are obtained in the direction perpendicular to the target surface, where the initial plasma dimension is only tens of micrometers.

Similar results emerge from the treatment by Anisimov et al. (Anisimov *et al*, 1993) and (Geohegan and David, 2009).

High expansion velocities

At PLD conditions in vacuum, typical velocities of the particles in the leading edge of the plume are in the range of $1\text{-}2{\cdot}10^4$ m/s. For an ablated atom or ion with a mass of 100amu, this corresponds to a kinetic energy of ~50-200 eV. In general, ion velocities are higher than those of neutral species.

Complex plume

The plume composition is complex, especially for multicomponent targets, and may change during expansion. In the first few millimeters of the plume expansion, emission from atoms and ions, multiple charged ions and possible molecules can typically be observed together with Bremsstrahlung emission in the plasma. After the first millimeters of expansion, Bremsstrahlung emission and emission from multiple charged ions are no longer observed. In absorption spectroscopy ground-state atoms and ions have been observed in the plume after the initial expansion.

Typically, non-emitting particles (i.e. ground-state atoms and ions) have Broader velocity distributions than emitting particles at PLD conditions. The existence of fast neutrals in the plume can be explained by recombination of fast ions with electrons and/or resonant charge exchange between fast ions and neutrals.

Electrons are more mobile than ions and neutrals, but are restricted from escaping the dense plasma by the strong space-charge field they build up by collectively moving away from the ions (Geohegan and David, 2009).

2.3.2 In a background atmosphere:

In the presence of a background atmosphere the plume particles will, in addition to colliding with themselves, collide with the gas particles, which can lead to scattering, attenuation and thermalisation of the plume. Thereby, important film growth parameters such as the spatial distribution, the deposition rate, and the kinetic energy distribution of the depositing species are altered. In addition, the plume particles can react chemically with the gas particles. As in the case of plume expansion in vacuum, plume expansion in a background atmosphere can be described by certain characteristics (Lowndes *et al*, 1996). However, depending on the background gas pressure and/or the difference in mass between the ablated species and the background gas particles, these characteristics will vary in strength or will not occur at all. The characteristics for plume expansion in a background atmosphere are the followings:

Increased fluorescence

Due to collisions on the expansion front of the plume and subsequent inter plume collisions, an increase in fluorescence from all species compared with the expansion in vacuum can usually be observed.

Sharpening of the plume boundary

As the plume propagates into the background atmosphere it seems to push the background gas ahead and a sharp plume boundary may be created at the plume front. This plume sharpening indicates the formation of a shock front.

A slowing of the plume

After a few microseconds of expansion and at sufficiently high background gas pressure, the plume slows down relative to the propagation in vacuum and eventually coalesces with slower moving material.

Plume splitting

At intermediate background gas pressures (in the millitorr range) the plume tends to split up into a fast (collisionless) and a slow (scattered) component.

Changes in angular distribution

Collision-induced broadening of the plume may appear when the mean free path of ablated species, Λ, is less than the target-substrate distance, h. For target substrate distances in the centimeter range, experiments indicate that changes in angular distribution become significant when h/Λ is around 10.

Plume thermalisation

With typical PLD target-substrate distances around a few centimeters and at sufficiently high background gas pressures, i.e. ≥ approximately 100 mtorr, the plume particles can thermalise completely (Lowndes *et al*, 1998).

Chemical reactions

Reactive scattering can, e.g., result in the formation of molecules or clusters in the plume.

2.4 Film deposition

The film growth process, i.e. deposition of ejected target material onto a growing film, can be described by the following sequence: Firstly, the arriving particles must adsorb on the surface1, after which they may diffuse some distance before they react with each other and the surface and start to nucleate. The way the particles nucleate may determine the structure or morphology of the growing film. Under certain circumstances (e.g. high substrate temperature) diffusional interactions within the film and with the substrate, beneath the growing film surface, may subsequently modify film composition and film properties.

In PLD, film growth is highly influenced by the process parameters.

In the following, some typical film growth modes will briefly be described and subsequently some PLD growth characteristics will be discussed. Finally, different film structures will be mentioned. The following subsections are mainly based on the references (Marozau *et al*, 2011).

2.4.1 Typical growth modes

In general, three conventional modes of nucleation and growth are considered:

1. Three-dimensional island growth called Volmer-Weber growth.

2. Two-dimensional full-monolayer growth called Frank - van der Merwe growth.

3. Two-dimensional growth of full monolayers followed by nucleation and growth of three-dimensional islands called Stranski-Krastinov growth.

The selection of one of these growth modes by a substrate-film system depends on the thermodynamics that relates the surface energies (film and substrate) to the film-substrate interface energy.

Volmer-Weber nucleation and growth

Figure 2-3 illustrates the different processes involved in the nucleation of clusters on a surface by vapour deposition of atoms. The balance between growth and dissolution processes for a given cluster will be governed by the total free energy of a cluster, ΔG, and relative to assemble of individual atoms. In general, for three-dimensional cluster growth, ΔG will have a maximum, ΔG^*, at a critical cluster size, which means that cluster sizes above this critical size are stable.

To a first approximation the nucleation rate is given as the product between (the arrival rates of atoms at critical-size nucleus) and (the concentration of critical nuclei). The former is proportional to the concentration of mobile atoms on the surface and to the surface diffusion coefficient. The latter is a strongly decreasing function of ΔG^*. As a rule, an increased cluster nucleation rate is desired in Volmer-Weber growth. In practice, this can be achieved by increasing the deposition rate (or decreasing the substrate temperature2) which gives a decrease in ΔG^*. Another possibility is to decrease the net surface/interface free energy (and thereby decrease ΔG^*), e.g. by creating interactions with a background gas.

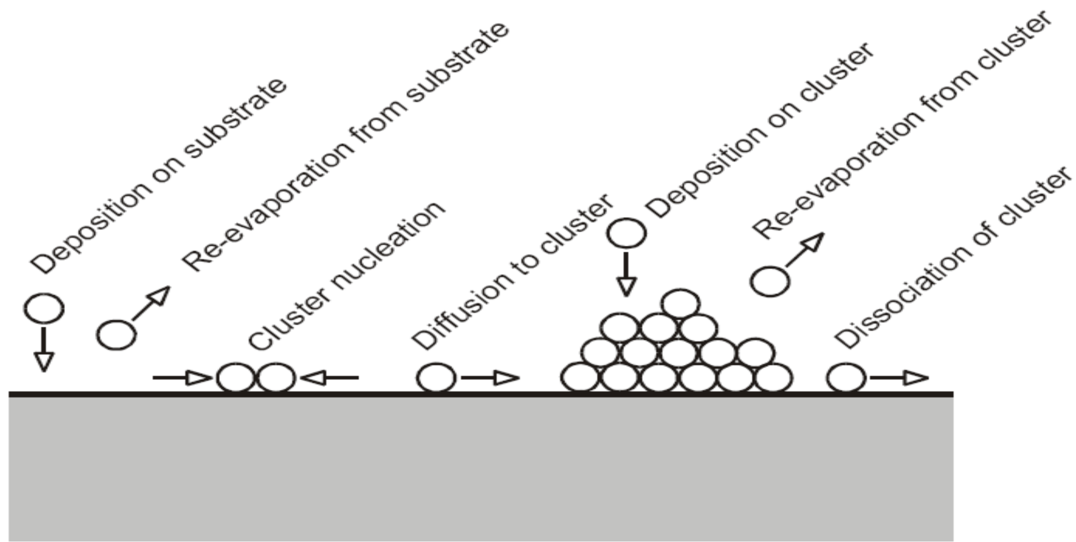

Fig (2-3) Frank - van der Merwe nucleation and growth

Full monolayer growth involves nucleation and growth of islands that are only one monolayer thick and grow to essential complete coalescence before significant clusters are developed on the next film layer. In this case there is no free energy barrier for nucleation (i.e. no ΔG^*). If the surface material is different from the film material, full monolayer nucleation will be promoted by strong film-substrate bonding, low film surface energy and high substrate surface energy.

Full monolayer growth may change to three-dimensional island growth after 1-5 monolayers due to a change in the energy situation with successive monolayers.

This could e.g. be an increase in stress with increasing layer thickness due to mismatched lattice spacing's.

2.4.2 Characteristics of PLD growth

Qualitatively, a possible event scheme for nucleation during a PLD cycle is as follows (assuming a high instantaneous vapour flux, (Horwitz and Sprague, 2009): A vapour pulse causes the nucleation of a high density of small subcritical clusters (i.e. the clusters are much smaller than those that would be stable for a much lower instantaneous deposition rate). The subcritical clusters are expected to be unstable once the vapour pulse has decayed after approximately 1ms.

• The subcritical clusters will tend to dissociate into mobile species. • The mobile species will nucleate new clusters on a different scale during the time of no vapour arrival-typically 100ms.

• The next pulse will initiate the same sequence with some of the mobile atoms being added to the clusters formed following the first pulse.

If the atomic process time constants, Tap's, (i.e. the time constants for all the relevant diffusion, accumulation and dissociation phenomena) are much smaller than the period of the PLD cycle, Tcycle, the pulsed vapour arrival should not affect the final film result significantly. However, if Tcycle ≈ Tap, then the film formation pattern may be altered. If the PLD is performed in a background gas e.g. oxygen, the background gas may promote stoichiometric film formation as oxide deposition. Furthermore, as mentioned above, the presence of a background gas may change film and substrate surface energies, possibly even the film growth mode. However, it is difficult to predict specific effects since they will depend on sticking coefficients, reaction rates and other factors. According to Metev, the two main thermodynamic parameters that determine film growth in PLD are the substrate temperature, Ts, and the supersaturation, m, where the latter is proportional to Ts and ln(Ra/Re). Here Rais the actual deposition rate and Re is the equilibrium deposition rate at temperature Ts. An increase in substrate temperature will, e.g., increase the rate of surface diffusion of the adsorbed particles. For typical PLD conditions, the actual deposition rate can be varied in a controlled manner by the experimental conditions over a wide range from Ra $\sim 10^{14} - 10^{22} \mathrm{cm}^{-2}\mathrm{s}^{-1}$. Other important process parameters that may influence the film growth are the flux, the energy, the ionisation degree and the type of condensing particles.

Surely, the physochemical properties of the substrate are essential for film growth as well. E.g. YBCO films are typically grown on non-interacting, nearly lattice-matched crystalline substrates such as <100> MgO, $SrTiO_3$ and $LaAlO_3$ (Horwitz and Sprague, 2009).

2.4.3 Structure development

The development of the deposited film structure changes with the amount of thermal motion that takes place during film growth and also with the amount of additional energy that is delivered to the growing surface as indicated above. According to Smith (Smith, 1995) important parameters are the ratio of the substrate temperature, Ts, to the melting point of the film, Tm (in Kelvin), and the distance between adsorption sites, *a*, compared with the diffusion length, ΛD, of the adsorbed particles. Four main structural forms (zones) have been identified in vapor- phase processes.

Zone 1

When Ts/Tmis so low that surface diffusion is negligible ($\Lambda D < a$), the film may consist of columns typically tens of nanometers in diameter separated by voids a few nanometers across. The columns have poor crystallinity or are amorphous. In thicker films this structure may be superimposed with an array of cones with wider voids between them, which terminate in domes at the surface.

Zone 2

When Ts/Tm> 0.3 approximately so that surface diffusion becomes significant, the film may consist of columns that have tight grain boundaries between them. The crystalline columns have fewer defects than in zone 1and zone T and are often facetted at the surface. The zone 2structure can also occur in amorphous films, where the plane boundaries are planes of reduced bonding rather than planes of crystallographic discontinuity.

Zone 3

When Ts/Tm > 0.5 approximately so that considerable bulk annealing of the film is taking place during deposition, the film may, under certain circumstances, consist of more isotropic or equiaxed crystallite shapes. For Ts/Tm > 0.5, zone 2 and zone 3structures are often associated with smooth film surfaces. However, the grain boundaries can develop grooves. In general, the “optimum” substrate temperature for high-quality thin-film

growth is when 0.3 < Ts/Tm < 0.5 approximately, where there is sufficient surface diffusion to allow surface atoms to minimise their surface energy (reach thermodynamically stable sites) (Hubler, 1994)

2.4.4 Particulate formation

One major problem in PLD is the presence of particulates on the film surface. Particulates can, e.g., originate from liquid droplets that are expelled from the target during irradiation, from ejected protruding surface features that are mechanically removed from the target by laser-induced thermal and mechanical shock, or from cluster condensation from vapour species due to supersaturation (Szela et al, 2013). The first particulate type is typically observed at laser power densities above 10^7 W/cm^2, and the last type is most likely observed in the presence of a background gas during film deposition. Typical particulate sizes are in the micron and submicron ranges, however, for particulates formed from the vapour state the size tends to be in the nanometer range. In general, the density and the size of particulates on the deposited film surface tend to increase with increasing laser fluence and with increasing laser wavelength. However, other process parameters such as laser spot size and ambient gas pressure are important as well. (Sezer, 2010).

2-4-5 Advantages and disadvantages of PLD

Pulsed laser deposition is receiving much interest because of the unique interesting features among these features.

1. Complex oxide compositions with high melting points can be easily deposited provided the target materials absorb the laser energy.
2. PLD allows the growth of films under a highly reactive gas ambient over a wide range of pressure.
3. The target composition is transferred instantaneously leading to a stoichiometry deposition and as such the turnaround time is much faster for initial optimization of the growth conditions with this technique. This is a major advantage whenever there is a need for experimenting with different target compositions.

4. The PLD technique is found to be very effective and well suited for developing epitaxial films, and allows fabrication of multilayer's, hetero-structures and super lattices on lattice matched substrates.

5. In the PLD process during film growth suitable kinetic energy in the range 10–100 eV and photochemical excitation exist in comparison to other deposition techniques, and is found to be beneficial for improving the quality of the deposited film.

Up scaling for industrial production and deposition on large area substrates is still a major concern. The technique is ideally suitable for deposition on small substrates, and yields high quality films useful for research and allows fabrication of discrete devices.

However, there are some disadvantages that causes detrimental effects on deposited films; (Seizer, 2010).

1- Laser droplets; subsurface boiling, recoil ejection and exfoliation.

2- Inhomogeneous flux and angular energy distributions within the plume.

3- Sometimes there are many macroscopic particulates that come from plasma plume on the film surface.

4- Crystallographic defects on the film caused by bombardment of high energetic ablation of particles.

5- Mechanisms of PLD are difficult to explain and dependence on parameters is very difficult to control.

2.5 The Optical Properties

Optical properties of films include (Sesham, 2012) index of refraction, reflectance, and absorptance which are a function of the wavelength, extinction (absorption) coefficient, optical scattering, and color. Optical absorption is an important effect for films used in high power laser technology where high or non-uniform absorption can give local failure of the coating color. Optical absorption is an important effect for films used in high power laser technology where high or non-uniform absorption can give local failure of the coating.

Optical Reflectance and Emittance:

Reflecting coatings reflect the incident radiation and what is not reflected is absorbed or transmitted. If there is spectral reflectance the surface is a mirror. If there is scattering, the surface is a diffuse reflector like a white paint. For deposited metal films, the difference is generally the surface finish a smooth surface is necessary to make a good mirror. Figure (2-4) shows the optical spectrum of solar radiation, the solar spectrum after it has passed through two standard air masses and the optical sensitivity of the human eye which ranges from 4500 nm to 7000 nm. (Khoshhesab *et al*, 2012) the diagram also shows the radiant energy from black-body surfaces at various temperatures. Most of the incident solar radiation is out of the range of human vision (61%) either in the long wavelength (>7000 nm) infrared region (53%) or the short wavelength (<4500 nm) ultraviolet region (8%). Artificial lights such as tungsten filament lamps emit a higher percentage of their radiation in the infrared than in the solar spectrum. The emission from halogen lamps and the new sulfur lamps, more nearly approach the solar spectrum. Figure 10-5 shows the reflectivity of metal surfaces. Aluminum (Al) and silver (Ag) are the most common reflector materials and gold (Au) is a good reflector in the infrared. A highly-reflective white paint is shown for comparison. A good metallic electrical conductor will completely reflect all of the incident radiation if it is about 1000 nm thick.

A thick and thinner film will let some of the radiation pass through to the underlying material. Metallization of a glass mirror can be done on the “back surface” or the “front surface”. If the metallization is on the back surface, there is some distortion and some radiation is lost in passing through the glass to and from the metallization, therefore a front surface mirror is a more efficient reflector. If the metallization is on the back surface it can be protected by a protective coating and silver is often used. However if the metallization is on the front surface, without a topcoat, it is exposed to corrosion and aluminum is the preferred material. Aluminum reflecting

surfaces are often given a topcoat to provide abrasion resistance as well as enhance corrosion protection.

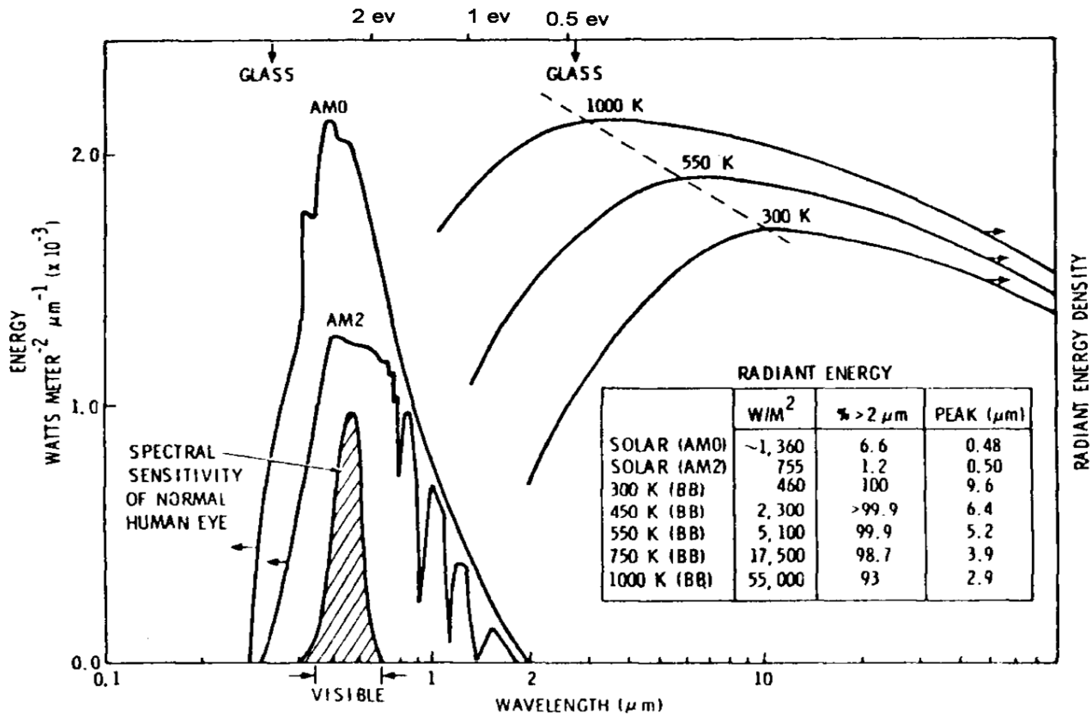

Figure (2-4) the optical spectrum of solar radiation.

Mirror surfaces can be over coated with a few or many transparent coatings (optical stacks) to further define the flux of radiation that is reflected, and the radiation that is absorbed by using optical interference effects. An optical stack of films consists of alternate layers of film material of specific thickness having high and low indices of refraction (Max Born, 2005). For example, by designing the optical stack so that the infrared is not reflected (i.e. adsorbed) a "cold mirror" can produce that minimizes the reflected heat from the light source. Such reflectors are used in light sources for hospital operating rooms and movie studios .A refractive surface can be over coated with transparent or semi-transparent polymer coatings that have color and/or texture, and these are often used for decorative coatings. for example, a Zinc die-cast lamp base, which has a rough surface, is flow – coated with a polymer basecoat to give a smooth surface, metalized with aluminum to give a reflective surface and then top coated with a colored lacquer to give a reflective, colored decorative finish to the lamp base. A molded polymer bottle cap can be coated with

aluminum and a lacquer topcoat to give a decorative coating. Metalized molded polymers are used as reflectors such as the auto headlight reflectors used with halogen light sources.

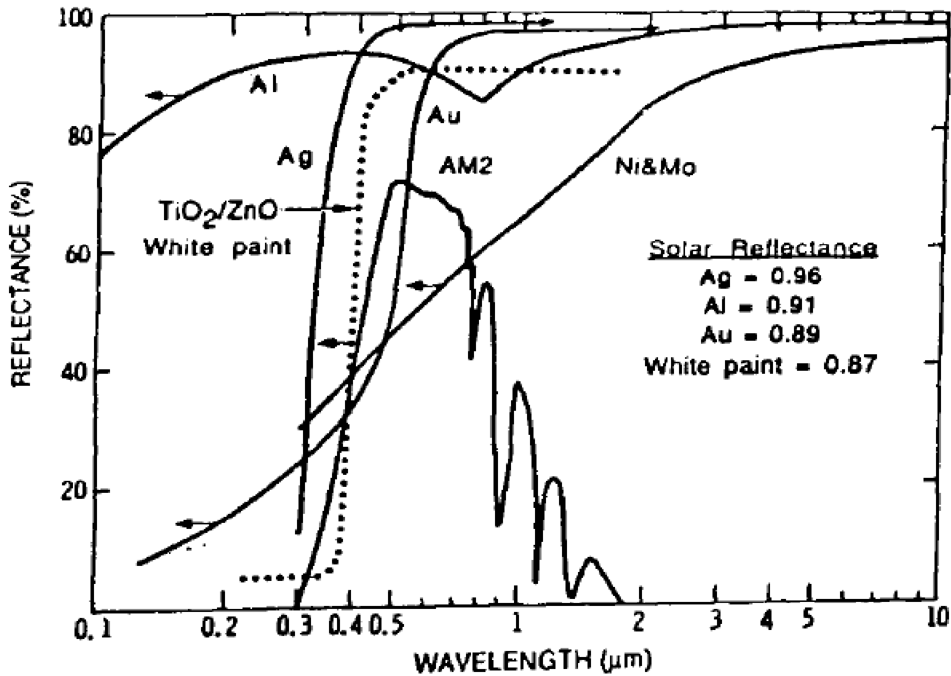

Figure (2-5): the solar reflectance spectrum

Mirrors can also be over coated with an electrically-active optical stack which can be made to be transparent or absorbing to varying degrees, by the application of an electric field. These types of optical stacks are call "electrochromic" coatings. Electrochromic coatings are composed of an ionic conductor (solid electrolyte) layer such as hydrated SiO_2, and an electrochromic material such as tungsten oxide, sandwiched between transparent electrical conductor films such as Indium-Tin-Oxide (ITO). When a voltage is applied across the sandwich, ions from the electrolyte enter the electrochromic material changing its transmittance.

When the potential is reversed the ions leave the electrochromic material the amount of incident power scattered by a surface as a function of angle is measured by scatterometry (Larson, 1996). This is normally done using a laser beam as the incident source and a detector that is moved in increments in a plane or sphere to determine the reflected power as a function of angle.

Thus restoring the transmission. Such electrochromic mirrors are available as anti-dazzling rear-view mirrors for automotive use.

2.6 Literature Review:

The efforts toward using Lasers in depositing thick films started soon after the invention of reliable high power lasers. Early observations of the ease with which the material could be vaporized by the intense interaction of high power laser pulses with material surface demonstrated that the intense laser radiation could be successfully used to deposit films of that material Titanium Oxide, Zinc oxide and Aluminum oxide films have attracting attention as one of the promising material with wide applications. It has been prepared and characterized by many workers and using different techniques, which greatly affected the obtained film characteristics. The first complete study about optical properties for crystalline material oxide type was prepared as crystal pieces by researcher.

In 1998 X. H. XU et al. studied the effect of calcinations temperatures on photocatalytic activity of TiO_2 films prepared by an electrophoretic deposition (EPD) method. TiO_2 films fabricated on transparent electro-conductive glass substrates and were further characterized by X-ray diffraction (XRD), X-ray photoelectron spectroscopy (XPS), field emission scanning electron microscope (FESEM), UV–vis diffuse reflectance spectra and Photoluminescence spectra (PL). FESEM images indicated that the TiO_2 films had roughness surfaces, which consisted of nano-sized particles.

In 2001 B. Farkas et al. prepared transparent TiO_2: Ni films with different Ni concentration 0.01, 0.015 and 0.03 at 600 °C on quartz substrates by (PLD) technique using Nd: YAG pulsed laser (λ=532 nm). Ni doping films showed a shift towards the visible in the absorption edge of the UV-Vis absorption spectra of the thick film.

The magnitude of this shift was found to increase with the amount of dopant. The values of band gap values for pure, 0.01, 0.015 and 0.03Ni concentration were determined to be 3.1, 2.76, 2.62, and 2.23 respectively.

In 2004, L.C.Tien et al. deposited TiO_2 films on sapphire by using ArF excimer laser (operating with wavelength 193 nm, pulse width 15ns, repetition frequency 10 Hz and power 100 mJ) at a substrate temperature of 500°C. The diagnostic of the ablation plume showed the interaction of the evaporated Ti particles with buffer O_2 gas. The dependence of the buffer O_2 gas pressure was studied by spectroscopy of ablation plume, thickness of films, morphology of the surface using SEM and AFM micrographs, XRD patterns and Raman spectra. The morphology showed the formation of nanostructure by interactions of evaporated Ti particles with the buffer O_2 gas. The structures of the PLD thin films showed epitaxial growths in the high substrate temperature (500°C) and an appearance of anatase at high buffer O_2 gas pressure owing to the contributions of the TiO molecules.

In2002,a series of ZnO films with various thicknesses were prepared by Park et al. on (0001) sapphire substrate by pulsed laser deposition (PLD) and Using a Nd: YAG pulsed laser with a wavelength of 355 nm. The laser repetition rate and energy density were maintained at 5 Hz and 2.5 J/cm^2, respectively. It is found that the crystalline quality, electrical and optical properties of the films strongly depend on the film thickness. It was believed that the films thicker than 400 nm were almost strain-free and exhibit the near-bulk ZnO properties.

Jin et al. in 2000 deposited ZnO films on sapphire by using Nd: YAG pulsed laser (λ= 355nm, 5Hz) with the laser energy density of 2.5 J/cm^2 at a substrate temperature of 400°C. It was concluded that the UV luminescence intensity depends strongly on the stoichiometry in the ZnO film rather than the micro-structural quality of the crystal. In the same year, ZnO films were grown on (0001) sapphire substrate by Bae et.al, 2000). The laser energy density was 2.5 J/cm^2. Pulsed Nd: YAG laser with a wavelength of 355 nm and a repetition rate of 5 Hz was used. Strong UV luminescence was obtained by increasing the substrate temperatures of ZnO films. This study suggests the possibility of using ZnO films in light emission device applications. In

2001,ZnO films were deposited by Jin et al on sapphire substrates by using an Nd: YAG pulsed laser (λ =355 nm, 5 Hz) with the laser energy density of 2.5 J/cm^2, at substrate temperatures of 4000C.The PL intensity of ultra-violet (UV) luminescence and the electrical resistivity generally increase as the oxygen pressure for the PLD of ZnO increases. The best quality with the minimum intensity ratio (defect related/ UV) is obtained from the ZnO sample.

In 2002,a series of ZnO films with various thicknesses were prepared by Park et al**.** On (0001) sapphire substrate by pulsed laser deposition (PLD) and Using a Nd: YAG pulsed laser with a wavelength of 355 nm. The laser repetition rate and energy density were maintained at 5 Hz and 2.5 J/cm^2, respectively. It is found that the crystalline quality, electrical and optical properties of the films strongly depend on the film thickness. It was believed that the films thicker than 400 nm were almost strain-free and exhibit the near-bulk ZnO properties.

Kaidashev et al. 2003 studied the high electron mobility of A multistep pulsed-laser deposition (PLD). Process was presented for epitaxial, ZnO films on c-plane sapphire substrates. They obtained high electron motilities in a narrow carrier concentration range. The samples showed flat surface structure with grain size of about (0.5–1) μm, where as the surfaces of low-mobility films consist of clearly resolved hexagonally faceted columnar grains of only (200-nm) size. In the same year (Barik et.al**.** 2003) deposited ZnO QDs embedded in Al_2O_3 matrix at room temperature. Third harmonic of Q-Switched Nd:YAG laser (355 nm, 6 ns, and 10 Hz) with a fluence of ~4 J/cm^2 have successfully grown a multilayer of alumina capped ZnO QDs using PLD and observed conspicuous size dependent blue shift in the band gap of such a QD matrix.

In 2004, Shan et al**,** prepared ZnO films on different substrate at different temperatures by using KrF Excimer laser (λ =248nm, τ =25ns) at about 1 J/cm^2 laser density. They found that all films showed (002) orientation at the

optimized conditions. Photoluminescence (PL) results indicate that the thick films fabricated at the optimized conditions show the intense near band PL emissions.

In this period of time Sans et al.2004, reported on the structural features and optical properties of wurtzite ZnO films epitaxial grown on sapphire, fluorite and mica substrates by means of pulsed laser deposition (PLD). Low cost mica substrates have been shown to be suitable to obtain ZnO films with optical and structural qualities suitable for optoelectronic applications.

Suchea et al. in 2005, prepared Zinc oxide transparent films (ZnO) with different thickness by dc magnetron sputtering and pulsed laser deposition (PLD) techniques using metallic and ceramic targets onto silicon and Corning glass substrates using XeCl Excimer Laser 308 nm wavelength. This work indicated that the film surface characteristics were strongly influenced by the deposition technique and conditions applied, thus providing a tool for the enhancement of the film sensing capabilities.

Also Lorenz, et. al.2006, studied the effect of N_2, N_2O and O_2 background gas on ZnO films grown by pulsed laser deposition (PLD) on α =-plane sapphire. Films with rough surface showed a broadening and splitting of the room-temperature CL peak into maxima at 3.21 and 3.26 eV, which could be due to either grain morphology or spatial variation of the electronic defect structure.

In 2006, Cho, observed the effect of substrate temperature on the structure and the exciton lifetime of ZnO films. The surface roughness generally increases as the substrate temperature increases. The lifetime for the ZnO film deposited at 400oC is found to be 168 ps. in the same year.

Zhao et.al.2006, studied ZnO films with c-axis (002) orientation growth on quartz glass substrate. High-quality ZnO films was obtained at such low temperature (100–250) °C. The ZnO films obtained at different substrate temperatures have nano-crystalline structure with grain size in the range of about 30– 45 nm. The as-deposited films showed ultraviolet emission and

accompanied deep-level emission in PL spectra. However, the ZnO film deposited at substrate temperature 200°C exhibited strong UV emission with no deep- level emission due to its low intrinsic defects.

In 2007, Yamaguchi et al. Fabricated ZnO films by PLD method with bias voltage to decrease defects in ZnO. The bias voltages of (-500 and +500) V were applied between the grid over substrate and the target to control the potential difference between the plume and the target. ZnO films were grown on Al_2O_3 substrates at substrate temperatures 20 and 700°C. However, applying bias voltage of -500V deteriorated the film surface condition and increased the density of defects. Also Novotny et al.2007, in the same time found that the resistivity and carrier concentrations of ZnO films grown by pulsed laser deposition in the presence of active ionic or neutral nitrogen species, generated in an electron cyclotron resonance N_2 plasma source, were measured as a function of the source microwave power and substrate temperature. Most of the films were n-type, although in conditions leading to increased activation of the ionic nitrogen species, p-type behavior was observed.

In2008, ZnO films were simultaneously deposited on sapphire (001) and Si (100) substrates at 5000C by pulsed laser deposition. The ZnO film grown on sapphire had a smoother surface and smaller grain size, and exhibited a sharper X-ray diffraction peak with a smaller full width at half maximum compared to those on Si. Simultaiously Sui, et al. deposited ZnO films on *c*-plane (0001) sapphire substrate at 250 °C. It is observed that the band gap energy red shifts nonlinearly from 3.345 to 3.153 eV with increasing temperature. These properties are highly advantageous for the design and fabrication of ZnO based fiber-optic temperature sensors, especially in the biological measurement.

Also Kang, et al, in2008 studied the relationship between the ultraviolet emission and electron concentration of ZnO films were deposited on (0001) Al_2O_3 substrates. And they found that the variation of electron concentration

of pure ZnO is more related to that of UV emission intensity than that of visible emission intensity. It is because that free-electron-neutral acceptor transition as origin of UV emission at room temperature is related to impurity concentration of pure ZnO.

In 2009, Wei and Zhang, using ZnO powder and ceramic target to prepared ZnO/Si films obtained in O_2 ambient at pressure 1.3Pa and study the effect of temperate on the structural and optical properties of these films investigated systematically by XRD, SEM, FTIR, and PL spectra. A pulsed Nd:YAG laser with a wavelength of 1064 nm (repetition rate is 10 Hz and the pulsed duration is 10ns).

At this time Zhaoyang, and Lizhong 2009 studied the effect of oxygen pressure on the structural and optical properties of ZnO films deposited on Si (111) by using KrF Excimer laser was operated at wavelength of 248 nm and repetition rate 5Hz. The laser energy density was about 2.5 J/cm^2.

They found that the increasing of oxygen pressure from 1 Pa to 50 Pa contributed to the size of ZnO grains and then promote the UV emission of the films. In the same year Premkumar et al, 2009 they deposited ZnO films on GaN and Sapphire substrate by PLD by using three different laser wavelengths Nd:YAG (1064nm, 532nm) and KrF(248nm). They found that the films grown at λ =532nm revealed the presence of ZnO nanorods and microrods, with diameter various from 250nm to 2µm and the length various between the 9 and 22µm.

Yu et al, 2009 studied the relationship between the photoluminescence and conductivity of undoped ZnO films grown on glass substrate with various oxygen pressures. The intensity of the deep-level-emission (DLE) and conductivity generally increased as the oxygen pressure decreased. The intensity of DLE peak was generally proportional to the conductivity. The band gap energy values, determined from transmittance spectra, were around 3.30–3.34eV, and decreased when the oxygen pressure increased.

Chapter Three

The Experimental Part

3.1 Introduction:

In this chapter, the details of the equipments, materials, various experimental procedures and the characterization techniques are described. Special aspects of experimental strategies are also pointed out and elaborated wherever necessary.

3.2 Deposition Equipments:

The basic components of the PLD-system, the laser, the preparation tools and the characterization equipment are introduced. The following sections consider the components inside the deposition experiments, namely, the laser, the targets and the substrate.

3.2.1 Nd: YAG Laser:

The laser source used for PLD was Q-switched Nd: YAG laser modelHS220E.It was supplied from Apolo Shanghai Medical Technology Company- China. The specifications of this laser are listed in table (3-1).

Table (3-1): The specifications of Nd: YAG Laser

Pulse energy-1064/532nm	1000/500mJ
Pulse duration	<10ns
Aiming beam	660 nm
Repetition rate	1~5Hz
Dimension	38cm*36cm*28cm (L*W*H)
power supply	220V
- Laser model	Q-switched Nd: YAG Laser
Laser wavelength	(1064 /532) nm.
Cooling method	inner circulation water cooling

The pulse energy of this laser was adjustable depending on the applied voltage pumping the flash lamps.

The whole system is made of light route system, power supply system, computer controlling system, cooling system, etc. The light route system is

installed into the hand piece, but power supply, controlling and cooling system are installed into the machine box of power supply.

3.2.2 Target holder:

The target holder keeps the target fixed in the vertical orientation during the deposition process.

3.2.3 Substrate holder:

The most important feature of a substrate holder is its movement relative to the target and plasma plume. Even with the simplest substrate holders, one should be able to adjust the distance between the target and the substrate. The adjustment of the target-substrate-distance provides an opportunity to control the deposition rate, as well as the energy of the particles hitting the substrate.

Glass substrates (3×2) cm^2 were used for deposition of films. The substrates were first cleaned in distilled water in order to remove the impurities and residuals from their surface. Then the substrate was cleaned in alcohol subsequently dried prior to film deposition experiment.

In this system, the substrate was placed parallel to the target surface at a 6mm distance.

3.3 Target materials:

Zinc Oxide (ZnO), Titanium dioxide (TiO_2), and Aluminum Oxide (Al_2O_3) powder with high purity (99.999%) were used as targets in form of disks by pressing them under (90 KN). The target should be as dense and homogenous as possible to ensure a good quality of the deposit. The target after being ablated is shown in Fig. (3.1).Three kinds of materials were used to fabricate the disks. Potassium Bromide was mixed with each disk to help in strength the disks.

Fig. (3.1): ZnO disk after being ablated by the laser.

3.3.1 Titanium Dioxide (TiO_2):

TiO_2 is an electrical insulating material which can be formed in three different phases, rutile, anatase, and brookite. The most stable phase of TiO_2 is the rutile phase with a body-centered tetragonal crystal structure, shown in Figure 3.3. Thermodynamically, rutile has the lowest total free energy compared to the other two metastable phases of TiO_2. The high refractive index of rutile phase (2.5 to 2.9) offers it to a variety of optical applications in a wide range of wavelengths (Agnarsson et al., 2013).

It has also been utilized for many applications in photochemistry, and electronics. The high refractive index and transparency of TiO_2 in the rutile phase make it a suitable candidate for low-emissivity and antireflective coatings, and optical devices such as Bragg mirrors and metal-insulator-metal devices for direct wavelength determination of monochromatic light (Wang and Melosh, 2013). Moreover, rutile TiO_2 is considered as a high-dielectric material (90 - 170 depending on lattice orientation) in microelectronics and has been used as a gate stack dielectric for metal-TiO_2-SiO_2-Si (MTOS) capacitors. Recently it has been suggested as a conductive protective layer on Si for photo cathodic H_2 evolution using solar energy where the conduction band alignment of TiO_2 compared to Si opens up the possibility of photocurrent detection.

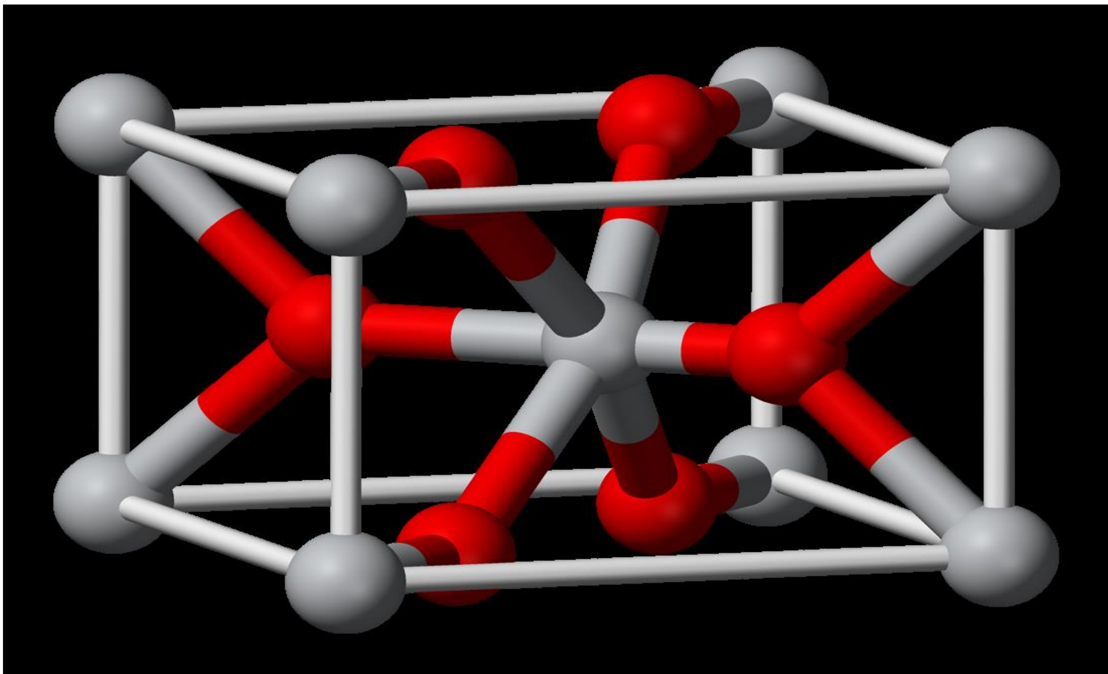

Figure 3.2: Crystal structure of TiO_2. Red and grey spheres are oxygen and titanium atoms, respectively.

3.3.2 Sapphire (Al_2O_3):

Single crystal sapphire possesses a unique combination of excellent optical, physical and chemical properties. The hardest of the oxide crystals, sapphire retains its high strength at high temperatures, has good thermal properties and excellent transparency. It is chemically resistant to common acids and alkali at temperatures up to 1000 °C as well as to HF below 300 °C. These properties encourage its wide use in hostile environments where optical transmission in the range from the vacuum ultraviolet to the near infrared is required. Sapphire is anisotropic hexagonal crystal. Its properties depend on crystallographic direction (relative to the optical C-axis).

Maximum available size for windows, lenses and blanks made of high purity optical grade single Kyropulos grown Sapphire: 250mm Dia x 120mm Thk and 175 mm Square x 120mm Thk.

Sapphire grown by EFG methods is available in form of round rods (1-8 mm Dia, up to 500 mm long), rectangular and square rods and ribbons (10-80 mm wide, 1-10 mm thick, 150-500 mm long), tubes, thermocouple sleeves, crucibles (1.5-50 mm ID, 0.5-4.0 mm wall thickness, up to 600 mm long) and

other custom cross-section configurations. Sapphire, Al_2O_3 has the properties listed in table (3.3)

Table (3.2): Sapphire, Al_2O_3Specifications

Chemical Formula	Al_2O_3
Crystal Class	Original
Molecular Weight	101.94
Density, g/cm^3 (20 °C)	3.98
Reflection Loss, % for two surfaces at 4 µm	12
Dielectric Constant for 10^3-10^9 Hz at 298 K parallel to C-axis perpendicular to C-axis	 11.5 9.3
Dielectric Strength, KV/mm	17
Resistivity at 20°C, Ohm cm	> 10^{16}
Melting Temperature, K	2300
Thermal Conductivity, W/(m K) at 300 K parallel perpendicular	 35.1 33.0
Thermal Expansion, 1/K at 293 K parallel perpendicular	 5.6×10^{-6} 5.0×10^{-6}
Specific Heat, cal/(g K) at 298 K	0.18
Bandgap, eV	9.9
Solubility in water	None
Mohs Hardness	9
Knoop Hardness, kg/mm^2	1370
Young's Modulus, GPa	335
Shear Modulus, GPa	148
Bulk Modulus, GPa at 273 K	240
Apparent Elastic Limit, MPa	275
Poisson's Ratio	0.25

3.3.3 Zinc oxide (ZnO):

The unique and fascinating properties of II-VI compound semiconductors have triggered tremendous motivation among the scientists to explore the

possibilities of using them in industrial applications. Zinc oxide (ZnO) is a piezoelectric, dielectric, transparent, semiconducting oxide and optoelectronic applications in UV-Blue spectral range. In addition, due to its wide band direct band gap and its large photo response, ZnO is also very suitable for UV photo-detector application. ZnO with a direct band gap of 3.37 eV at room temperature and a large excitation binding energy (60 meV), which is 2.4 times the effective thermal energy (KBT=25meV) at room temperature, and biexcitation energy is 15meV. This is one of the key parameters that ZnO exhibits near-UV emission, transparency, conductivity, and resistance to high temperature electronic degradation. ZnO crystallizes into a rugged Wurtzite structure which has two interpenetrating hexagonal sub-lattices of Oxygen and Zinc atoms respectively, shifted along the c-axis by 5c/8. Another crystalline phase of ZnO which is cubic Zinc bland, although rarely observed, has also been reported by a few groups ((Jagadish, 2006). The high cohesive energy of ZnO which is ~1.89eV makes it a highly stable and perhaps the most radiation hard material amongst the direct band gap semiconductor family, which ensures a long life and a high degradation threshold of ZnO based optoelectronic devices. The high melting and boiling points of ZnO allow one to explore a variety of heat treatments required for alloying purposes and device formation. Being an oxide, ZnO also enjoys the extreme stability against the oxidation problem which can severely affect the device performance as in case of some of the III-V and II-V semiconductors such as GaAs, InAs and ZnS etc (Cao, 1998).

The grown films exhibited hexagonal grains of size ~ 50 nm well arranged in a honey comb fashion. The grain boundary between the grains served as cavity mirrors. The observed low threshold of pumping for efficient stimulated emission was attributed to the excitonic recombination. Quantum confinement of excitons can further enhance the excitonic binding energy and may result in other interesting properties including extremely low threshold of lasing. Table (3.4) shows a compilation of the basic physical parameter for

ZnO. Still some uncertainty exists in these values. For example, in few reports it has been mentioned physical properties of wurtzite ZnO and therefore the whole mobility and effective mass. (Yousif. 2010).

Table (3.4): Physical properties of ZnO wurtzite structure

property	value
Lattice parameters at 300 K	
$a_\circ$,$c_\circ$ U	0.3249nm, 0.52069 nm 0.345
Density	5.606gcm^{-3}
Stable phase at 300K	Wurtzite
Bond length	1.77µm
Melting point	1975 °C.
Thermal conductivity	0.6 W.cm^{-1}.C^{-1}
Linear expansion coefficient(/C)	$a_\circ$:6.5×10^{-6}, $c_\circ$: 3.9×10^{-6}
Static dielectric constant	8.656
Refractive index for Zinc blend For Wurtzite structure	2008 2.029
Energy gap	3.4 eV, direct
Intrinsic carrier concentration	<10^{6}cm^{-3}
Exciton bending energy	60meV
Electron effective mass	0.24
Electron Hall mobility at 300 K for Low n-type conductivity	200cm^{2}V^{-1}s^{-1}
Minimum pressure at melting point	7.82atm
Ionicity	62%
Heat capacity Cp	9.6cal/mol K

3.3.4 Potassium Bromide (KBr):

Potassium Bromide is used for windows and prisms when transmission through the 0.25µm -26µm range is desired. Potassium Bromide is water soluble and must be protected against moisture degradation of polished surfaces. The material cleaves readily, and can be used at temperatures up to 300°C. Irradiation of Potassium Bromide produces color centers. Potassium Bromide has the properties which are listed in the table (3.2). (www.semiconductors.co.uk)

Table (3.2): Potassium Bromide properties

Chemical Formula	KBr
Molecular Weight	119.01
Crystal Class	Cubic
Lattice Constant, Å	6.60
Density, g/cm^3 at 300 K	2.75
Absorption Coefficient, 1/cm at 2.7 µm at 3.8 µm	 1.2×10^{-4} 1.6×10^{-4}
Reflection Loss for two surfaces at 10 µm, %	8.4
Dielectric Constant for 10^2-10^{10} Hz at 298 K for 10^2-10^{10} Hz at 360 K	 4.9 4.97
Melting Temperature, K	1000
Thermal Conductivity, W/(m K) at 319 K	4.8
Thermal Expansion, 1/K at 300 K	38.5×10^{-6}
Specific Heat, cal/(g K) at 273 K	0.104
Debye Temperature, K	174
Bandgap, eV	7.6
Solubility, g/100 g H_2O at 273 K	53.48
Knoop Hardness, kg/mm^2	7.0 [100]
Young's Modulus, GPa	26.87
Rupture Modulus, GPa	0.0039
Shear Modulus, GPa	5.08
Bulk Modulus, GPa	15.02

3.4 The Pressing Machine and its Parts:

An old classical pressing machine was used here in order to produce solid rigid disks by pressing them in disk shape. The load provided by this machine extended from 0.0 to 15.0 tons. The part accompanied with this Machine is of an internal radius of about 15mm and a height of about 100mm. the base, the sides, the cover of this part are all very smooth. Figure (3.3) shows a photograph of the used pressing machine and figure (3.4) shows a photograph for three material disks obtained by the compression method

Fig (3.3): A press with a matrix and a punch for pressing of powder of material into a disk.

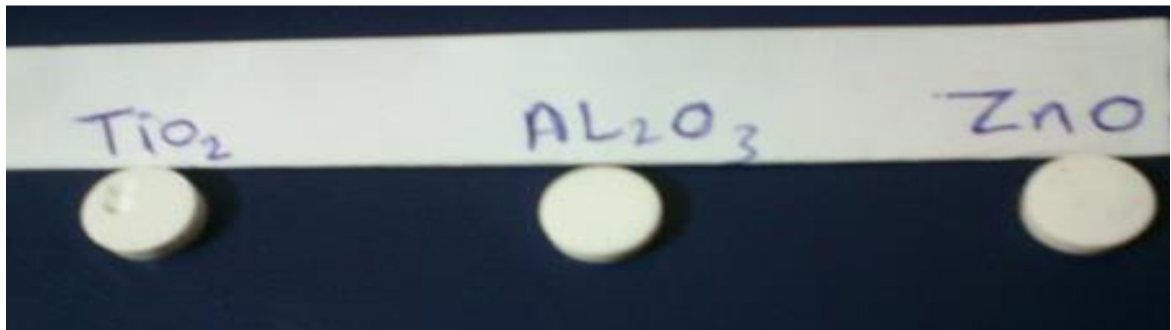

Fig (3.4). Tablets of three group of material obtained by the compression method**.**

3.5 Procedure of PLD:

All the pulsed laser deposition experiments were performed at ambient pressure and room temperature. The set-up of laser deposition is shown in fig.3.5. The focused Nd:YAG (SHG Q-switching laser beam) was incident on the target surface in a direction making an angle of 45° between them. The substrate was placed in front of the target with its surface parallel to that of the target. Sufficient gap was kept between the target and the substrate so that the substrate holder does not obstruct the incident laser beam.

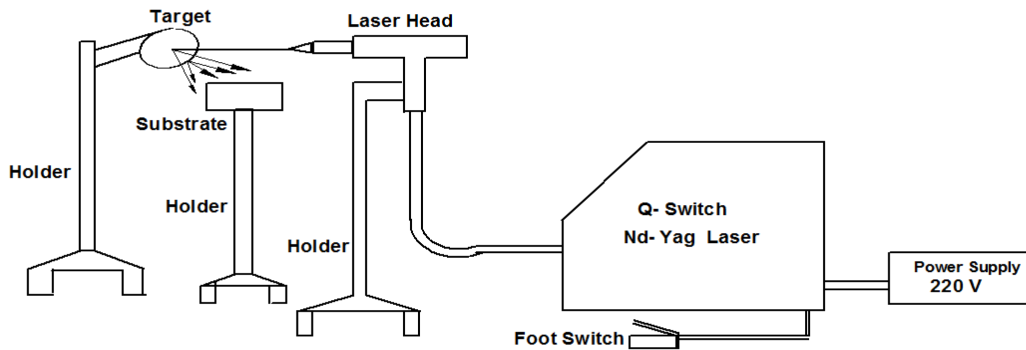

Figure 3-5: Schematic diagram of PLD technique setup

3.6 Fabrication of the thick films by (PLD):

Conceptually and experimentally, Pulsed Laser Deposition (PLD) is simple; it was performed at ambient pressure and room temperature. The schematic diagram and setup have been shown in Figure: (3-5) and figure: (3-7) respectively. It consist the Target, Substrate, Holders and Laser source (Nd-YAG Q- switched laser). And the experiment procedure was followed by steps:

1-The target –substrate distance was fixed at 6 mm.

2- The laser – target distance was fixed at 1.2 cm

3-The laser beam was incident on the target by angle of incident 45°, the wave length 1064nm was selected (Nd: YAG laser) and pulse duration 10ns.

4-The laser pulse energy was varied from (500-700) mJ with increment 100mJ in each step, and with laser repetition rate (20, 30,40Hz).

5- Repeat step (4) to all group (TiO_2, Al2O3 and ZnO) respectively.

3.7 Scanning Electron Microscope:

Scanning electron microscopy (SEM) is a technique similar to optical microscopy but offers a higher resolution. Light microscopes have a magnification of ~1000 times and allow features separated by ~ 200 nm to be resolved, however the resolution power of a microscope is not solely limited by the number and quality of lenses but is limited by the wavelength of light. Therefore visible light only allows features to be resolved that are separated by ~ 200nm. Electrons in a vacuum travel in a straight line with wave-like properties ~ 100,000 times shorter than visible light. Electronic and magnetic

fields are used to shape the electron beam (similar to a glass lenses in a light microscope). This allows electron microscopes to resolve features separated by ~ 0.05 nm. Although the wavelength associated with electrons is ~ 100,000 times smaller than the wavelength of light (~ 550 nm) this does not translate to a 1000,000 times better resolution due to a combination of beam voltage, aperture size and lens aberrations. The resolution also depends on electron spot size, working distance and interaction volume.

There are several basic modes of operation for scanning electron microscope;

- Secondary electron imaging

- Backscattered electron imaging

- X-ray analysis and mapping (EDX – Energy Dispersive X-ray Analysis)

When the incident electron beam interacts with the samples surface, secondary electrons arise from the ionization of electrons associated with the atoms in the samples surface. Secondary electrons are low energy (< 50 eV) electrons which have escaped from the top 1 – 30 nm of the sample. Once the escaped electrons (from different points in the sample) are detected, an image is formed of the surface topography.

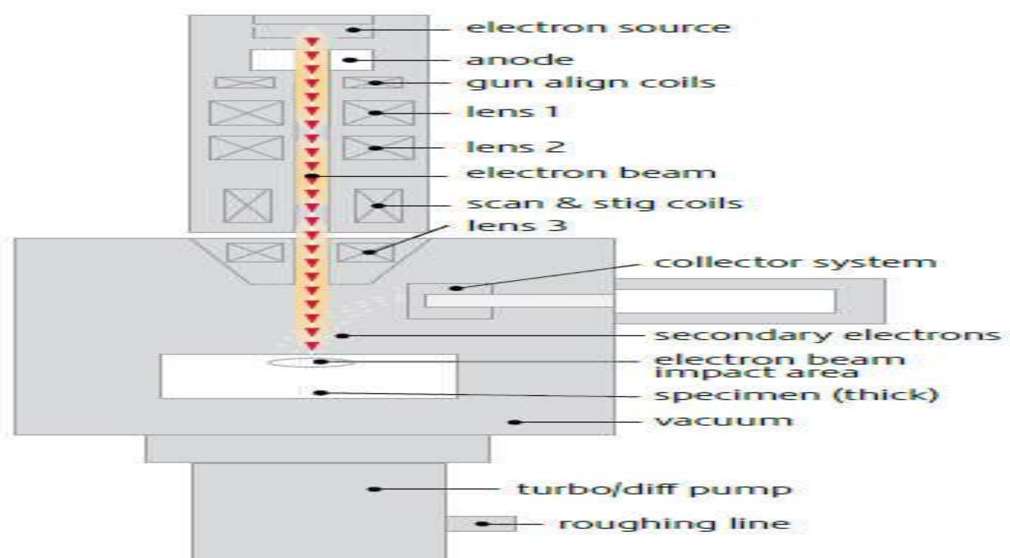

Fig (3.6). Schematic representation of a scanning electron microscope

Another imaging technique using the scanning electron microscope is known as backscattered electron imaging. This technique is used to image subsurface

detail and is possible when higher energy electrons are backscattered from the top 10 – 100 nm of the samples surface. This is achievable when higher incident beam energy is emitted from the electron gun (1–20 keV). The intensity of the backscattered electrons is dependent on the average atomic number and can therefore be used to image atomic number contrast if the effects of topography have been removed (e.g. polishing). When the incident beam electrons travel deeper into the samples surface they progressively spread out with increasing depth into the sample, which reduces the image resolution. Therefore secondary electrons are usually used when high resolution images of the sample are required. X-rays are emitted when incident beam electrons interact with matter. As the electron beam is scanned across the sample surface x-rays are emitted from all the different points the electron beam is scanned. Different elements in the sample produce x-rays of characteristic wavelengths which allow the distribution of elements in the sample surface (interaction of ~ 1 μm below the sample surface) to be mapped. In this work the scanning electron imaging was used to image the topography of the surface and measuring the thickness of thin films as figure (3.9) below. X-rays were used to map the elemental distribution before and after pulsed laser exposure. The SEM used in this work was a LEO1530 Gemini FEG-SEM fitted with an Oxford Instruments UTW EDX detector, running ISIS software. Images were taken at an operating voltage of 3 kV and a working distance of ~ 2 - 3 mm.

3.8 Characterization of thick films:

In this study, varieties of the light sources were used to determine the optical properties of the thick films. Of particular interest was the determination of the optical parameters from visible –infrared transmission spectrum in the spectral range (532-915nm) using different laser sources and the film thickness from Scanning electron microscope (SEM).

3.8.1 The Lasers Sources:

A number of laser sources were used to investigate the transmission spectrum of each thick film, and then it's for each wavelength. These lasers are:

3.8.1.1 Diode Laser (532nm):

This laser source was used to irradiate the thick films in order to measure the transmission spectrum of each film. It was supplied for and its specifications are listed in table (3.5).

Table (3.5): Specifications of diode Laser (532nm)

Wavelength	532nm
Output power maximum	4mW
Operating mode	Continues
Class	2

3.8.1.2 Monochromatic LED (660 nm):

This is a light emitting diode (L E D) used to aim the beam of Nd:YAG laser and to simply the alignment of the beam to the desired destination, the aiming beam of the Q-switched Nd:YAG (Model Name HS 220 E) manufactured by Shanghai Apolo Medical Technology Co.ltd (Shanghai Apolo Medical Technology Co.ltd,2011) was used in this study. It emits 660 nm wavelengths, 5mW output power.

3.8.1.3 He-Ne Laser (632.8nm):

He-Ne laser used here was supplied from PHYWE Company – Germany. Its specifications are illustrated in table (3.6).

Table (3.6): Specification of He-Ne Laser (632.8nm)

Wavelength	632.8nm
Output power maximum	1mW
Operating mode	Continues
Class	2

3.8.1.4: Diode laser (675 nm):

This laser also was supplied from omega XP, CW with 30mWoutput power, its specifications are listed in table (3.8) below.

Table (3.8) specifications of the diode laser (675) nm:

Wavelength	675nm
Output power	30mW
Operating mode	Pulse >5μs
Classification	Class 111-B

3.8.1.5 Diode Laser (820 nm):

This laser was supplied from omega XP Company – United Kingdom. Its specifications are listed in table (3.7).

Table (3.7): Specifications of diode Laser 820nm..

Wavelength	820nm
Output power	20W
Operating mode	Pulse >5μs
Class	4

3.8.1.6: Diode laser (915nm)

This laser was supplied from omega XP, CW mode, with200mW output power, it was manufactured by Omega Company –England, and its specifications are listed in table (3.9) below, (Botech health, 1996)

Table (3.8) specifications of infrared prope 915nm:

Wavelength	915 nm
Coherence	Laser
power	200mW
Output power	30mW
Classification	Class 111-B
Power density	1.60 W/cm^2

3.9 Determination of the films optical properties:

The laser beam was focused on the middle of each thick film that by guiding the probe of each laser source directly in front of the detector and concentrate the laser beam spot on it. The intensity (I_0) without the film was measured, as a voltage, displayed on the digital multimeter. Each film from the three groups was tested by putting the thick film above the detector and read the

transmitted intensity, displayed also on the digital millimeter. All the components (laser probe, detector, thick film) were aligned.

The procedure was repeated for all lasers sources and the transmission spectrum for each thick film was plotted.

The experimental setup was arranged as shown in the fig (3.7) below.

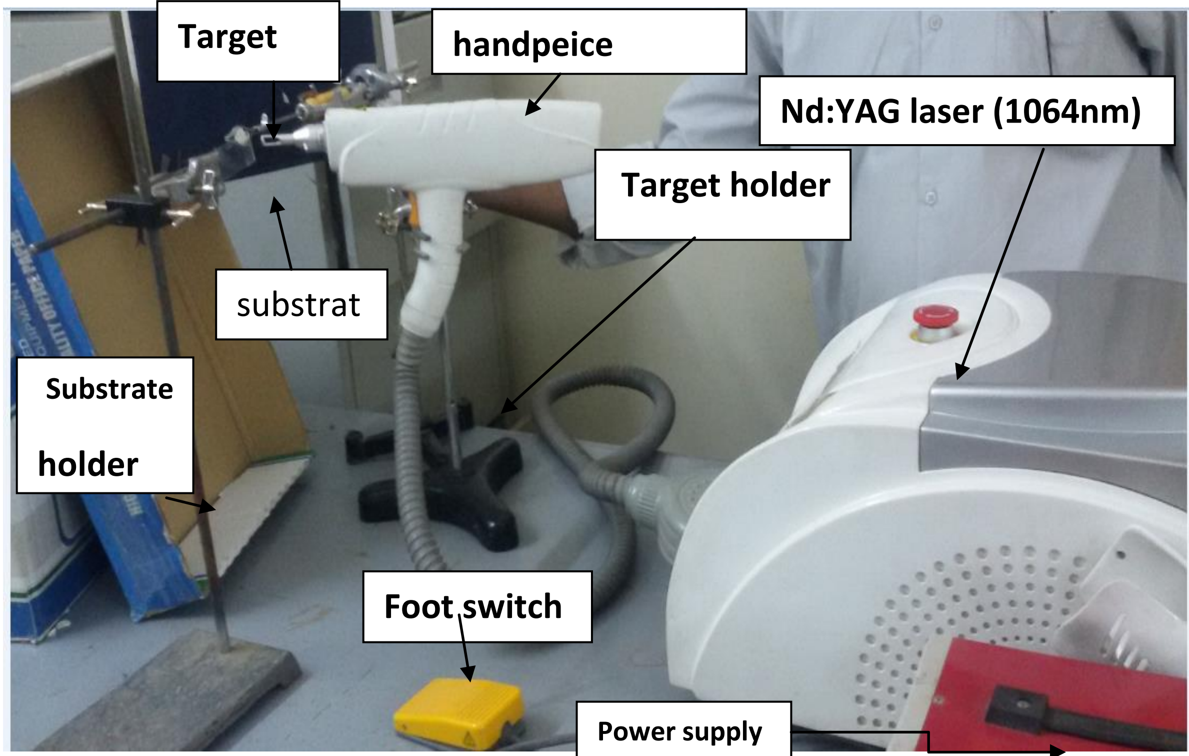

Fig (3.7) a photograph of the PLD setup.

The absorption coefficient and the refractive index for each film were calculated using the measured reflectivity R and the glass refractive index n_s according to :(Mousa, Ponpon, 2006) and (Elhadi, 2007)

$$I = I_{\circ} e^{-\propto d} \qquad (3\text{-}1)$$

Where (I) represent the transmitted intensity,($I_{\circ}$) the incident intensity before deposition,($\propto$) is the absorption coefficient, and (d) the thickness of the thick film.

$$n = \sqrt{\left\{\frac{n_s(1+\sqrt{R})}{(1-\sqrt{R})}\right\}} \qquad (3\text{-}2)$$

$$n_s = \frac{1}{T_S}\sqrt{\left[\frac{1}{T_S^2} - 1\right]} \quad \text{(3-3)}$$

Where T_S represents the transmission of glass substrate, ns is the refractive index of substrate, n represent the refractive index of the thick film.

The absorption coefficient and the refractive index were plotted as a function of wavelength for each thick film.

Chapter four

Results and discussion

4.1 Introduction:

The basic objective of this chapter is to present and discuss the results obtained from the experimental work of this study. Some of the results were measured and the others were calculated to determine the optical properties of the thin films.

This work was limited to the case of a single layer film deposited on a glass substrate practically.

In general, each thin film is characterized by its absorption coefficient (α), its refractive index (n), and its thickness (d).

In this work, different samples were prepared from oxides materials TiO_2, Al_2O_3 and ZnO on glass substrate by pulsed laser deposition as thin films under different laser energies with different repetition rates as listed in table (4-1) below:

Table (4.1): samples that were prepared by Nd:YAG (1064 nm) laser

Material	Samples Code	Laser Energy	R.R(Hz)
TiO_2	A_1,A_2,A_3	500mJ	20,30,40Hz
	A_4, A_5, A_6	600mJ	
	A_7,A_8, A_9	700mJ	
Al_2O_3	B_1 ,B_2,B_3	500mJ	20,30,40Hz
	B_4 , B_5,B_6	600mJ	
	B_7 , B_8, B_9	700mJ	
ZnO	C_1, C_2, C_3	500mJ	20,30,40Hz
	C_4, C_5, C_6	600mJ	
	C_7 , C_8, C_9	700mJ	

All the data for these samples are listed in tables and plotted in figures.

The measured values of the incident and transmitted intensity of different lasers wavelengths are listed in tables from one up to 26 in the appendix.

4.2 Thickness measurement:

One of the important points of this work is the measurement of the films thicknesses, using the scanning electronic microscope (SEM). Figures (4.1) to

(4.11) show the images of the thick films gained by the (SEM).The measured thickness of the thick films are tabulated in table (4-2). Figures (4.12) and (4.13) show the relation between the thickness of the films and the (R.R) for the cases of 500 mJ and 700 mJ , we get from these results of thickness two equations (4-1) and (4-2) vs. between RR and thickness respectively.

Figure (4. 1): SEM image of the T iO_2thick film (sample A1)

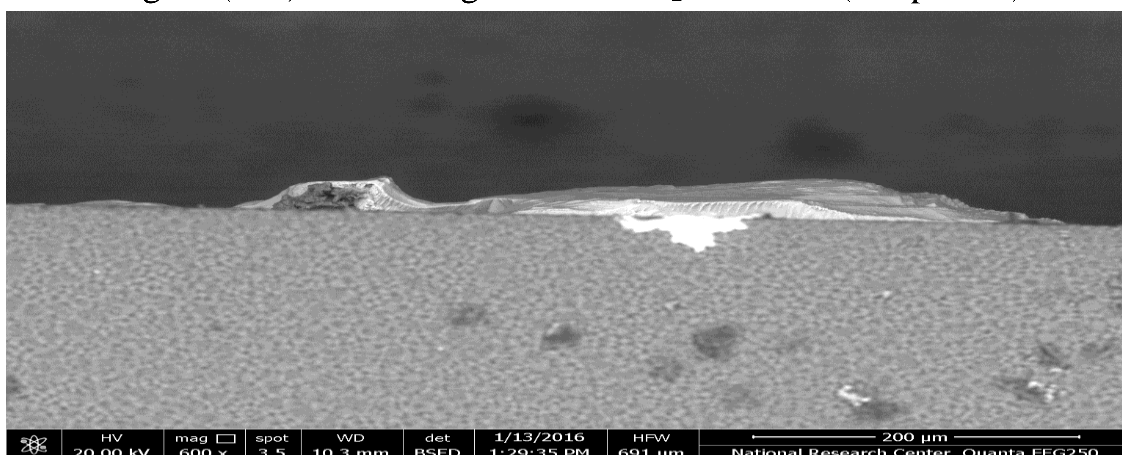

Figure (4.2): SEM image of the TiO_2 thick film (sample A2)

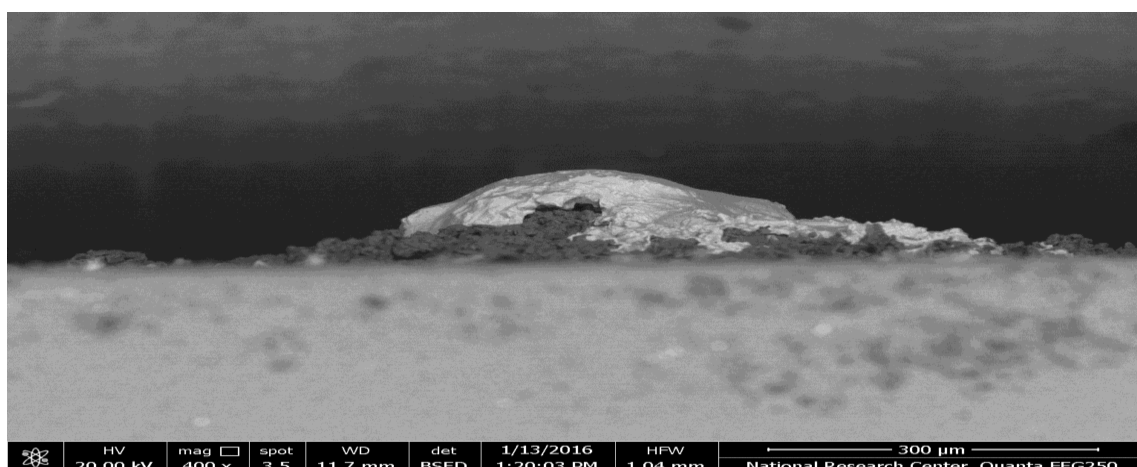

Figure (4.3) SEM image of the TiO_2 thick film (sample A3)

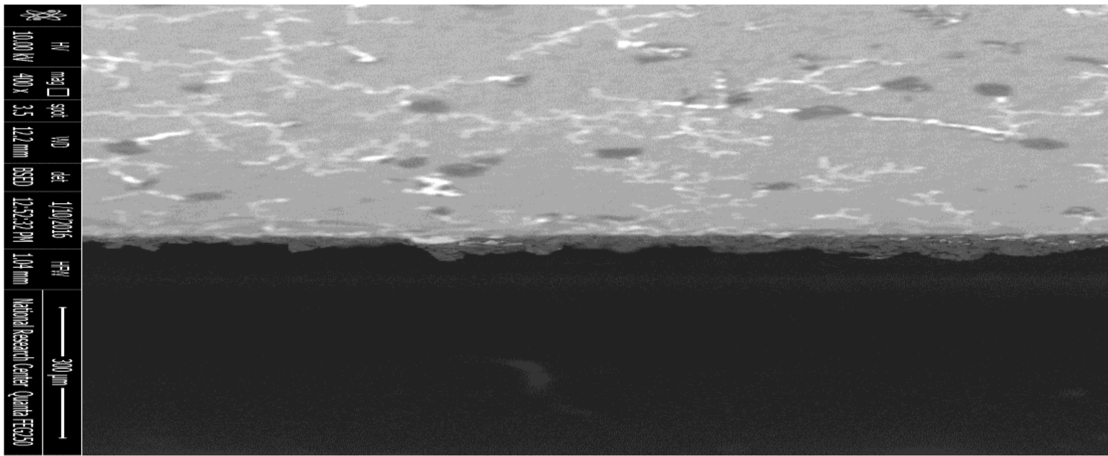

Figure (4.4) SEM image of the TiO_2 thick film (sample A6)

Figure (4.5) SEM image of the TiO_2 thick film (sample A7)

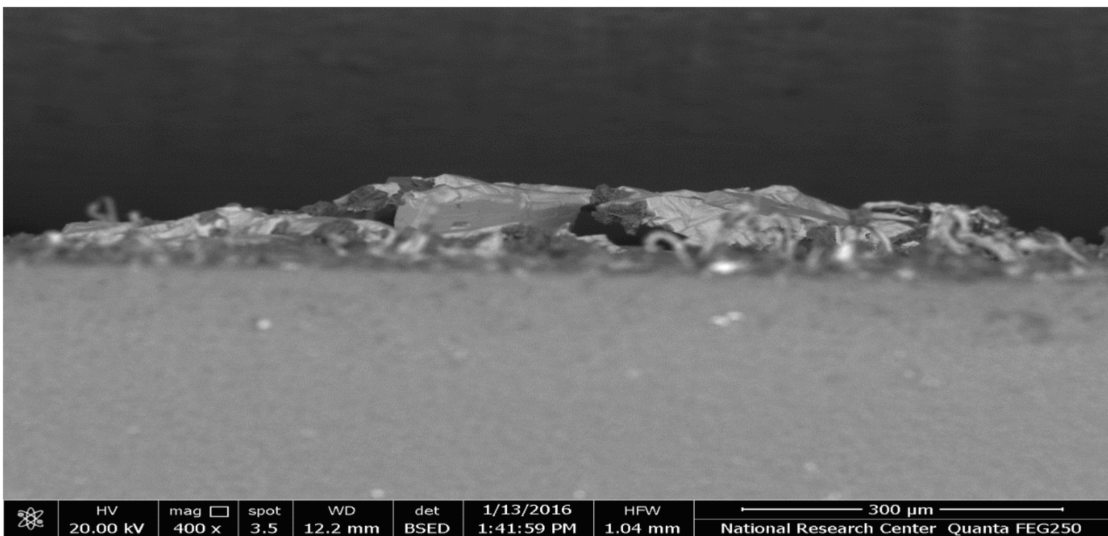

Figure (4.6) SEM image of the TiO_2 thick film (sample A8)

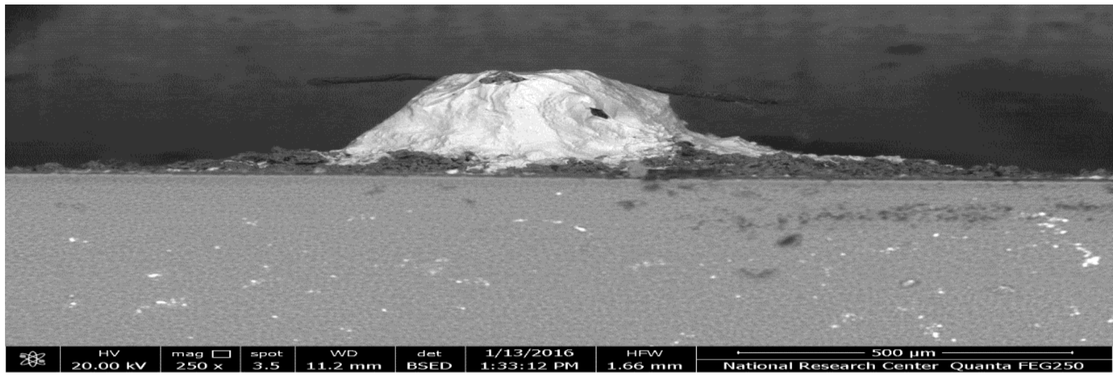

Figure (4.7) SEM image of the TiO_2 thick film (sample A9)

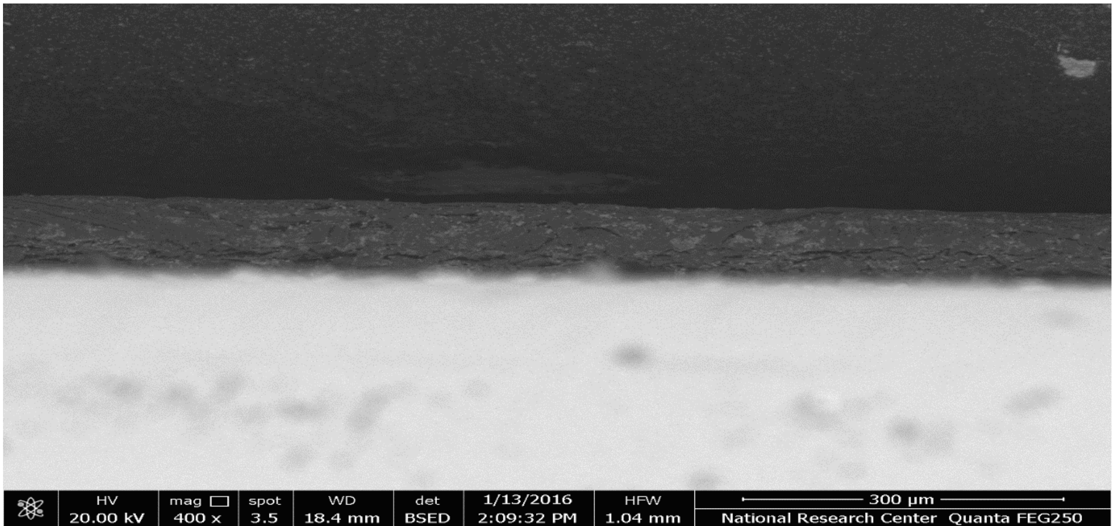

Figure (4.8) SEM image of the Al_2O_3 thick film (sample B1)

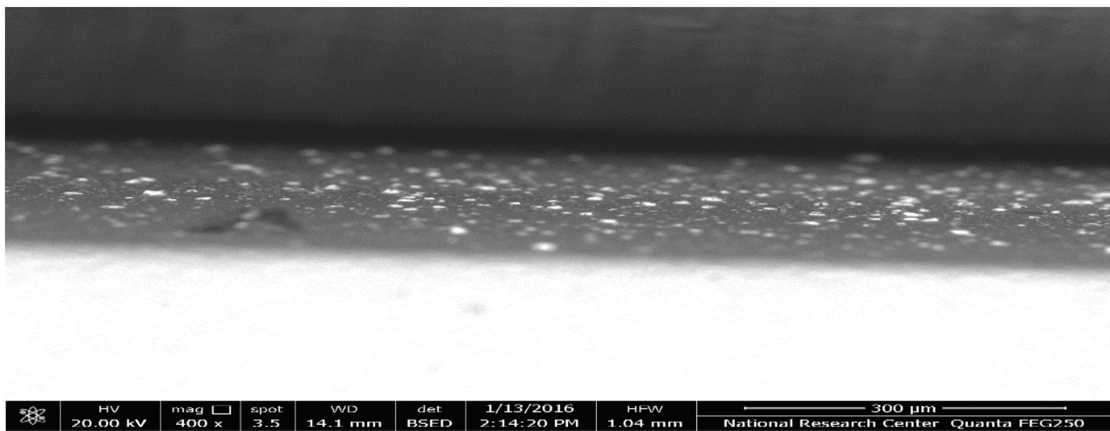

Figure (4.9) SEM image of the Al_2O_3 thick film (sample B2)

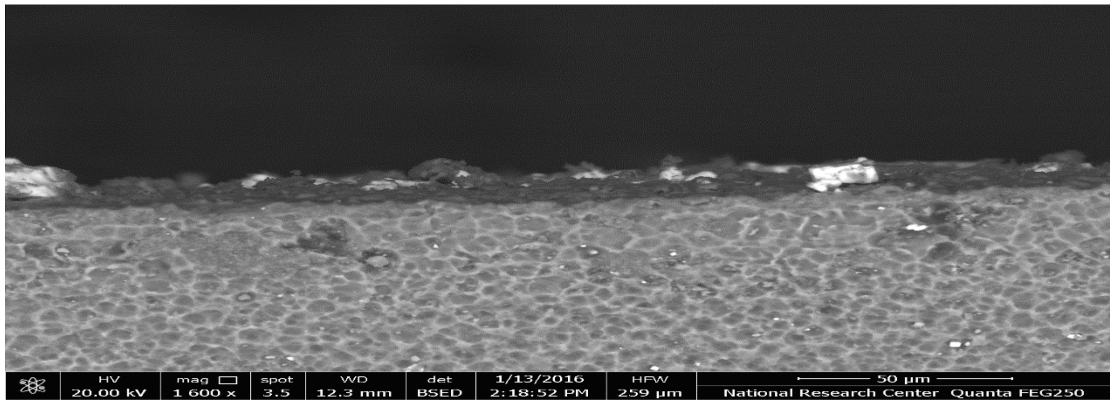

Figure (4.10) SEM image of the Al_2O_3 thick film (sample B3)

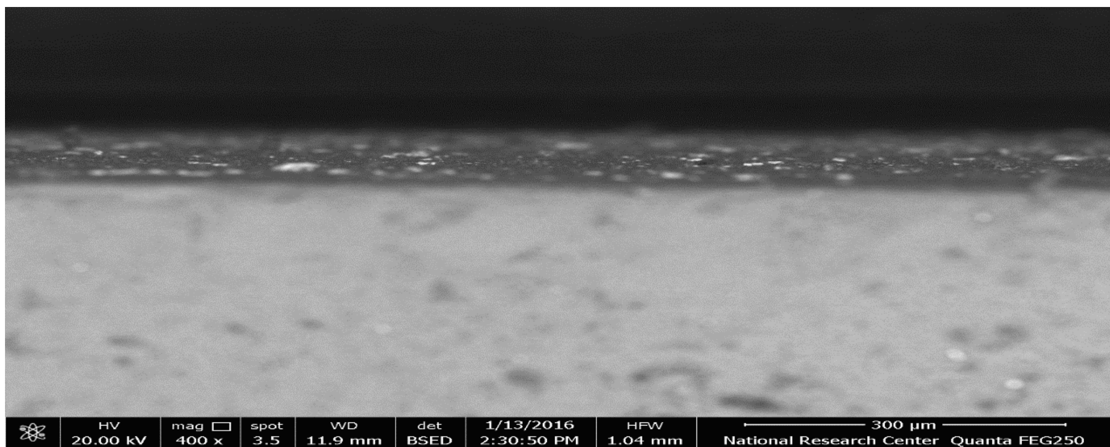

Figure (4.11) SEM image of the Al_2O_3 thick film (sample B4)

Table (4-2): The measured thicknesses of the thick films

Laser energy	R.R. (Hz)	Thickness(µm)	Samples
500mJ	20	81.35	A_1
	30	106.54	A2
	40	116.23	A3
700mJ	20	96.66	A7
	30	103.12	A8
	40	107.63	A9

$$\text{Thickness} = -0.056RR^2 + 5.1686R \qquad (4\text{-}1)$$

$$\text{Thickness} = -0.0942RR^2 + 6.4227R \qquad (4\text{-}2)$$

Thickness = -0.0942RR^2 +6.4227R

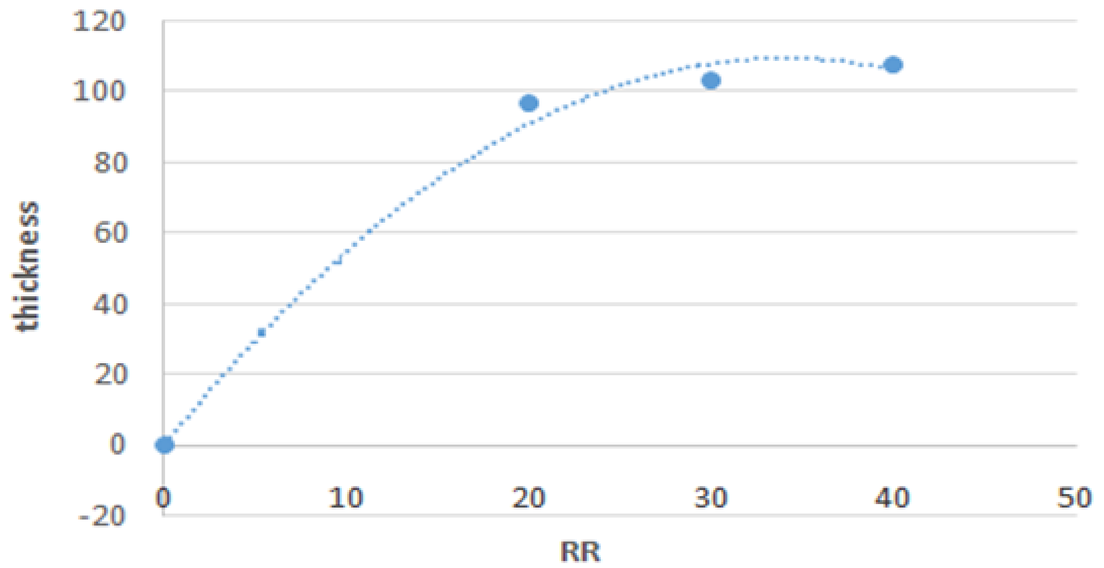

Figure (4.12): The thickness of TiO_2thick films Vs. the Repetition Rate (20, 30 and 40Hz) at pulse energy (500mJ)

Thickness = -0.056RR^2 +5.1686R

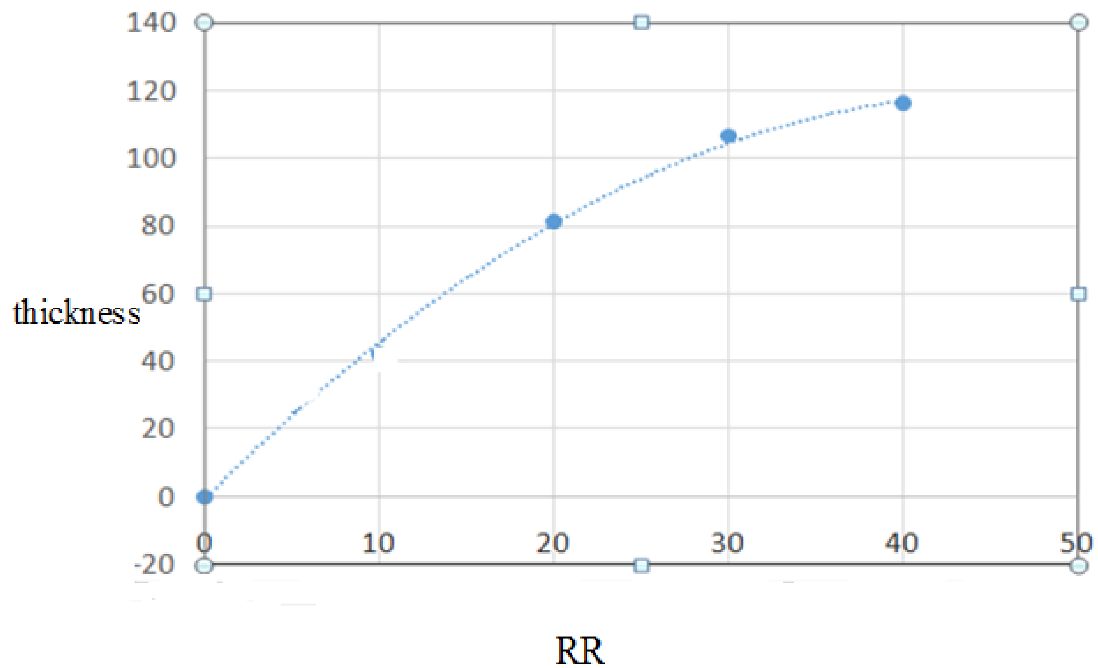

Figure (4.13): The thickness of TiO_2thick films Vs. The Repetition Rate (20, 30 and 40Hz) at pulse energy (700mJ).

4.3 The optical properties of (TiO_2) thick films:

Titanium dioxide (TiO_2) samples were deposited on glass substrate that has a refractive index equal to (1.3) and thickness (1mm) at room temperature. The measured values of the incident and transmitted intensities of different laser wavelengths are listed in tables ((1)-(9)) in the appendix.

By using Beer Lambert law and knowledge of the film thickness and from the results in tables ((1)-(9)), the absorption coefficients (∝) for these samples were calculated at different wavelengths, By using the following relationship[$\propto = \frac{1}{d} \ln \frac{1}{T}$], where d is the thickness of the film and T is the optical transmittance (E.V. Bufa et al, 2008), and the results are listed in tables ((37)-(45)) in the appendix. The refractive index was calculated using the following relationship.

$$n = \left\{ \frac{n_s(1+\sqrt{R})}{1-\sqrt{R}} \right\}^{\frac{1}{2}} \tag{4.3}$$

Where (n) is the refractive index of the film, (n_s) is the refractive index of the glass substrate, and (R) is the reflectance of the film. The results are tabulated in tables ((28)-(36)) in the appendix.

These parameters (thickness, absorption coefficient, and refractive index) represent the optical properties of samples (A1-A9) which are the most important parameters for any thin film (Macleod, 1987).

The transmission spectra, the absorption coefficients and the refractive indices for the TiO_2 samples, are shown in figures ((4.14)-(4.23) below.

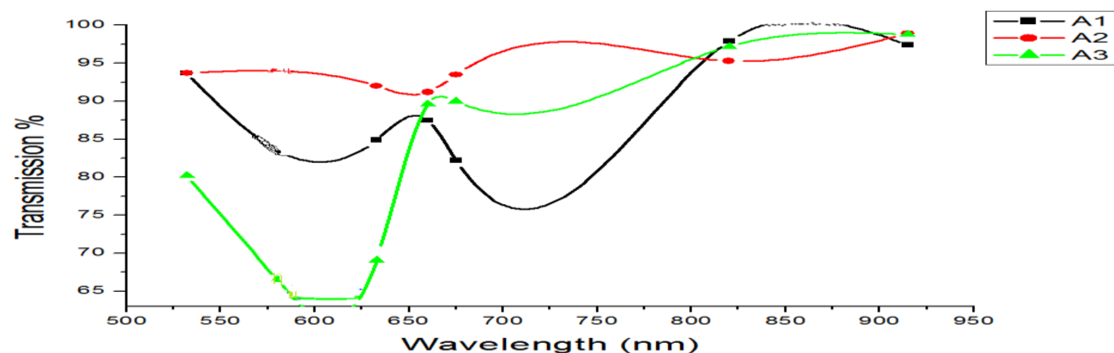

Fig (4-14): The transmission spectra of samples (A1, A2, A3).

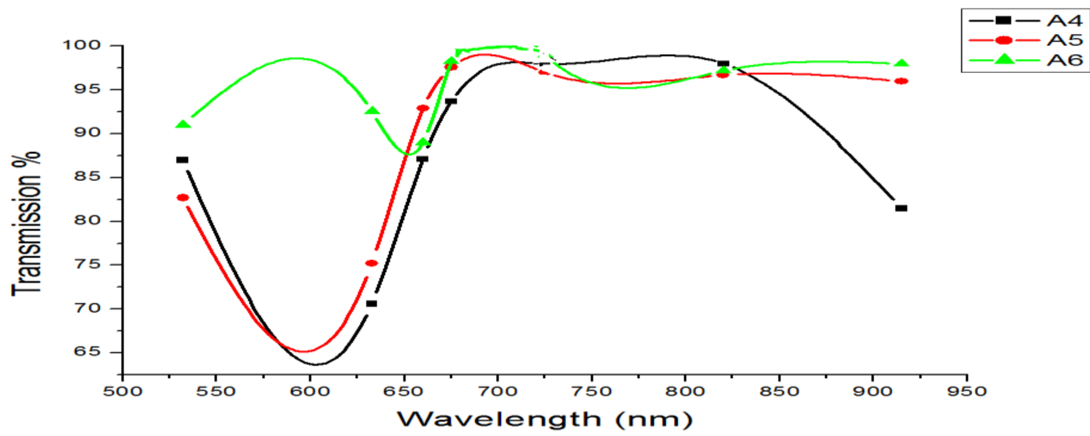

Fig (4-15): The transmission spectra of samples (A4, A5, A6).

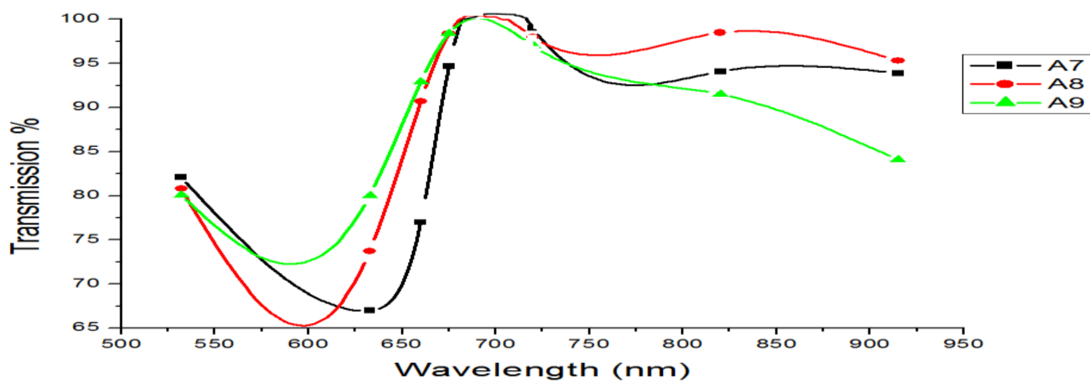

Fig (4-16): The transmission spectra of samples (A7, A8, A9).

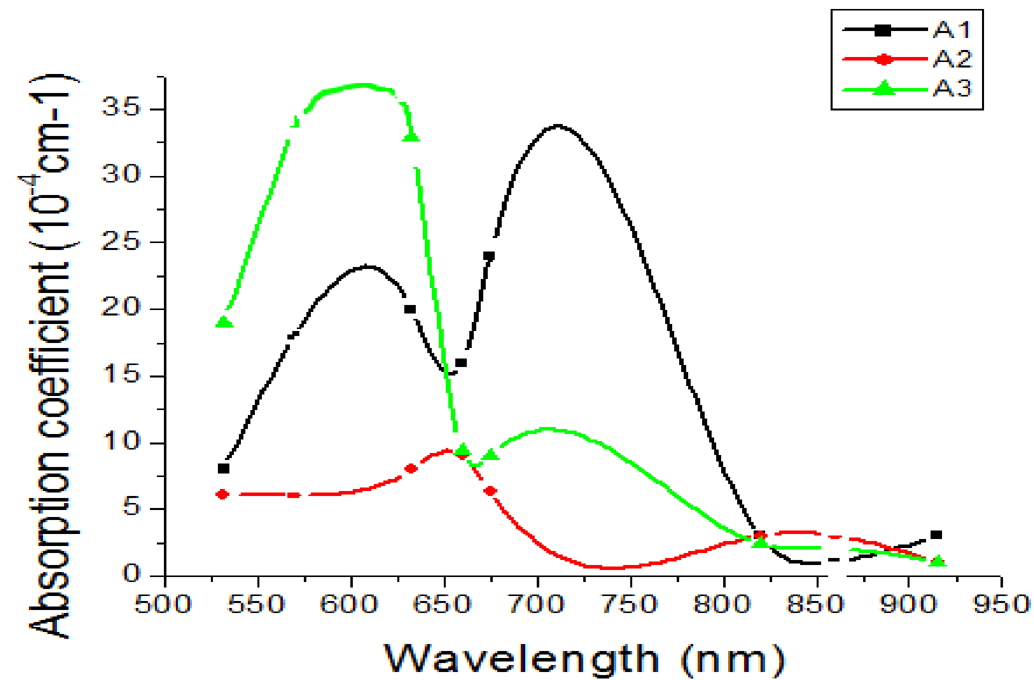

Fig (4.17): The absorption coefficients of samples (A1, A2, A3).

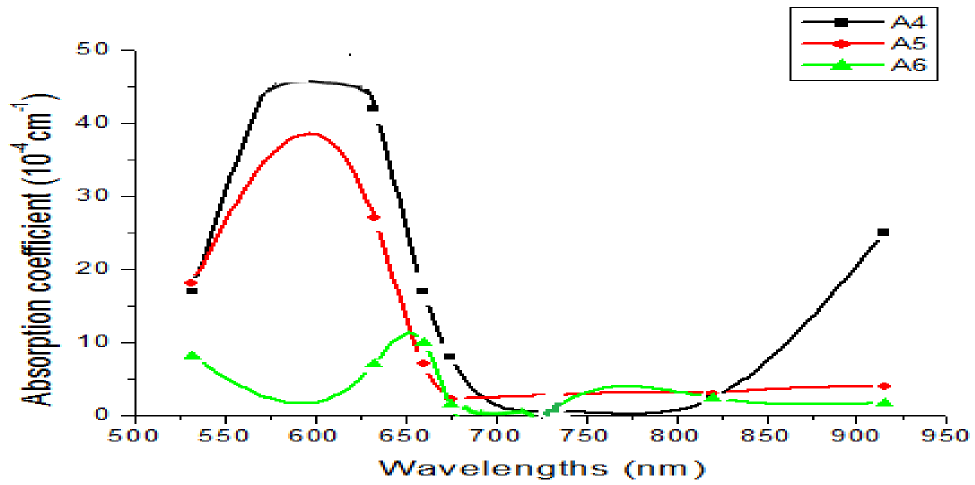

Fig (4.18): The absorption coefficients of samples (A4, A5, A6).

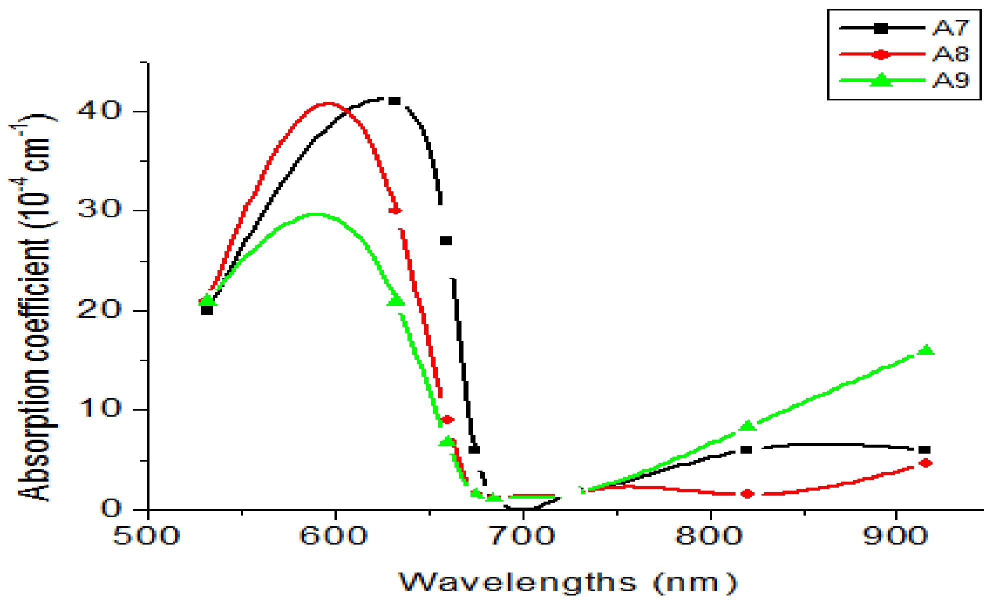

Fig (4.19): The absorption coefficients of samples (A7, A8, A9)

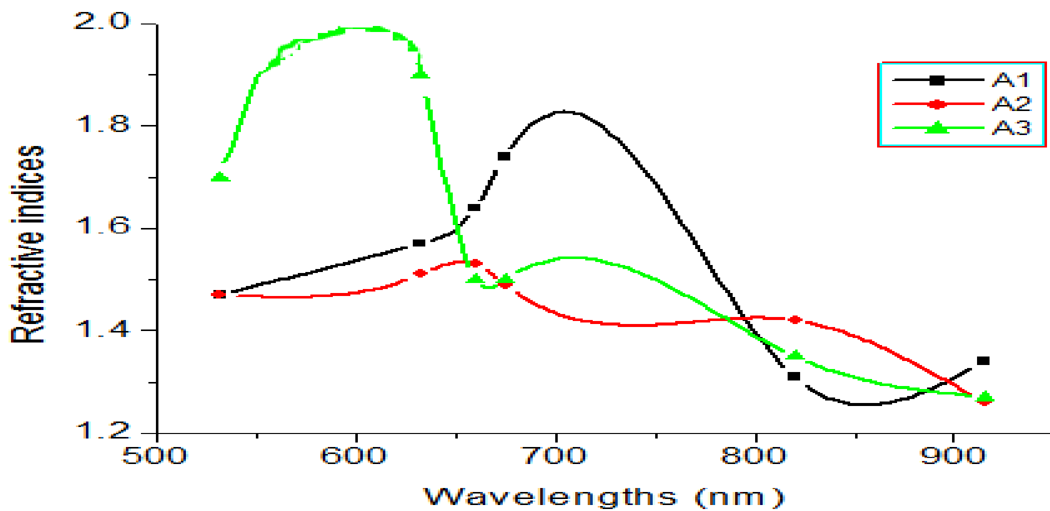

Fig (4.20): The refractive indices of samples (A1,A2,A3) .

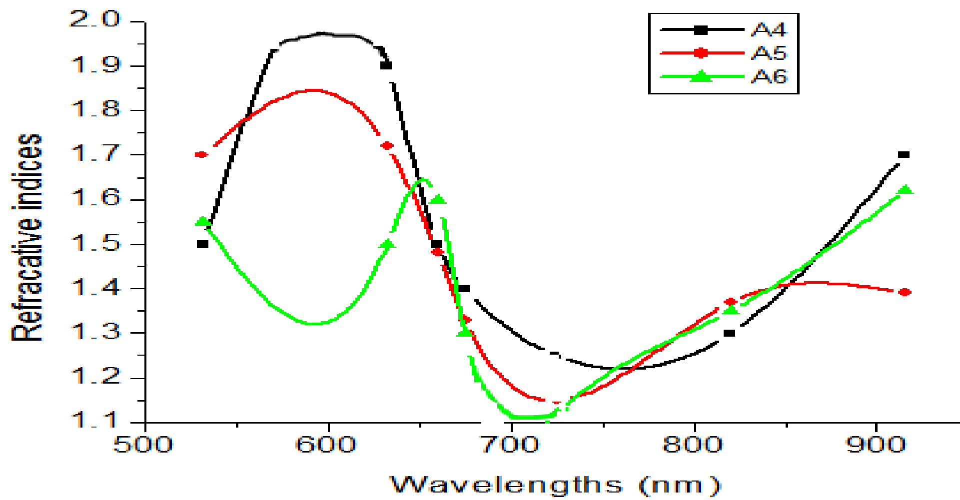

Fig (4.21): The refractive indices of samples (A4, A5, A6).

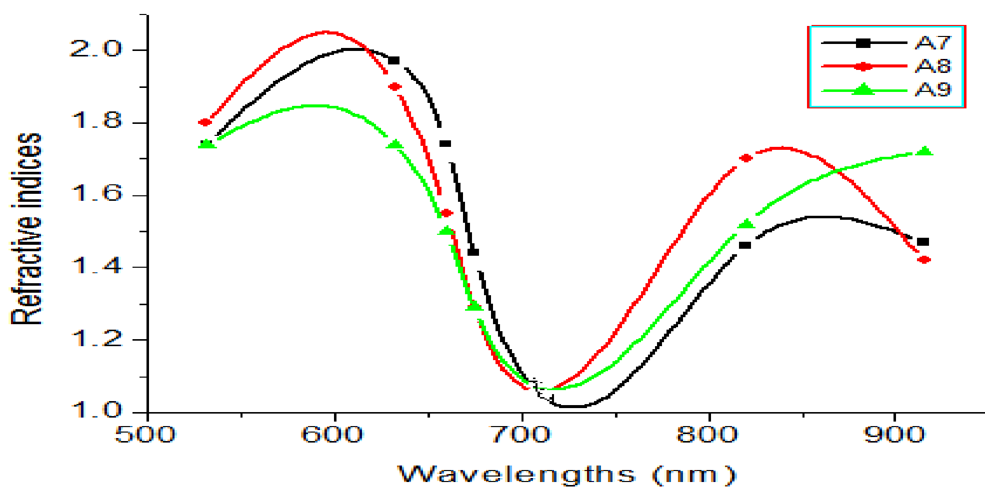

Fig (4.22): The refractive indices of samples (A7, A8, A9).

Typical results for the TiO_2 Transmission are shown in Figures (4.14) to (4.16). The figures show 9 samples of TiO_2 ((A_1, A_2, A_3), (A_4, A_5, A_6) and (A_7, A_8, A_9)), in three groups. In Fig (4.14) the transmission (%) for sample (A1) is very high at (532), (820) and (915) nm compared with the other wavelengths. It is a good indicter to use this property to produce an optical filter at these wavelengths. If we look to the transmission spectrum of sample (A2), one can see that the transmission percentages (> 90%), this indicates an optical transparency. Also for sample (A3) the average transmittance in the visible –near infrared part of the spectra (660-915 nm) is about 80-90%. For

the wavelength (632.8) nm, one can see that the transmission percentage is lower than other wavelengths.

As shown in Fig (4.15) it is clear that the fabricated TiO_2 thick film has a high transmission (≫ 80%) in the wavelengths (532), (660), (675), 820 and 915 nm. It is a good indicter to use this sample as a window in these wavelengths, but in the wavelength (632.8) nm the transmission percentage is 67%. This value indicates that this thick film can be used as reflector at this wavelength. Fig (4.16) shows a similar plot of the transmittance vs. wavelength for (A7, A8 and A9 samples) deposited on glass substrate at pulse energy of 700 mJ, with repetition rate 20, 30, and 40Hz, respectively. This figure shows that the transmission percentage increased by increasing the repetition rate in 532,632.8, and 660 nm, but in the 690 nm the three samples have the same transmission (=98%) which makes them suitable for sensor applications. The optical properties in the range from 500nm to 920nm at various R.R reveal that the transmittance depends on the thicknesses as shown in Fig (4-16). It is also found that the average transmittance of the TiO_2films exceeded 90% in the range (670-950) nm except sample A9 which showed a transmittance less than 90% at the wavelength 920nm. This indicates that this TiO_2film can be used as a window material in solar cells. For all the films analyzed it is observed that the optical transmittance decreases slightly with increasing the thickness and R.R.

Figures (4.17),(4.18) and (4.19) show the relationships between the absorption coefficient of samples (A_1,A_2,A_3), (A_4,A_5,A_6) and (A_7,A_8,A_9) and the wavelengths at laser pulse energy of 500 mJ,600 and 700mJ, and repetition rate 20,30,40 Hz. These figures supported the idea to use these samples as absorption filters or as reflectors in certain wavelengths, because the absorption coefficient of these films at these wavelengths are very large compared with other wavelengths. By noting the absorption coefficients at (820) and (915) nm for sample (A1), it may be used as a transmission filter, because its absorption coefficient at these wavelengths is very low.

Lastly, figures (4.20),(4.21)and (4.22) show a plot for the refractive indices of samples (A1,A2,A3) , (A4,A5,A6) and samples (A7, A8,A9) versus wavelength at pulse energy of 500, 600 and 700 mJ, respectively with repetition rates of 20,30,40 Hz . The values of the refractive index for these films varied between 1.2 to 2.2, one can see from figures (4.20), (4.21) and (4.22), that when the absorption coefficient is high, the refractive indices are also high at the same wavelengths.

4.4Theoptical properties of Al_2O_3 thick films:

Information concerning optical transmittance is important for evaluating the optical performance of the Al_2O_3 thin films. The optical transmittance spectrum of the Al_2O_3films deposited on glass substrate at 500, 600, 700mJ and at R.R (20, 30, 40Hz), respectively, are shown in figures below. Figure (4.23) shows the transmittance of the Al_2O_3 deposited on glass. As it can be seen, the Al_2O_3 films are optically transparent. At the wavelength of 660nm, the transmittance of the deposited films (B_1, B2) was found to be (>98%). In this figure the transmittance decreased as the R.R increased in the wavelengths range 500-675nm, but in range 675 -915nm, the transmittance spectra increased by increasing the repetition rate.

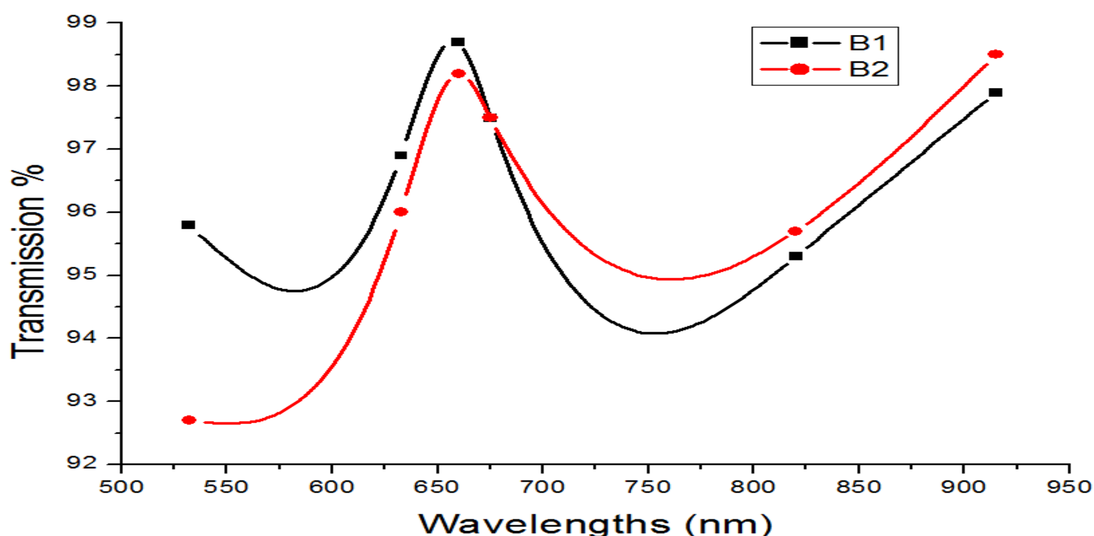

.

Fig (4.23): The transmission spectra of samples (B1, B2).

The transmission spectra of samples (B4, B5, B6) are illustrated in figure

(4.24). All the films exhibit high optical transparency (~ 80 %) in the visible and near infrared (NIR) range which is crucial in order to get films act as transparent conductive oxides (TCO) for solar cells (Stein Hauser, 2008).

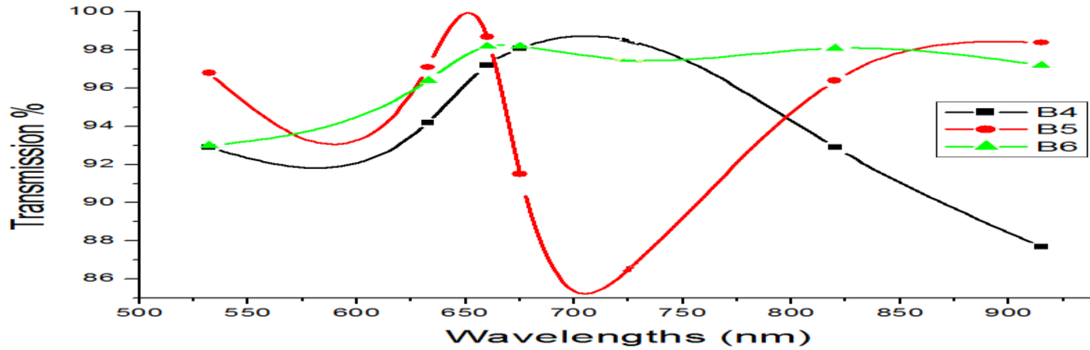

Fig (4.24): The transmission spectra of samples (B4, B5, B_6).

Figure (4.25) shows the transmittance of the alumina (Al_2O_3) coatings deposited on glass. One can observe the transmittance decreases slightly as the thickness of the samples increases, and that is due to the higher absorption of the films. Despite this fact, the transmittance is higher than 65% for all samples (B_7, B8, B9), this value indicates that this thick film can be used as reflector at these wavelengths

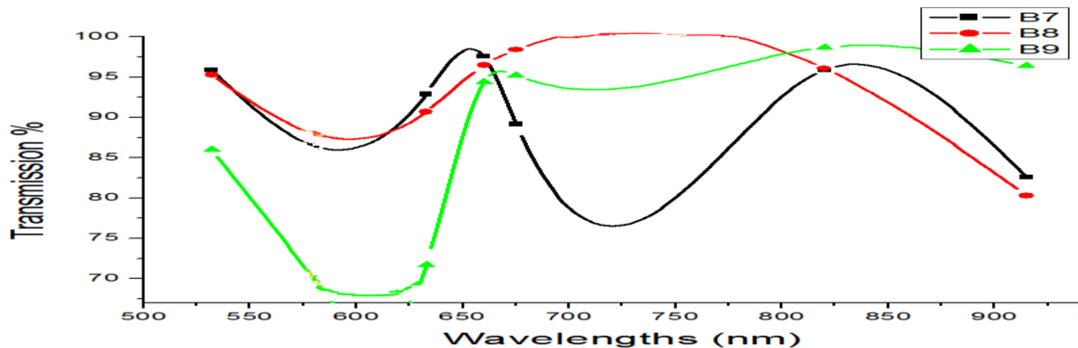

Fig (4.25): The transmission spectra of samples (B_7, B8, B_9).

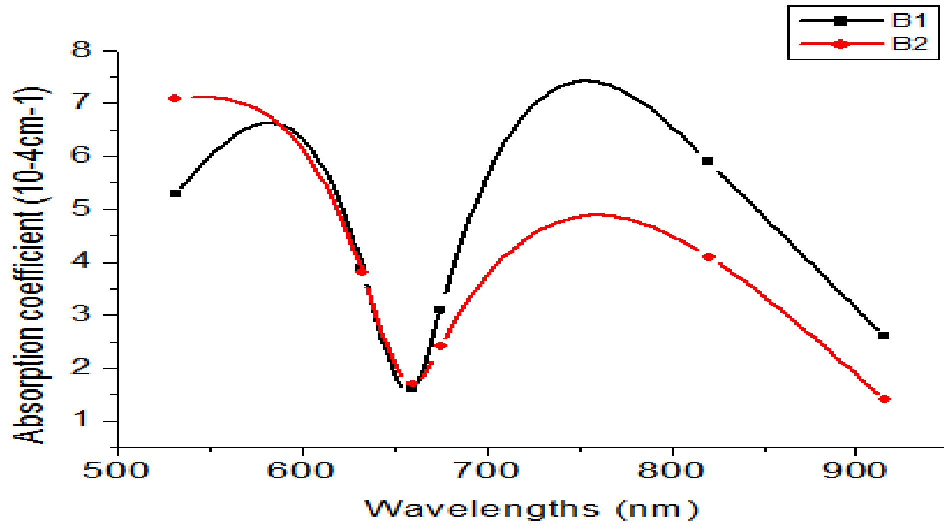

Fig (4.26): The absorption coefficients of samples (B_1, B2).

The relation between the absorption coefficients of (Al_2O_3) thick films and the wavelength is shown in Figure (4.26). The absorption coefficient of samples (B_1, B2) is found to be low ($\alpha=1.5\times10^{-4}cm^{-1}$) in the wavelength 655 nm and it is increased rapidly with the decrease in wavelength. This makes these thick films suitable to act as window in the solar cells.

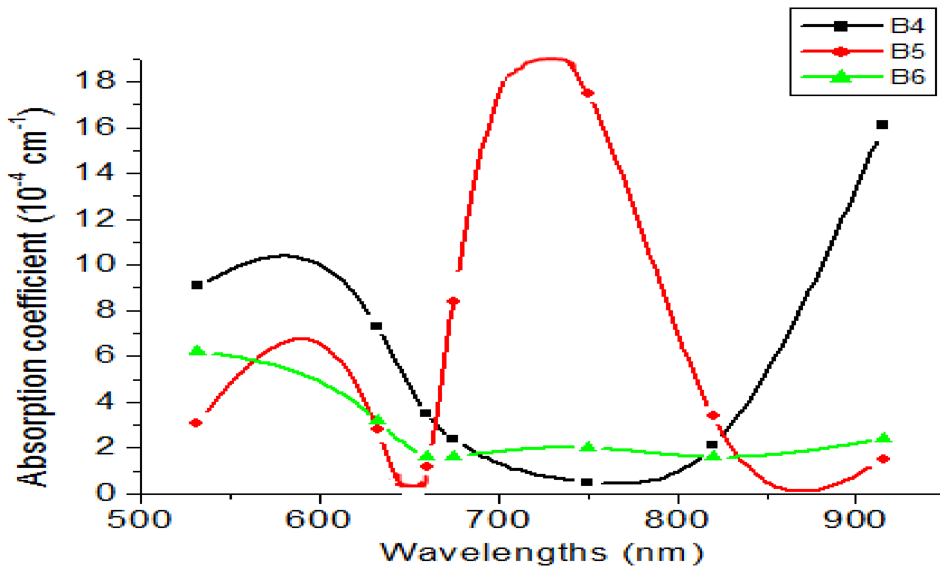

Fig (4.27): The absorption coefficients of samples (B4, B5, B6).

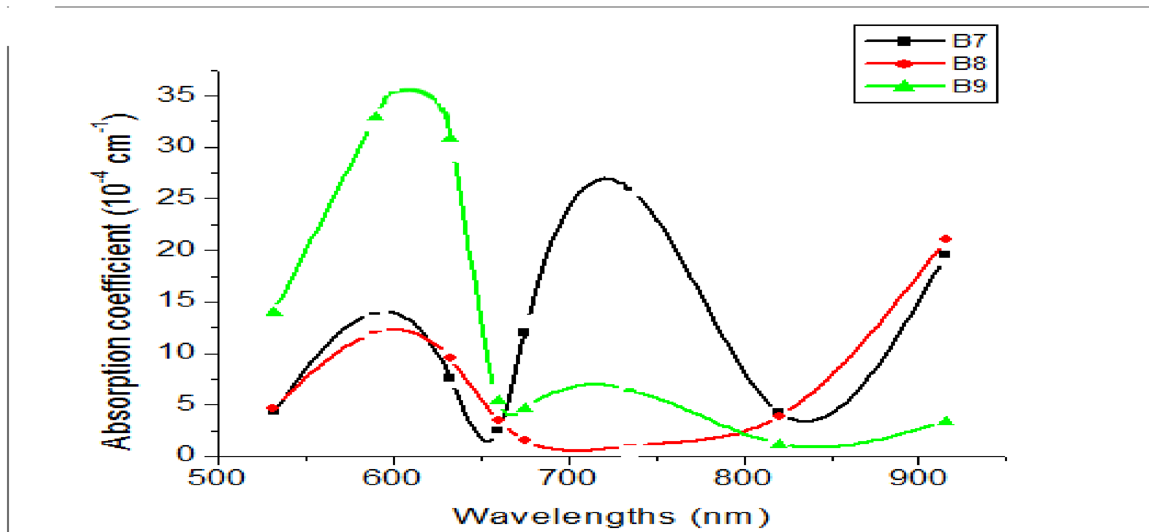

Fig (4.28): The absorption coefficients of samples (B7, B8, B9).

Figure (4.27) displays the absorption coefficient of samples (B4, B5, B6) as a function of wavelengths. Samples B5 and B4 have high absorption coefficients (= 18×10^{-4} cm^{-1} and $16\times10^{-4}cm^{-1}$) at 750 nm and 915 nm, respectively, but at the other wavelengths samples B4 and B6 have low absorption coefficient (< $3\times10^{-4}cm^{-1}$). These results show that the fabricated Al_2O_3 thick films could be used in solar cells due to their low absorbance in the visible region.

Fig (4.28)shows the plot of the absorption coefficients of samples (B7, B8, B9) versus wavelengths at pulse energy of 700 mJ with repetition rate of 20, 30, 40 Hz. These plots supported the idea to use these samples as absorption filters because the absorption coefficients of these films at wavelengths of 610 nm and 720 nm for samples B9 and B7 are very large compared with the other wavelengths. One can see from figure (4.28) that the absorption coefficient decreases slightly as the R.R increases.

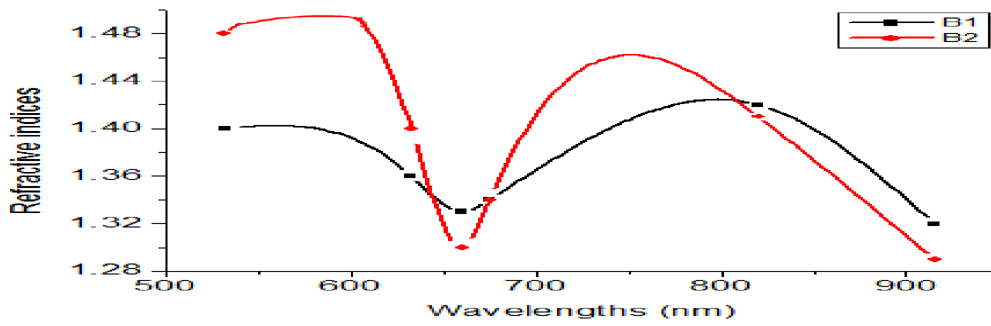

Fig (4.29): The refractive indices of samples (B_1, B2).

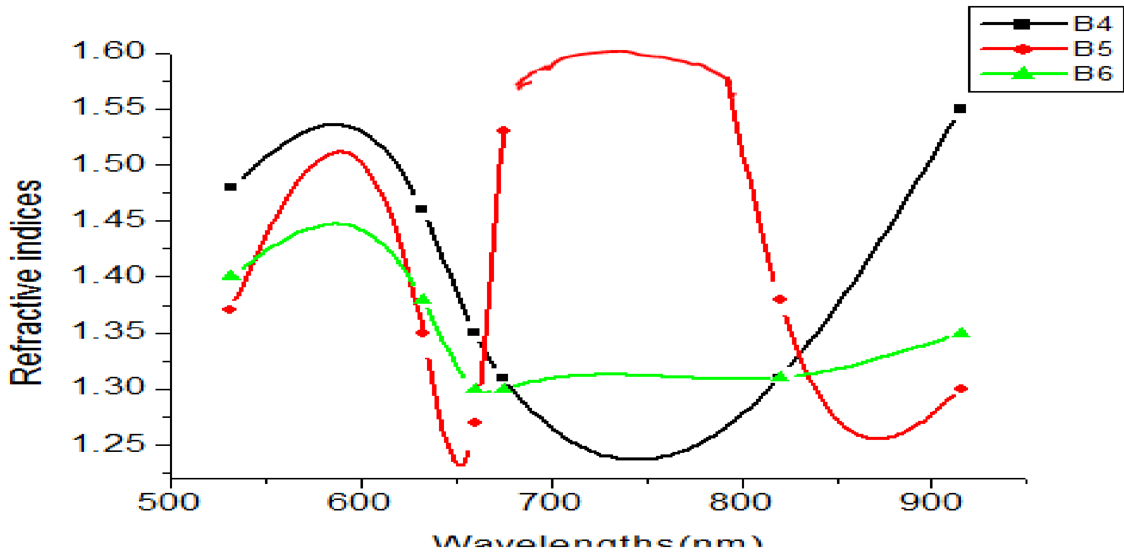

Fig (4.30): The refractive indices of samples (B_4, B5, B6).

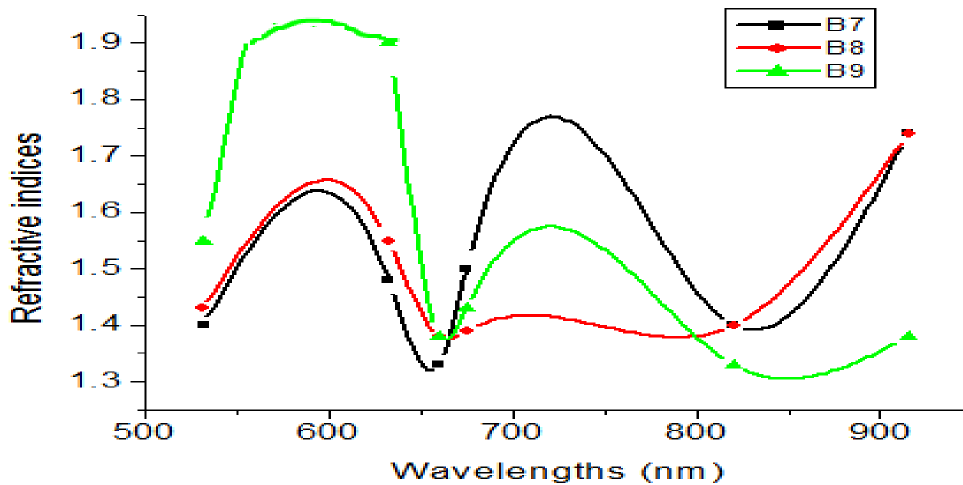

Fig (4.31): The refractive indices of samples (B7, B8, B9).

Fig (4.29) shows the relation between the refractive index of samples B7, B8 and B9 with the wavelengths. It is clear from this figure that the films are influenced by the film thicknesses. The refractive indices of these films are

slightly increases due to the increasing in the R.R and thicknesses. The refractive index can be determined from the reflectance (R) using the relation (4.2) (Habubi, 2012).

4-5 The optical properties of (ZnO) thick films:

The transmittance spectra of the ZnO films were measured to investigate their optical properties and they are shown in Figures (4.32), (4.33) and (4.34) which revealed an optical transmittance above 90%in the visible and near infrared range (500–920nm).

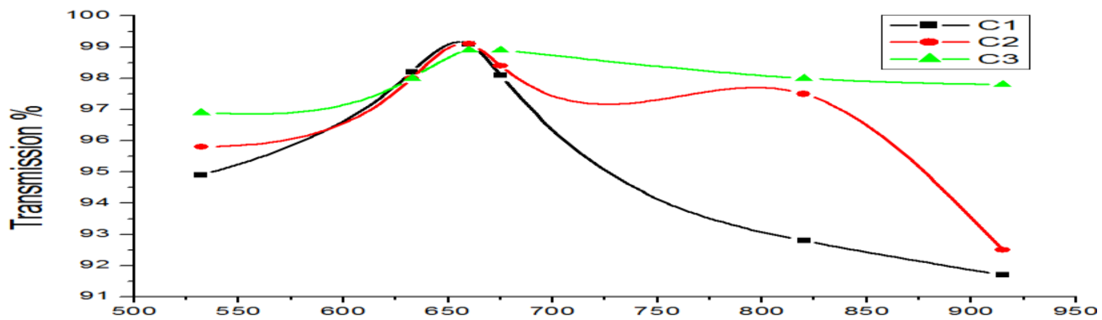

Fig (4.32): The transmission spectra of samples (C1, C2, C_3).

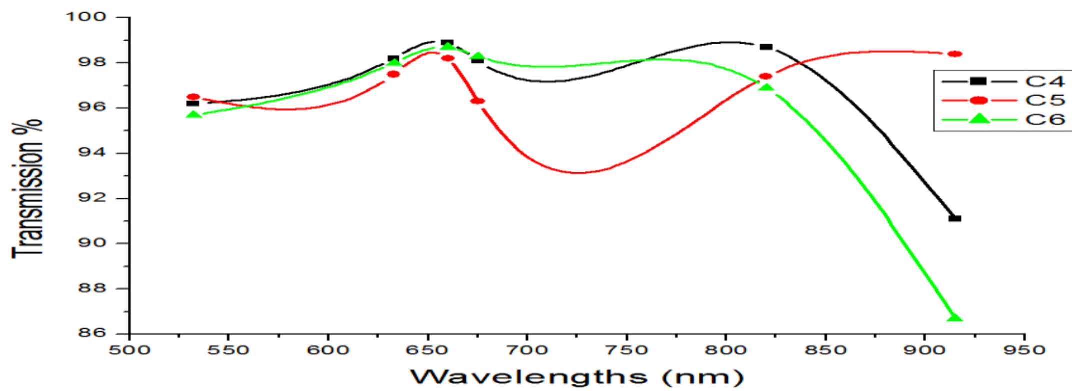

Fig (4.33): The transmission spectra of samples (C4, C5, C6).

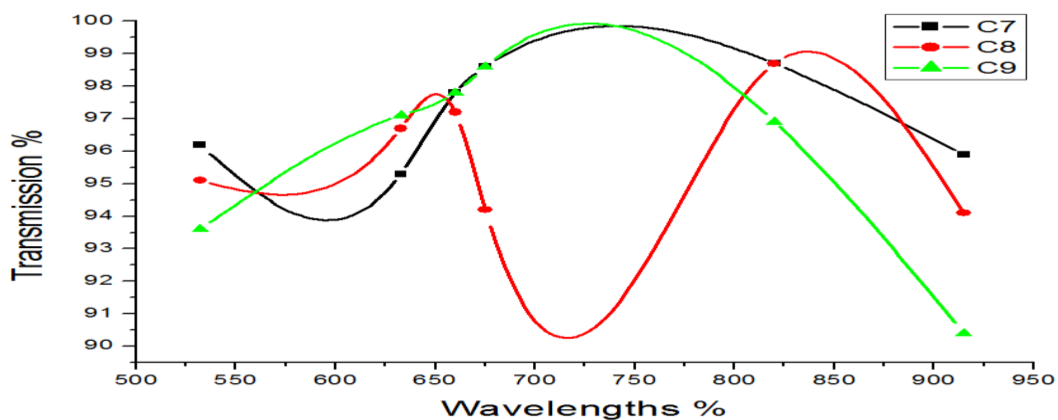

Fig (4.34): The transmission spectra of samples (C7, C8, C9).

From the transmission spectra it is clear that the transmission of the films increases with the increase of R.R. Sample C4 exhibits maximum transparency (98%). All other samples have over than 86% transparency in the visible region and it continuous to near infrared region. This value indicates that this film can be used as a window for solar cells (Sriram, 2012). The relation between the absorption coefficients of the thin films of ZnO, having different thickness, and the wavelengths are shown in figures (4.35)-(4.37). These figures reveal the low absorbance of these films in the visible region.

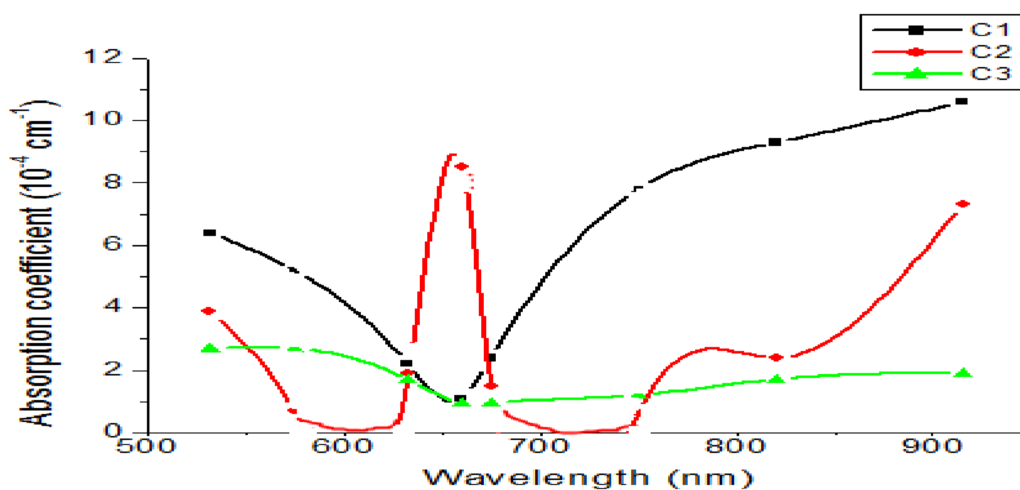

Fig (4.35): The absorption coefficients of samples (C_1, C2, C3).

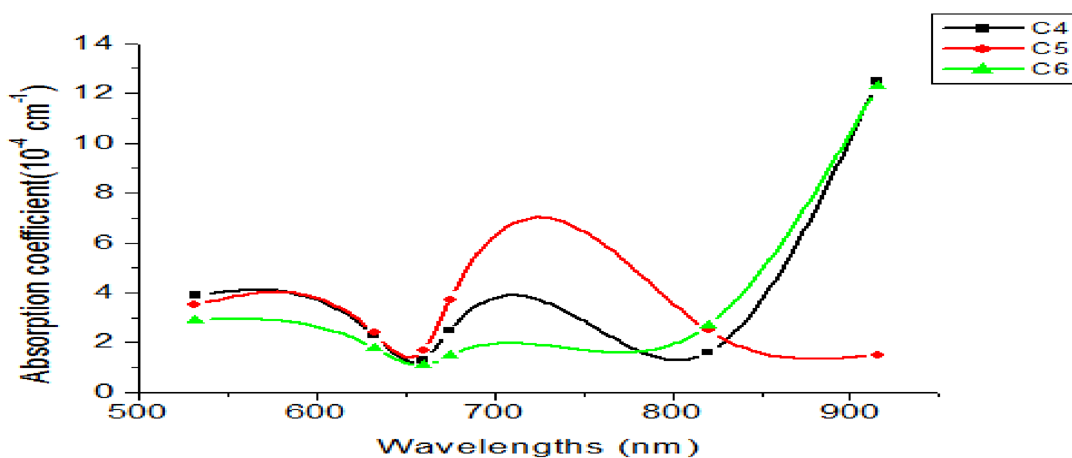

Fig (4.36): The absorption coefficients of samples (C4, C5, C6).

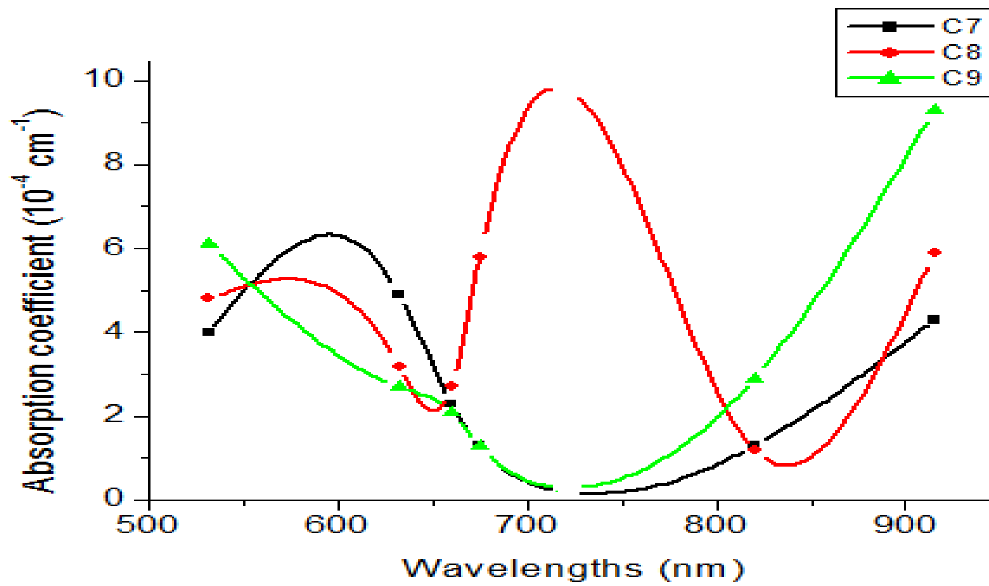

Fig (4.37): The absorption coefficients of samples (C7, C8, C9).

It can be noticed that the absorption coefficient increased with increasing the wavelength. Also it can be noticed that the absorption coefficient increased with the increasing of film thickness.

Studying the refractive index will complete the fundamental study of the optical properties and optical behavior of the material. The values of the refractive indices for the films at different R.R varied from 1.2 to 1.55. This is attributed to the structural characteristics of the films (Yahiya, 2010).

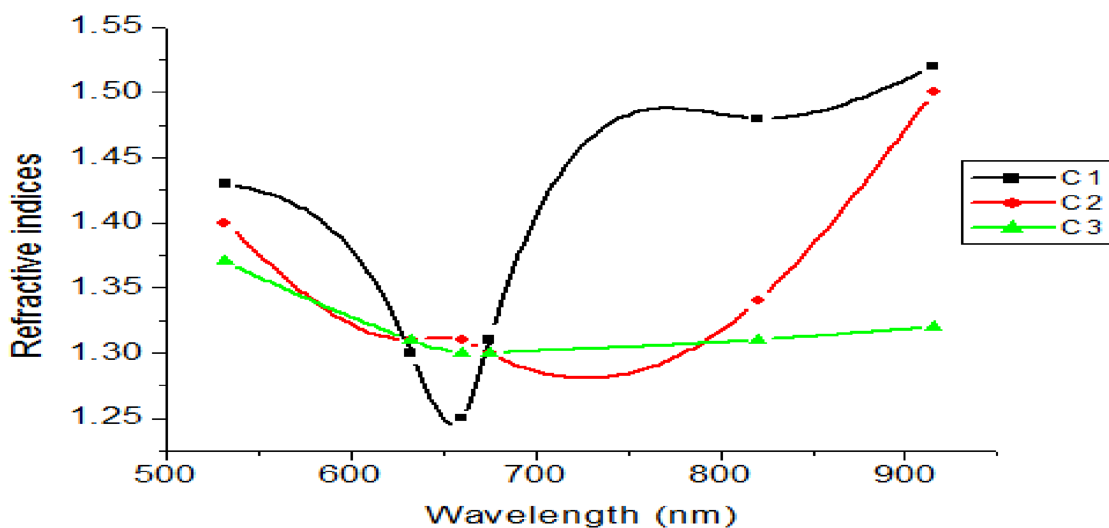

Fig (4.38): The refractive indices of samples (C1, C2, C3).

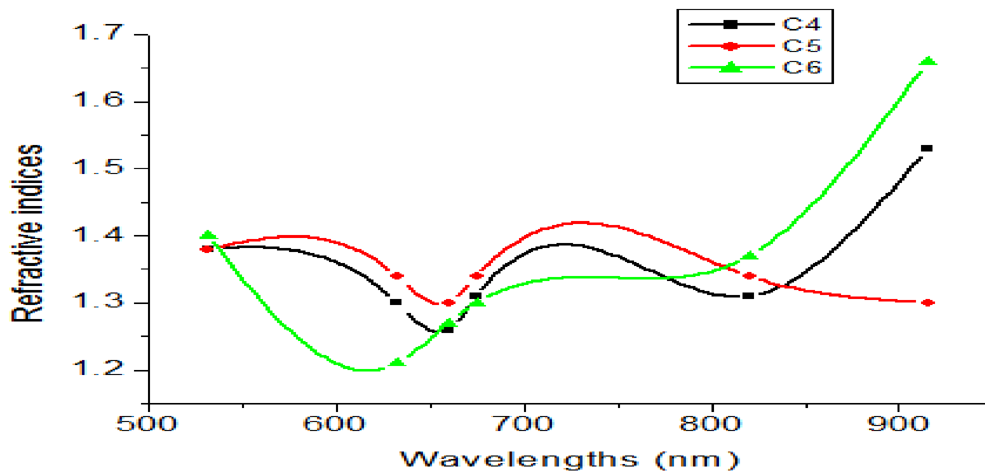

Fig (4.39): The refractive indices of samples (C4, C5, C6).

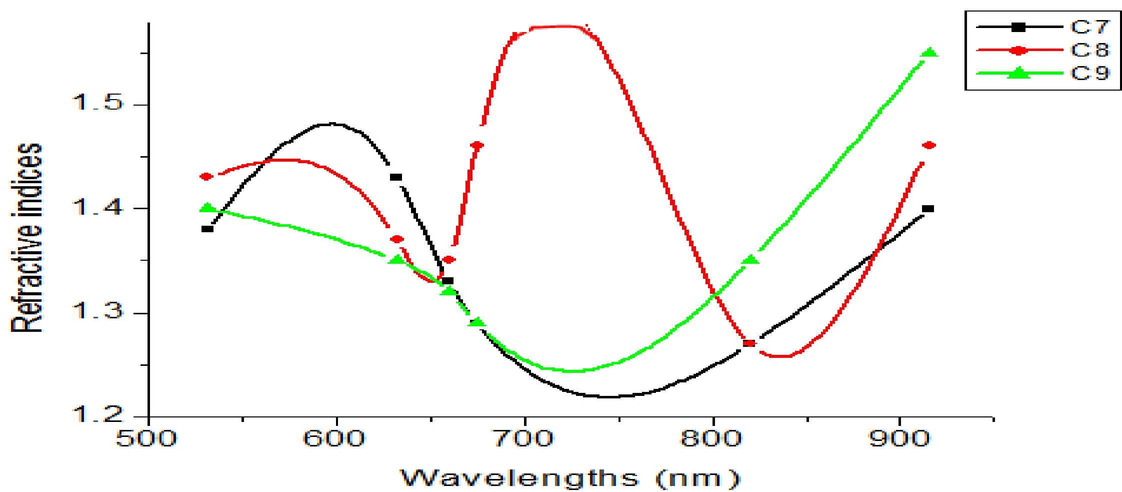

Fig (4.40): The refractive indices of samples (C7, C8, C9).

It is found that the refractive index at 632.5 and 675 nm is equal 1.3 compared with other wavelengths. The refractive index increased due to the increasing of R.R and thickness as can be seen in figure (4.40).

4.6 Conclusions:

From the results obtained in this work, one can conclude that:

1- The thickness of the thick film increased with the increasing of pulse energy and R.R.

2- The three materials can be used to produce optical components in the spectral range (532) to (915) nm.

3- The transmittance is higher than 65% for all samples of Al_2O_3, the refractive indices of these samples are slightly increases with the increase in the films thickness and R.R at different pulse energy.

4- ZnO films can be applied as solar cell window because of their high transmittance in the visible region.

5- The refractive index increased due to the increasing of R.R and thickness.

4.7 Recommendations:

The followings can be recommended as future work:

1- Fabrication of thick films of the same groups by pulsed laser deposition in chamber to decrease the contamination during deposition.
2- Measuring the thickness of the thick film by ellipsometry.
3- Annealing the glass substrate after deposition.
4- Increasing the number of laser sources to investigate the transmission spectrum of the thick films more accurately.

References

Allmen, M .V. Blatter, A. (1998), *Laser-Beam Interactions with Materials*

Anisimov, S. I. Bäuerle, D.and Luk yanchuk, B. S. (1993), Gas dynamics and film profiles in pulsed-laser deposition of materials. *Physical Review B,* 48(16), p. 12076.

Bae, S. H. Lee, S. Y. Jin B. J. and Im, S., (2000), *Pulsed Laser Deposition of ZnO Thin Films for Applications of Light Emission,* Appl. Sur. Sci. 154-155, P.458.

Bae, S. H. Lee, S. Y. Jin B. J.and Im, S. (2001), *Growth and Characterization of ZnO Thin Films Grown by Pulsed Laser Deposition"*, Appl. Sur. Sci. 169-170, P. 525.

Barik, S. Srivastava, A. K. Misra, P. Nandedkar R. V., Kukreja, L. M. (2003), *Alumina Capped ZnO Quantum Dots Multilayer Grown by Pulsed Laser Deposition,* Sol. Stat. Com. 127, P. 463.

Burnside, D.E., Macosko, C.W., and Scriven, B., (1989), Spin coating: Onedimensional model. *Journal of Applied Physics ,* 11(66), pp. 5185 -5186.

Cao, H. Wu, J Y. Ong, H. C. Dai, J. Y. and Change, P. H., (1998). Second harmonic generation in laser ablated zinc oxide thin films. *Applied Physics Letters ,* 73(5), pp. 572-574.

Chakrabarti, S. B. Doggett, R. O'Haire, E. McGlynn, M. O. Henry, A. Meaney, J. P. Mosnier, (2007), *Characterization of Nitrogen – Doped ZnO Thin Films Grown by Plasma- Assisted Pulsed LaserDeposition on Sapphire Substrates*, Superlattices and Microstructures 42, P. 21.

Cheung, J. , Horwitz, J., (2013), Pulsed Laser Deposition History and Laser-Target Interactions. *Materials Research Society,* 17(2), pp. 30-36.

Cho, S. (2006), *Structural and Optical Properties of ZnO Films Grown on Sapphire Substrates Subjected to Substrate Temperature*, J. of the Kor. Phys. Soc., 49, 3, P. 985.

Chowdhury, S. and Ichimura, M., (2010), Photochemical Deposition of GaSxOy Thin Films from Aqueous Solutions. *Japanese Journal of Applied Physics,* 49(6R).

Christoulakis, S. Suchea, M. Katharakis, M. Katsarakis, N. Koudoumas, E. And Kiriakidis, G. (2005), *ZnO Nanostructured Transparent Thin Films by PLD"*, Rev. Adv. Mater. Sci. 10, P. 331.

Coutal, C. Azéma, A. Roustan , J. C., (1996), Fabrication and characterization of ITO thin films deposited by excimer laser evaporation. *Thin Solid Films,* 288(1-2), p. 248–253.

Dijkkamp, D. Gozdz, A. S. and Venkatesan,T.,(1987), Evidence for the Thermal Nature of Laser-Induced Polymer Ablation. *Physical Review Letters,* 58(20), p. 2142.

Ehadi, S.E., (2007), *Utilization of Different Laser Systems to Determine the Optical Properties of Chloroform and Rhodamine 6G Thin-Films in Nanometer Scale*, M.Sc. Thesis in laser application in physics, College of Graduate Studies- Sudan University of Science and Technology.

Ferrante1, G. Zarcone1, M. and Uryupin, S. A., (2001), Inverse bremsstrahlung in a plasma with electron temperature anisotropy. *Phys. Plasmas,* 8(11), p. 4745.

FYu, C- Sung, Hann, S. Chen, Sun, S.J ,(2009)*, Relationship between the photoluminescence and conductivity of undoped ZnO thin films grown with various oxygen pressures,* Appl. Surf. Sci. 245, 5675.

Geohegan, Dr. David B., (2009), Distinguished Service Award, International Conference on Laser Ablation. *Materials Research Society,* 3(12), pp. 55-76.

Gossard, A. C., (1988), Growth of Microstructures by Molecular Beam Epitaxy. *Quantium eclctronic,* 22(9), pp. 1649-1652.

Grainger, S. Blunt, J., (1998), *Engineering Coatings, Design and Application.* 2nd ed. U.S.A: Woodhead Publishing.

Greer, J. A.Tabat, M. D.Lu, C., (1997), Future trends for large-area pulsed laser deposition. *Elsevier ,* 121(1), pp. 357-362.

Habubi, N. Oboudi, S. F. Chiad, S.S., (2012), Study of some optical properties of mixed SnO2-CuO Thin Films,*Nano- and Electronic Physics* · Vol. 4No 4, (January 2012) 04008(4pp).

Han, Mei .L. Liu .C, Pedro. C., Alves .E., (2008),*Comparison of ZnO Thin Films Grown by Pulsed Laser Deposition on Sapphire and Si Substrate*, Physica E 40 ,P. 699.

Hansen, T.N., (1997), *UV laser ablation of metals in vacuum*. M.Sc. Thesis in Danish: University of Copenhagen.

Higgins, B. G., (1986), Film flow on a rotating disk. *Physics of Fluids,* 29(11), p. 3522.

Horwitz J.S., and Sprague, J.A., (2009*), Film nucleation and film growth in pulsed laser deposition of ceramics*, in ref. 3, pp.229-254.

Hubler, G. K., (1994), *Comparison of vacuum deposition techniques, in pulsed laser deposition of thin films.* 327 ed. New York: John Wiley & Son.

Jagadish, P., (2006),*Zinc Oxide Bulk, Thin Films and Nanostructures Processing, Properties, and Applications,* U.S.A: Elsevier Science,Hugonnot, E. Delville, M. Deliville,J. (2007), Statistical physics. *Physical Review E,* 75(6).

Jianting, H. Huizhao, X. Chengshan, Z. ShuyunH. Lijun, and X. Shoubin, (2006), *Effect of SubstrateTemperature on Microstructural and Optical Properties of ZnO Films Grown by Pulsed Laser Deposition*, Rare Metals. 25, 2, P. 161.

Jin, B. J. Woo, H. S. Im, S. Bae, S. H. Lee, S. Y, (2001), *Relationship between Photoluminescence and Electrical Properties of ZnO Thin Films Grown by Pulsed Laser Deposition*, Appl. Sur. Sci. 169-170 P. 521.

Jo, J. H. Kwak, J. S. Kwon, Y. H. Hwang D. Y.and Kim, H. K. (2005), *Effects of Oxygen Pressure on the Crystalline of ZnO Films Grown on Sapphire by PLD Method"*, J. of the Kor. Phys. Soc., 47,P. S300.

Joseph, M., Tabata, H., Sacki, H., Ueda, K., Kawai,T.,(2001),*Fabrication of the low-resistive p-type ZnOby codoping method*, Physica B302-303 :P 140-141.

Kaczmarek, S.M., (1997), *Pulsed laser deposition--today and tomorrow*,warsaw, Poland: Slawomir Kaczmarek.

Kaidashev, E. M. Lorenz, M .Wenckstern, A. Rahm, H. C. Semmelhack, (2003) *,High Electron Mobility of Epitaxial ZnO Thin Films on c- Plane Sapphire Grown by Multistep Pulsed – Laser Deposition*, Appl. Phys. Lett. 82, 22, P. 3901.

Kamiya Toshio, a. H., (2005), Electronic Structures and Device Applications of Transparent Oxide Semiconductors: What Is the Real Merit of Oxide Semiconductors?. *Applied Ceramic Technology,* 2(4), p. 285–294.

Kang, H. S. Kim, G. H. Lim, S. H. Chang, H. W. , Lee, S. Y.(2008), *Relation Between Ultraviolet Emission and Electron Concentration of ZnO Thin Films"*, Thin Solid Films, 516 ,P. 3147.

Khoshhesab, M. Sarfaraz,M. and Asadabad, A., (2012), Preparation of ZnO nanostructures by chemical precipitation method,. *Synthesis and Reactivity in Inorganic, Metal-Organic and Nano-Metal Chemistry,,* 41(7), p. 814–819.

Kim, B.I. Kim, S.C. Shin, B.C. Kim, T.S. Jung, M.Y. Yu, Y.S. (2006), *High-Pressure Oxygen Treatment of ZnO Thin Films*, Physica B 376–377, P752.

Kim, S. S. Lee, B. T. (2004), *Effect of Oxygen Pressure on the Growth of Pulsed Laser Deposited ZnO Films on Si (001)*, Thin Solid Films 446, P. 307.

Larson, T., (1996), Measuring Haze on Deposited Metals with Light-Scatteringbased Inspection Systems,. *Micro,* 14(8), p. 310.

Liu, M. Sun, G. Z.G. Zhang, X.Q. Wei, C.S. Chen, C.S. Xue, and B.Y. Man, (2006), *Effects of Focus Lens Position on Pulsed Laser Deposition of ZnO Films*, Eur. Phys. J. Appl. Phys. 34, P. 73.

Liu, M. Wei, X.Q. Zhang, Z.G. Sun, G. Chen, C.S. Xue, C.S. Zhuang, H.Z. Man, B.Y. (2006), *Effect of Temperature on Pulsed Laser Deposition of ZnO Films"*, Appl. Sur. Sci. 252, P. 4321.

Look, D. C., Reynolds, D. C., Litton, C. W., Jones, R. L., Eason, D. B., & Cantwell, G. (2002), *Characterization of Homoepitaxial p-Type ZnO Grown by Molecular Beam Epitaxy.* puplished Phd thesis.American Institute of Physics.

Lorenz, M. Hochmuth, H. Lenzner, J. Nobis, T. Zimmermenn, G. Diaconu, M. Schmidt, H. Wenckstern, H. V., Grundmann, M. (2005), *Room-Temperature Cathodoluminescence of n-Type ZnO Thin Films Grown by Pulsed Laser Deposition In N2, N2O and O2 Background Gas*, Thin Solid Films 486, P. 205.

Lowndes, H. D, Rouleau, M. C, Geohegan, D. B, Puretzky, A. A, Strauss, M.A, Pedraza, A. J., Park, J.W., Budal and Poker, D. B., (1998), *Pulsed Laser Ablation Growth and Doping of Epitaxial Compound Semiconductor Films*, Mat. Res.Soc.Vol.397. P. 107-118.

Macleod, H.A., (1987), Thin – Film Optical Coatings, *Applied Optics and optical Engineering,* Academic Press, San Diego, Vol. 10.

Marozau, I. Shkabko, A. Döbeli, M. Lippert, T. Mallepell, M. Schneider, C.W. Weidenkaff, A. Wokaun, A. (2011), *Pulsed laser deposition and characterisation of perovkite-type* $LaTiO_{3-x}N_x$ *thin films* Acta Material. 59, 7145.

Max., B. Emil., W, (2005), *Principles of optics Electromagnetic theory of propagation,.* Edinburgh: cambridge university press.

Meaney, A. Duclere, J. R. McGlynn, E. Mosnier, J. P. O'Haire, R. Henry, M.O. (2005), *Comparison of Structural, Optical and Electrical Properties of Undoped ZnO Thin Films Grown on r - and c-Al2O3 Substrates Using Pulsed Laser Deposition"*, Superlattices and Microstructures 38, P. 256.

Mohamed, A. A, (2015), *Effect of Laser Pulse Energy and Repetition Rate on Optical Transmittance Spectra of Fe2O3 Thin Films*, M.Sc. Thesis in

Laser application in physics; College of Graduate Studies – Sudan University of Science and Technology.

Mousa A.M. and Ponpon, J.P., (2006), *Growth of Pb Te films by laser induced evaboration of pressed Pb Te Pellets,* Eur. Phys. J. Appl. Phys. 34 (01): 1-5

Nakata, Y. Okada, T. Maeda, M. (2002), *Deposition of ZnO Film by Pulsed Laser Deposition at Room Temperature*, Appl. Suf. Sci. 197-198, P 368.

Narayana, M. V . Gibson, J. M., (2002), *Handbook of Thin Film Deposition.* 2nd ed. California: William Andrew.

Novotny, M. Duclere, J. R. McGlynn, E. Henry, M. O'Haire, O. Mosnier, J. P. *Nitrogen Doping of ZnO Thin Films Grown by Plasma- Assisted Pulsed Laser Deposition*, J. of Phys.: Conference series 59 P. 505.

Park, M. C., Yoon, W. H., Lee, D. H.Myoung, J. M. Bae, S. H. Lee S. Y. and Yun, I. (2002), *Effect of Misfit Strain on Properties of ZnO Films Grown by Pulsed Laser Deposition*, Mat. Res. Soc. Symp. Proc. 696. P. N3.25.1.

Podder, J. Kobayashi, R. Ichimura, M. (2005), Photochemical deposition of Cu x S thin films from aqueous solutions. *Thin Solid Films,* 472(1), pp. 71-75.

Premkumar, P. Manoravi, Panigrahi, K. Baskar, T. (2009), *Particulate assisted growth of ZnO nanorods and microrods by Pulsed; laser deposition*, Appl. Surf. Sci. 255, 6819.

Ramamoorthy, K. Sanjeeviraja, C. Jayachandran, M. Sankaranarayanan, K. Pankaj Misra, Kukreja, L.M. (2006), *Development of a Novel High Optical Quality ZnO Thin Films by PLD for III–V Optoelectronic Devices*, Cur. Appl. Phys. 6, P. 103.

Sans, J. A. Segura, A. Mollar, M. Mari, B. (2004), *Optical Properties of Thin Films of ZnO Prepared by Pulsed Laser Deposition*, Thin Solid Films 453-454, P. 251.

Sezer, B. S, (2010), *Fabrication of Lu doped YBCO thin films by pulsed laser deposition technique and their characterization*. Published M.Sc. Thesis, *Physical Principles and Applications*, [Online] Available From:

http://download.springer.com/static/pdf/442/bok% [Downloaded: 24 February 2016].

Shan, F. K. Shin, B. C. Jang, S.W. Yu, Y. S. (2004), *Substrate Effect of ZnO Thin Films Prepared by PLD Technique,* J. of the Eur. Cer. Soc. 24, P. 1015.

Singh, R. K. Narayan, J., (1998), Pulsed-laser evaporation technique for deposition of thin films: Physics and theoretical model. *Physical Review B,* 41(13), p. 8843.

Smith, D., (1995), *Thin-Film Deposition: Principles and Practice.* 1st Edition ed. New York: McGraw-Hill.

Sriram, S. and Thayumanavan , A., (2012), Optical and electrical properties of Nitrogen Doped ZnO Thin Films Prepared by Low Cost Spray Pyrolysis Technique, *Journal of Electron Devices*, 15, pp. 1215-1224.

Stein .Hauser. J., (2008), *Deposition Zinc Oxide for Silicon Thin Film Solar Cells Optical and Electric Properties,* Unpublished PhD thesis, University of Neuchatel Institute of MicrotechnologyI.

Suchea, M. Christoulakis, S. Katharakis, M. Katsarakis N.and Kiriakidis, G. (2005), *Surface Characterization of ZnO Transparent Thin Films*, J. of Phys. Conference Series 10, P. 147.

Sui, C., Chen. N., Xu, X., Wei, G., Cai, P., Zhou, H.,(2008) , *High–Temperature- Dependent Optical Properties of ZnO Film on Sapphire Substrate*, Thin Solid Films, 516,P. 1137.

Sun, Y. W. Gospodyn, J. Kursa, P. Sit, J. DeCorby, R. G. Tsui, Y. Y. (2005), *Dense and Porous ZnO Thin Films Produced by Pulsed Laser Deposition*, Appl. Sur. Sci. 248, P. 392.

Szela, W., Sloyan, A., Parsonage, L., Mackenzie, I., Eason, W.,(2013), Laser operation of a Tm:Y2O3 planar waveguide. *Optics Express,* 21(10), pp. 12460-12468.

Tonooka, K. Te-Wei, C. Kikuchi, N., (2009), Preparation of transparent conductive TiO. *Applied Surface Science* , 255(12), p. 9695–9698.

Toshio, K, and Hideo. H., (2005), Electronic Structures and Device Applications of Transparent Oxide Semiconductors: What Is the Real Merit of Oxide Semiconductors?. *Applied Ceramic Technology,* 2(4), p. 285–294.

Vilanova. (2006), *Development of a Thick Film Gas Sensor for Oxygen Detection at Trace Levels*, Published PhD Thesis, University College Tarragona.

Villanueva, Y. D. Liu, P. T. Cheng, (2006*), Pulsed Laser Deposition of Zinc Oxide*, Thin Solid Films.501, P. 366.

Wei. X., Zhang .Q. Z, Yu. Y. X., Man. B. Y., (2009)*, Comparative Study on Structural and Optical Properties of ZnO Thin Films Prepared by PLD Using ZnO Powder Target and Ceramic Target,* Optics & Laser Technology , Article in press.

Yamaguchi, H. Komiyama, T. Yamada, K. Sato, T. Aoyama, (2007), *Fabricated of ZnO Films by PLD Method with Bias Voltage* , Physica B 401-402, P. 391.

Yousif, A., (2010)**,** *Characterization of ZnO Film Grown on Different Substrates Using PLD*, Ph.D Thesis in Bagdad*:* University of Technology.

Zeng, J. N. Low, J. K. Ren, Z. M. Liew, T. Lu, Y. F. (2002), *Effect of Deposition Condition on Optical and Electrical Properties of ZnO Films Prepared by Pulsed Laser Deposition*, Appl. Sur. Sci. 197-198P.362.

Zhao, J. . Hu, L W. Liu, Z. Wang, (2007), *Properties of ZnO Thin Films Grown on Si Substrates in Vacuum and Oxygen Ambient by Pulsed Laser Deposition*, Appl. Sur. Sci. 253, P. 6255.

Zhao, J. Lian, Y. Liu, Q. Jian, (2006) *,Structural and Optical Properties of ZnO Thin Films Deposited on Quartz Gla,, ss by Pulsed Laser Deposition*, Appl. Sur. Sci. 252, P 8451.

Zhaoyang, Lizhong, W. H., (2009)*, Effect of Oxygen Pressure on the Structural and Optical Properties of ZnO Thin Films on Si (111) by PLD,* Vacuum 83, P.906.

Zhao-Yang, W. Li-Zhong, H. Z. Jie, S. Jie, W. Zhi-jun, (2005), *Effect of The Variation of Temperate on The Structural and Optical Properties of ZnO Thin Films Prepared on Si (111) Substrate Using PLD*, Vac. 78, P. 53.

Zhu, B. L. Sun, X. Z. Zhao, F. H. Su, G. H. Li, X. G. Wu, J. Wu, R. Wu, Liu. J., (2008), *The Effect of Substrate Temperature on The Structure and Properties of ZnO Films Prepared by Pulsed Laser Deposition*, Vac. 82, P. 495.

Appendix

Table (1): The incident and transmitted intensity of different lasers wavelengths for sample A_1

λ((nm)	I_0(v)	I(v)
532	386	362
632.8	452	384
660	466	408
675	400	329
820	437	428
915	501	488

Table (2): The incident and transmitted intensity of different lasers wavelengths for sample A_2

λ(nm)	I_0(V)	I(V)
532	386	362
632.8	451	415
660	466	425
675	400	374
820	448	427
915	497	492

Table (3): The incident and transmitted intensity of different lasers wavelengths for sample A_3

λ(nm)	I_0(V)	I(V)
532	399	320
632.8	448	310
660	466	418
675	400	360
820	439	427
915	500	494

Table (4): The incident and transmitted intensity of different lasers wavelengths for sample A_4

λ(nm)	I_0(V)	I(V)
532	388	340
632.8	450	318
660	466	406
675	382	358
820	413	405
915	498	406

Table (5): The incident and transmitted intensity of different lasers wavelengths for sample sample A_5

λ(nm)	I_0(V)	I(V)
532	377	312
632.8	452	340
660	466	433
675	382	373
820	397	384
915	461	443

Table (6): The incident and transmitted intensity of different lasers wavelengths for sample A_6

λ(nm)	I_0(V)	I(V)
532	370	337
632.8	450	417
660	466	415
675	372	366
820	442	430
915	503	493

Table (7): The incident and transmitted intensity of different lasers wavelengths for sample A_7

λ(nm)	I_0(V)	I(V)
532	382	314
632.8	452	303
660	466	361
820	413	389
915	499	469

Table (8): The incident and transmitted intensity of different lasers wavelengths for sample A_8

λ(nm)	I_0(V)	I(V)
532	427	343
632.8	454	335
660	466	423
675	381	375
820	419	413
915	496	473

Table (9): The incident and transmitted intensity of different lasers wavelengths for sample A_9

λ(nm)	I_0(V)	I(V)
532	419	336
632.8	455	364
660	466	433
675	675	675
820	400	366
915	498	419

Table (10): The incident and transmitted intensity of different lasers wavelengths for sample B_1

λ(nm)	I_0(V)	I(V)
532	388	372
632.8	454	440
660	466	460
675	402	392
820	430	410
915	498	485

Table (11): The incident and transmitted intensity of different lasers wavelengths for sample B_2

λ(nm)	I_0(V)	I(V)
532	384	356
632.8	455	437
660	466	458
675	402	393
820	424	406
915	499	487

Table (13): The incident and transmitted intensity of different lasers wavelengths for sample B_4

λ(nm)	I_0(V)	I(V)
532	381	354
632.8	452	426
675	371	364
820	425	418
915	499	438

Table (14): The incident and transmitted intensity of different lasers wavelengths for sample B_5

λ(nm)	I_0(V)	I(V)
532	379	367
632.8	452	439
660	466	460
675	401	367
820	428	413
915	500	492

Table (15): The incident and transmitted intensity of different lasers wavelengths for sample B_6

λ(nm)	I_0(V)	I(V)
532	387	360
632.8	451	435
660	466	458
675	401	394
820	434	426
915	500	486

Table (16): The incident and transmitted intensity of different lasers wavelengths for sample B_7

λ(nm)	I_0(V)	I(V)
532	391	375
632.8	452	420
660	466	455
675	383	342
820	424	407
915	500	413

Table (17): The incident and transmitted intensity of different lasers wavelengths for sample B_8

λ(nm)	I_0(V)	I(V)
532	383	365
632.8	456	414
660	466	450
675	383	377
820	413	397
915	498	400

Table (18): The incident and transmitted intensity of different lasers wavelengths for sample B_9

λ(nm)	I_0(V)	I(V)
532	381	328
632.8	450	323
660	466	440
675	380	362
820	402	397
915	457	441

Table (19): The incident and transmitted intensity of different lasers wavelengths for sample C_1

λ(nm)	I_0(V)	I(V)
532	379	360
632.8	455	447
660	466	462
675	382	375
820	418	388
915	498	457

Table (20): The incident and transmitted intensity of different lasers wavelengths for sample C_2

λ(nm)	I_0(V)	I(V)
532	388	372
632.8	453	444
660	466	462
675	382	376
820	414	404
915	499	462

Table (21): The incident and transmitted intensity of different lasers wavelengths for sample C_3

λ(nm)	I_0(V)	I(V)
532	389	377
632.8	453	444
660	466	461
675	382	378
820	411	403
915	458	402

Table (22): The incident and transmitted intensity of different lasers wavelengths for sample C_4

λ(nm)	I_0(V)	I(V)
532	378	364
632.8	454	446
660	466	461
675	382	375
820	410	405
915	498	454

Table (23): The incident and transmitted intensity of different lasers wavelengths for sample C_5

λ(nm)	I_0(V)	I(V)
532	376	363
632.8	453	442
660	466	458
675	384	370
820	399	389
915	447	440

Table (24): The incident and transmitted intensity of different lasers wavelengths for sample C_6

λ(nm)	I_0(V)	I(V)
532	380	364
632.8	453	444
660	466	460
675	367	361
820	379	385
915	498	432

Table (25): The incident and transmitted intensity of different lasers wavelengths for sample C_7

λ(nm)	I_0(V)	I(V)
532	374	360
632.8	454	433
660	466	456
675	368	363
820	400	395
915	446	428

Table (26): The incident and transmitted intensity of different lasers wavelengths for sample C_8

λ(nm)	I_0(V)	I(V)
532	370	352
632.8	456	441
660	466	453
675	384	362
820	400	395
915	445	419

Table (27): The incident and transmitted intensity of different lasers wavelengths for sample C_9

λ(nm)	I_0(V)	I(V)
532	378	354
632.8	452	439
660	466	456
675	402	387
820	394	382
915	449	406

Table (28): The transmission, reflectance, absorption coefficient and refractive indices of different lasers wavelengths for sample A_1

λ(nm	T%	R	α($10^{-4}cm^{-1}$)	n
532	93.7	0.063	8	1.47
632.8	84.9	0.151	20	1.57
660	87.5	0.125	16	1.64
675	82.2	0.178	24	1.74
820	97.9	0.021	3	1.31
915	97.4	0.026	3	1.34

Table (29): The transmission, reflectance, absorption coefficient and refractive indices of different lasers wavelengths for sample A_2

λ(nm)	T%	R	α($10^{-4}cm^{-1}$)	n
532	93.7	0.063	6.1	1.47
632.8	92.0	0.080	8	1.51
660	91.2	0.088	9	1.53
675	93.5	0.065	6.3	1.49
820	95.3	0.047	3	1.42
915	98.9	0.011	1	1.26

Table (30): The transmission, reflectance, absorption coefficient and refractive indices of different lasers wavelengths for SampleA_3

λ(nm)	T%	R	α(10^{-4}cm^{-1})	n
532	80.2	0.198	19	1.7
632.8	69.1	0.309	33	1.9
660	89.6	0.104	9.4	1.5
675	90.0	0.100	9	1.5
820	97.2	0.028	2.4	1.35
915	98.8	0.012	1	1.27

Table (31): The transmission, reflectance, absorption coefficient and refractive indices of different lasers wavelengths for Sample A_4

$\lambda(nm)$	T%	R	α(10^{-4}cm^{-1})	n
532	87.0	0.130	17	1.5
632.8	70.6	0.284	42	1.9
660	87.1	0.129	17	1.5
675	93.7	0.063	8	1.4
820	98.0	0.020	2.4	1.3
915	81.5	0.185	25	1.7

Table (32): The transmission, reflectance, absorption coefficient and refractive indices of different lasers wavelengths for Sample A_5

λ(nm)	T%	R	α(10^{-4}cm^{-1})	n
532	82.7	0.173	18	1.7
632.8	75.2	0.248	27	1.72
660	92.9	0.071	7	1.48
675	97.6	0.024	2.3	1.33
820	96.7	0.033	3	1.37
915	96.0	0.040	4	1.39

Table 33): The transmission, reflectance, absorption coefficient and refractive indices of different lasers wavelengths for Sample A_6

λ(nm)	T%	R	α(10^{-4}cm^{-1})	n
532	91.0	0.090	8	1.55
632.8	92.6	0.074	7	1.50
660	89.0	0.110	10	1.60
675	98.3	0.017	1.5	1.30
820	97.2	0.028	2.4	1.35
915	98.0	0.120	1.7	1.62

Table (34): The transmission, reflectance, absorption coefficient and refractive indices of different lasers wavelengths for Sample A_7

λ(nm)	T%	R	$\alpha(10^{-4}cm^{-1})$	n
532	82.1	0.179	20	1.74
632.8	67.0	0.330	41	1.97
660	77.0	0.230	27	1.74
675	94.7	0.053	6	1.44
820	94.1	0.059	6	1.46
915	93.9	0.061	6	1.47

Table (35): The transmission, reflectance, absorption coefficient and refractive indices of different lasers wavelengths for Sample A_8

λ(nm)	T%	R	$\alpha(10^{-4}cm^{-1})$	n
532	80.8	0.192	21	1.80
632.8	73.7	0.263	30	1.9
660	90.7	0.093	9	1.55
675	98.4	0.016	1.5	1.29
820	98.5	0.015	1.5	1.7
915	95.3	0.047	4.6	1.42

Table (36): The transmission, reflectance, absorption coefficient and refractive indices of different lasers wavelengths for sample A_9

λ(nm)	T%	R	$\alpha(10^{-4}cm^{-1})$	n
532	80.1	0.199	21	1.74
632.8	80.0	0.200	21	1.74
660	92.9	0.071	6.8	1.50
675	98.4	0.016	1.5	1.29
820	91.5	0.085	8.3	1.52
915	84.1	0.159	16	1.72

Table (37): The transmission, reflectance, absorption coefficient and refractive indices of different lasers wavelengths for Sample B_1

λ(nm)	T%	R	$\alpha(10^{-4}cm^{-1})$	n
532	95.8	0.042	5.3	1.40
632.8	96.9	0.031	3.9	1.36
660	98.7	0.023	1.6	1.33
675	97.5	0.025	3.1	1.34
820	95.3	0.047	5.9	1.42
915	97.9	0.021	2.6	1.32

Table (38): The transmission, reflectance, absorption coefficient and refractive indices of different lasers wavelengths for Sample B_2

λ(nm)	T%	R	$\alpha(10^{-4}cm^{-1})$	n
532	92.7	0.073	7.1	1.48
632.8	96.0	0.040	3.8	1.4
660	98.2	0.018	1.7	1.3
675	97.5	0.025	2.4	1.34
820	95.7	0.043	4.1	1.41
915	98.5	0.015	1.4	1.29

Table (40): The transmission, reflectance, absorption coefficient and refractive indices of different lasers wavelengths for Sample B_4

λ(nm)	T%	R	$\alpha(10^{-4}cm^{-1})$	n
532	92.9	0.071	9.1	1.48
632.8	94.2	0.058	7.3	1.46
660	97.2	0.028	3.5	1.35
675	98.1	0.019	2.4	1.31
820	98.3	0.017	2.1	1.31
915	87.7	0.123	16.1	1.55

Table (41): The transmission, reflectance, absorption coefficient and refractive indices of different lasers wavelengths for sample B_5

λ(nm)	T%	R	$\alpha(10^{-4}cm^{-1})$	n
532	96.8	0.032	3.1	1.37
632.8	97.1	0.029	2.8	1.35
660	98.7	0.013	1.2	1.27
675	91.5	0.085	8.4	1.53
820	96.4	0.036	3.4	1.38
915	98.4	0.016	1.5	1.3

Table (42): The transmission, reflectance, absorption coefficient and refractive indices of different lasers wavelengths for sample B_6

λ(nm)	T%	R	$\alpha(10^{-4}cm^{-1})$	n
532	93.0	0.070	6.2	1.4
632.8	96.4	0.036	3.2	1.38
660	98.2	0.018	1.6	1.3
675	98.2	0.018	1.6	1.3
820	98.1	0.019	1.6	1.31
915	97.2	0.028	2.4	1.35

Table (43): The transmission, reflectance, absorption coefficient and refractive indices of different lasers wavelengths for sample B_7

λ(nm)	T%	R	$\alpha(10^{-4}cm^{-1})$	n
532	95.9	0.041	4.3	1.4
632.8	92.9	0.071	7.6	1.48
660	97.6	0.024	2.5	1.33
675	89.2	0.108	12	1.5
820	95.9	0.041	4.3	1.4
915	82.6	0.174	19.6	1.74

Table (44): The transmission, reflectance, absorption coefficient and refractive indices of different lasers wavelengths for sample B_8

λ(nm)	T%	R	$\alpha(10^{-4}cm^{-1})$	n
532	95.3	0.047	4.7	1.43
632.8	90.7	0.093	9.5	1.55
660	96.5	0.035	3.5	1.38
675	98.4	0.016	1.6	1.39
820	96.1	0.039	3.9	1.4
915	80.3	0.197	21	1.74

Table (45): The transmission, reflectance, absorption coefficient and refractive indices of different lasers wavelengths for sample B_9

λ(nm)	T%	R	$\alpha(10^{-4}cm^{-1})$	n
532	86.0	0.140	14	1.55
632.8	71.7	0.293	30.9	1.9
660	94.4	0.036	5.4	1.38
675	95.2	0.048	4.6	1.43
820	98.7	0.023	1.2	1.33
915	96.4	0.036	3.4	1.38

Table (46): The transmission, reflectance, absorption coefficient and refractive indices of different lasers wavelengths for sample C_1

λ(nm)	T%	R	$\alpha(10^{-4}cm^{-1})$	n
532	94.9	0.051	6.4	1.43
632.8	98.2	0.018	2.2	1.3
660	99.1	0.009	1.1	1.25
675	98.1	0.019	2.4	1.31
820	92.8	0.072	9.3	1.48
915	91.7	0.083	10.6	1.52

Table (47): The transmission, reflectance, absorption coefficient and refractive indices of different lasers wavelengths for sample C_2

λ(nm)	T%	R	α($10^{-4}cm^{-1}$)	n
532	95.8	0.042	3.9	1.40
632.8	98.0	0.020	1.9	1.31
660	99.1	0.019	8.5	1.31
675	98.4	0.016	1.5	1.3
820	97.5	0.025	2.4	1.34
915	92.5	0.075	7.3	1.50

Table (48): The transmission, reflectance, absorption coefficient and refractive indices of different lasers wavelengths for sample C_3

λ(nm)	T%	R	α($10^{-4}cm^{-1}$)	n
532	96.9	0.031	2.7	1.37
632.8	98.0	0.020	1.7	1.31
660	98.9	0.011	0.95	1.3
675	98.9	0.011	0.95	1.3
820	98.0	0.020	1.7	1.31
915	97.8	0.032	1.9	1.32

Table (49): The transmission, reflectance, absorption coefficient and refractive indices of different lasers wavelengths for sample C_4

$\lambda(nm)$	T%	R	α($10^{-4}cm^{-1}$)	n
532	96.2	0.038	3.9	1.38
632.8	98.2	0.018	2.3	1.3
660	98.9	0.011	1.3	1.26
675	98.1	0.019	2.5	1.31
820	98.7	0.013	1.6	1.31
915	91.1	0.089	12.5	1.53

Table (50): The transmission, reflectance, absorption coefficient and refractive indices of different lasers wavelengths for sample C_5

λ(nm)	T%	R	α($10^{-4}cm^{-1}$)	n
532	96.5	0.035	3.5	1.38
632.8	97.5	0.025	2.4	1.34
660	98.2	0.018	1.7	1.3
675	96.3	0.027	3.7	1.34
820	97.4	0.026	2.5	1.34
915	98.4	0.016	1.5	1.3

Table (51): The transmission, reflectance, absorption coefficient and refractive indices of different lasers wavelengths for sample C_6

λ(nm)	T%	R	α($10^{-4}cm^{-1}$)	n
532	95.7	0.043	2.9	1.40
632.8	98.0	0.020	1.8	1.21
660	98.7	0.013	1.1	1.27
675	98.3	0.017	1.5	1.3
820	96.9	0.031	2.7	1.37
915	86.7	0.133	12.3	1.66

Table (52): The transmission, reflectance, absorption coefficient and refractive indices of different lasers wavelengths for sample C_7

$\lambda(nm)$	T%	R	α($10^{-4}cm^{-1}$)	n
532	96.2	0.038	4	1.38
632.8	95.3	0.047	4.9	1.43
660	97.8	0.022	2.3	1.33
675	98.6	0.014	1.3	1.29
820	98.7	0.013	1.3	1.27
915	95.9	0.041	4.3	1.4

Table (53): The transmission, reflectance, absorption coefficient and refractive indices of different lasers wavelengths for Sample C_8

$\lambda(nm)$	T%	R	α($10^{-4}cm^{-1}$)	n
532	95.1	0.049	4.8	1.43
632.8	96.7	0.033	3.2	1.37
660	97.2	0.028	2.7	1.35
675	94.2	0.058	5.8	1.46
820	98.7	0.013	1.2	1.27
915	94.1	0.059	5.9	1.46

Table (54): The transmission, reflectance, absorption coefficient and refractive indices of different lasers wavelengths for Sample C_9

λ(nm)	T%	R	α($10^{-4}cm^{-1}$)	n
532	93.6	0.044	6.1	1.40
632.8	97.1	0.029	2.7	1.35
660	97.8	0.022	2.1	1.32
675	98.6	0.014	1.3	1.29
820	96.9	0.031	2.9	1.35
915	90.4	0.096	9.3	1.55